1992

# Monte Carlo Studies of the Critical Phenomena in Carbon Monoxide Oxidation.

Bing Yu
*Louisiana State University and Agricultural & Mechanical College*

Order Number 9317008

# Monte Carlo studies of the critical phenomena in CO oxidation

Yu, Bing, Ph.D.

The Louisiana State University and Agricultural and Mechanical Col., 1992

U·M·I
300 N. Zeeb Rd.
Ann Arbor, MI 48106

# MONTE CARLO STUDIES OF THE CRITICAL PHENOMENA IN CO OXIDATION

A Dissertation

Submitted to the Graduate Faculty of the
Louisiana State University and
Agricultural and Mechanical College
in partial fulfillment of the
requirements for the degree of
Doctor of Philosophy
in
The Department of Physics and Astronomy

by
Bing Yu
B.S. Louisiana State University, 1985
M.S. Louisiana State University, 1987
December 1992

TO MY PARENTS

# ACKNOWLEDGMENTS

I am indebted to my advisor, Prof. Dana Browne, for his guidance and kindness, and I wish to express my utmost gratitude to him. This work would not have been possible without his constant caring and encouragement. During the years, I have benefited immensely from his ingenuity and knowledge. He has provided me with an enormous opportunity to develop my professional career by encouraging me to attend various professional conferences. His concern for the development of my professional life is deeply appreciated.

I also would like to thank Prof. Peter Kleban of University of Maine for his invitation to work with him. I am grateful for his kindness and generosity.

Thanks are due to the Department of Physics and all its faculty members and staff who have made my graduate study here an enjoyable and memorable experience.

Additionally, I also would like to express my thanks to LSU SNCC for providing me with excellent computational resources and LSU Library for providing me with an excellent collection of books and professional journals.

Moreover, I would like to thank all my friends here at LSU who have made my life pleasant.

Finally, I would like to thank a special friend, Sonia Granera, for the wonderful time we have together. Her friendship is deeply appreciated.

# CONTENTS

**Acknowledgments** iii

**List of Tables** vi

**List of Figures** x

**Abstract** xi

**Chapter 1. Introduction** 1

1.1 Critical Phenomena of Equilibrium Systems . . . . . 1
1.1.1 Early Work on Critical Phenomena . . . . . 2
1.1.2 Modern Theory of Critical Phenomena . . . . . 7
1.2 Critical Phenomena of Nonequilibrium Systems . . . . . 17

**Chapter 2. Review of Catalytic Oxidation of CO** 25

2.1 Introduction . . . . . 25
2.2 Experimental Results of CO Oxidation . . . . . 25
2.2.1 Reaction Mechanism . . . . . 26
2.2.2 Adsorption and Desorption of CO . . . . . 28
2.2.3 Adsorption and Desorption of O . . . . . 29
2.2.4 Diffusion . . . . . 30
2.2.5 Experimental Phase Diagram . . . . . 30
2.3 The ZGB Model . . . . . 33
2.3.1 Kinetic Rules . . . . . 33
2.3.2 Phase Diagram of the ZGB Model . . . . . 35
2.3.3 Review of Literature on the ZGB Model . . . . . 37
2.4 Objectives of This Study . . . . . 40

**Chapter 3. Anisotropic ZGB Model** 42

3.1 Introduction . . . . . 42
3.2 Description of Anisotropic Model . . . . . 42
3.3 Results on the Anisotropic ZGB Model . . . . . 46
3.3.1 Phase Diagram with no Diffusion . . . . . 46
3.3.2 Behavior with Diffusion . . . . . 50

3.3.3 Limiting Cases of ZGB Model . . . . . 51
3.3.4 Critical Behavior and Critical Exponents . . . . . 54
3.4 Conclusion . . . . . 60

**Chapter 4. ZGB Model with Finite Reaction Rate** **62**

4.1 Introduction . . . . . 62
4.2 Comparison of the Models . . . . . 62
4.3 Tricritical Point . . . . . 68
4.3.1 Characteristic Time Scale and Susceptibility . . . . . 76
4.3.2 Critical Behavior and Critical Exponents . . . . . 83
4.3.3 A Theory of the Tricritical Point . . . . . 97
4.3.4 Effects of Anisotropy and Diffusion on Tricritical Points 112
4.5 Conclusion . . . . . 115

**Chapter 5. Mechanism of Dynamical Phase Transition** **117**

5.1 Introduction . . . . . 117
5.2 A Master Equation Approach . . . . . 118
5.3 The Master Equation as a Transfer Matrix . . . . . 119
5.4 Noise and Universality Class . . . . . 122
5.5 A Case Study . . . . . 124
5.5.1 Review of Group Theory . . . . . 125
5.5.2 Finite Size Scaling of Eigenvalues . . . . . 129
5.6 Conclusion . . . . . 131

**Chapter 6. Conclusions** **135**

**Appendix A. Computational Considerations** **146**

**Appendix B. Random Number Generations** **152**

**Vita** **160**

# LIST OF TABLES


1 Critical exponents from static scaling for various anisotropy $R_x$ 58

2 Critical exponents from dynamical scaling for various anisotropy $R_x$. . . . . 58

3 Dynamical and static critical exponents at $R_x = 0.5$ . . . . . 91

# LIST OF FIGURES


1 Phase diagram of water . . . . . 4

2 Universal behavior of different chemical compounds . . . . . 8

3 A pictorial illustration of the renormalization group . . . . . 15

4 A pictorial illustration of the tricritical point and the crossover phenomenon . . . . . 16

5 Experimental phase diagram of the ZGB model . . . . . 32

6 Phase diagram of the ZGB model . . . . . 36

7 Structure of the (110) surface of a fcc crystal . . . . . 44

8 Oxygen coverage $n_0$ *vs.* $y_{co}$ for various values of $R_x$ for a 100x100 lattice . . . . . 47

9 The location of the first order transition $y_2$ *vs.* $R_x$ . . . . . 48

10 The phase diagram for the anisotropic model with no CO diffusion . . . . . 49

11 Oxygen coverage $n_O$ *vs.* $y_{co}$ for various diffusion rates with $R_x = 0.25$ on a 100x100 lattice . . . . . 52

12 The mean lifetime $\tau$ *vs.* system size $L$ for various choices of $y_{co}$ 57

13 A scaling plot of $\log(\psi L^{\beta/\nu})$ *vs.* $\log(|y_{co}/y_1 - 1|L^{1/\nu})$ for various system sizes with $R_x = 0.2$ . . . . . 59

14 First and second order transition points *vs.* anisotropy $R_x$ at $r = 0.9$ . . . . . 63

15 First and second order transition points *vs.* anisotropy $R_x$ at $r = 0.4$ . . . . . 64

16 First order and second order transition points *vs.* reaction rate at $R_x = 0.5$ . . . . . 66

17 Steady state CO concentration as a function of reaction rate at $R_x = 0.5$ . . . . . 67

18 Magnification of the tricritical region . . . . . 69

19 Concentration of CO and vacancies as a function of time . . . 71

20 A typical steady state at the second order transition . . . . . 72

21 A typical steady state at the first order transition . . . . . 73

22 A typical steady state at the tricritical point . . . . . 74

23 Characteristic time $\tau$ *vs.* $y_{co}$ at $r = 0.9$ and $R_x = 0.5$ . . . . . 77

24 Derivative of characteristic time $\tau$ *vs.* $y_{co}$ at $r = 0.9$ and $R_x = 0.5$ . . . . . 78

25 Characteristic time $\tau$ *vs.* $y_{co}$ at $r = 0.6$ and $R_x = 0.5$ . . . . . 79

26 Derivative of characteristic time $\tau$ *vs.* $y_{co}$ at $r = 0.6$ and $R_x = 0.5$ . . . . . 80

27 Characteristic time $\tau$ *vs.* $y_{co}$ at $r = 0.01$ and $R_x = 0.5$ . . . . 81

28 Derivative of characteristic time $\tau$ *vs.* $y_{co}$ at $r = 0.01$ and $R_x = 0.5$ . . . . . 82

29 Vacancy susceptibility as a function of $y_{co}$ . . . . . 84

30 CO and vacancy concentration as a function of time at $r = 0.9$ and $R_x = 0.5$ . . . . . 86

31 CO and vacancy concentration as a function of time at $r = 0.4$ and $R_x = 0.5$ . . . . . 87

32 CO and vacancy concentration as a function of time at $r = 0.9$ and $R_x = 0.5$ . . . . . 88

33 $\log(n_{vac+co})$ *vs.* $\log(L)$ at $r = 0.02$ and $R_x = 0.5$ . . . . . 90

34 Local slope of the growth rate *vs.* the reciprocal time at $r = 0.02$ and $R_x = 0.5$ . . . . . 92

35 $\log(n_{vac+co})$ *vs.* $\log(L)$ at $r = 0.9$ and $R_x = 0.5$ . . . . . 93

36 $\log(\tau)$ *vs.* $\log(L)$ at $r = 0.9$ and $R_x = 0.5$ . . . . . 94

37 A scaling plot of $\log(n_{co+vac}L^{\beta/\nu})$ *vs.* $\log(|y_{CO}/y_1 - 1|L^{1/\nu})$ for various system sizes with $r = 0.9$ and $R_x = 0.5$ . . . . . 95

38 $He^3 - He^4$ phase diagram . . . . . 99

39 Phase boundary in a-b space . . . . . 104

40 $c_2$ as a function of reaction rate at $R_x = 0.5$ . . . . . 107

41 Phase diagram computed using extracted $c_2$ at $R_x = 0.5$ . . . 108

42 CO-O concentration from simulation and calculation assuming $c_2 = 0$ and $r = 0.9$ . . . . . 109

43 CO-O concentration from simulation and calculation assuming $c_2 = 0$ and $r = 0.025$ . . . . . 110

44 CO-O concentration from simulation and calculation assuming $c_2 = 0$ and $r = 0.018$ . . . . . 111

45 Projections of the tricritical line onto $R_x - r$ plane . . . . . 113

46 Projections of the tricritical line onto $R_x - y_{co}$ plane . . . . . 114

47 Effect of diffusion on the tricritical point at $r = 0.01$ . . . . . 116

48 Phase diagram of the Schizo model . . . . . 126

49 Relaxation of two slowest modes . . . . . 130

50 Plots of $\ln(\tau)$ *vs.* $\ln(L)$ for various $p$ values . . . . . 132

51 A plot of $\ln(\tau L^{-z})$ *vs.* $\ln\left((p - p_c)L^{1/\nu}\right)$ for various lattice sizes showing the collapse of the data on a single universal curve . . . . . 133

52 One dimensional distribution of linear congruent random numbers on a linear lattice . . . . . 155

53 Two dimensional distribution of linear congruent random numbers on a square lattice . . . . . 156

54 One dimensional distribution of Fibonacci random numbers on a linear lattice . . . . . 158

55 Two dimensional distribution of Fibonacci random numbers on a square lattice . . . . . 159

# ABSTRACT

It is well established that anisotropy does not affect the critical behavior of a system in thermodynamic equilibrium undergoing a second order phase transition. We study here an anisotropic kinetic model for heterogeneous catalysis which mimics the oxidation of CO on the (110) surface of a transition metal like Pd. In this model, the oxidation process occurs at an infinite reaction rate. We mapped out the phase diagram of possible steady states for various anisotropic reaction and absorption processes as a function of the $O_2$/CO adsorption rate and the CO diffusion rate. The phase diagram depends upon the amount of anisotropy and exhibits both a first order and a second order phase transition. We also examined the critical behavior at the second order phase transition with finite size scaling and found that this model belongs to the directed percolation universality class irrespective of the anisotropy. Furthermore, we extended this model to include finite reaction rates. We found evidence of a new feature here, namely a tricritical point. We have developed a theory to account for this new feature. The critical behavior of this modified model belongs to the same universality class as the original model except at the tricritical point. To better understand the physics of nonequilibrium transitions, we studied the behavior of various dynamic modes utilizing the master equation and finite size scaling. This master equation approach indicated that dynamic phase transition is a consequence of the emergence of new steady states. This approach affords a connection with the traditional method of transfer matrix.

# CHAPTER 1

# INTRODUCTION

## 1.1 Critical Phenomena of Equilibrium Systems

Throughout history, mankind has engaged in unravelling the mysteries of nature. This endeavor brought many fundamental changes in our understanding of the world. The first such fundamental change came from the success of the Newtonian mechanics, which elucidated the regularity of the universe amidst the diversity of natural phenomena. Since then deterministic thinking has dominated the scientific community. Our universe was considered as a *clock*, and random process was regarded as a disorganizing force. It was not recognized until recently that many systems under the influence of random external forces can organize themselves. These new discoveries changed our traditional view of the random process. Consequently, these discoveries had a profound impact on our understanding of the behavior of systems with many degrees of freedom, including examples from physics, chemistry, biology, sociology, geology and economics.

Organization of a system from a macroscopically disordered state to an ordered state occurs frequently in nature; the formation of ice from water is an example. The phenomenon of changing from one state to the other is commonly known as a phase transition. Systematic studies of this phenomenon began almost a century ago. Since then we have accumulated a wealth of knowledge about phase transitions of thermodynamic systems. In recent years, a significant amount of effort has been devoted to broaden the study of phase transitions and related critical phenomena to include dynamical

systems. This shift of emphasis from equilibrium systems to nonequilibrium systems is a step forward towards understanding more complicated systems such as catalytic reactions. The focus of this thesis is on the critical phenomena of catalytic reactions. Before proceeding, we will give an overview of the ideas and language used in describing critical phenomena and phase transitions.

### 1.1.1 Early Work on Critical Phenomena

Phase transitions occur in a wide variety of systems which are entirely different in nature. Nevertheless, seemingly unrelated systems such as fluids and magnets have some common characteristics as they approach their transition point. These *universal* characteristics of critical phenomena are indicative of some underlying fundamental similarities. To elucidate these similarities is the task of the theory of critical phenomena.

Theoretical work on critical phenomena began with the work of Van der Waals in 1873[1]. His work gave a good description of the critical phenomenon in a liquid-gas system such as water. Fig. 1, which shows the phase diagram of water, delineates the temperature and pressure boundaries of distinct forms of water. The liquefaction of steam below certain pressure gives off latent heat in a so-called first order phase transition as shown in Fig. 1, consequently, the entropy of the system changes abruptly as the system crossing the phase boundary. This condensation process is clearly visible because of the density difference between the liquid and gas, and it occurs at a variety of pressure and temperature, forming the vapor-pressure line. On this line liquid and gas can exist simultaneously.This first

order transition line eventually terminates at a point known as the critical point.

The transition occurs at the critical point is completely different from the first order transition; the distinction between the liquid and gas disappears, and liquefaction is no longer possible. A system at the critial point is dominated by large density fluctuations. These fluctuations cause a clear liquid to become milky due to enhanced ability of the liquid to scatter light. This phenomenon is known as critical opalescence. In addition to large fluctuations, the entropy does not have a singular behavior; no latent heat is given off during the transition. However, the singular behavior does occur in the specific heat of the system. This type of transition is known as a second order transition. The behaviors of a system undergoing a second order transition near a critical point is referred to as critical phenomena.

The most fundamental difference between a first and second order phase transition is in the behavior of the thermodynamic free energy. In a first order transition, the first derivative of the thermodynamic free energy or entropy is singular while second and higher order derivatives are singular in a second order transition. This smoothness of the free energy and its derivative is the basis of Ehrenfest's classification. According to Ehrenfest, if the $i^{th}$ order and all higer order derivatives are singular, the transtion is referred to as an $i^{th}$ order phase transition.

In addition to classifying a transition, it is necessary to quantify certain characteristics of a transition. For example, no density difference exists at the critical point in a liquid-gas system. To facilitate a description of this fact, we define a quantity known as the order parameter. The chief purpose of this quantity is to serve as an indicator which measures the

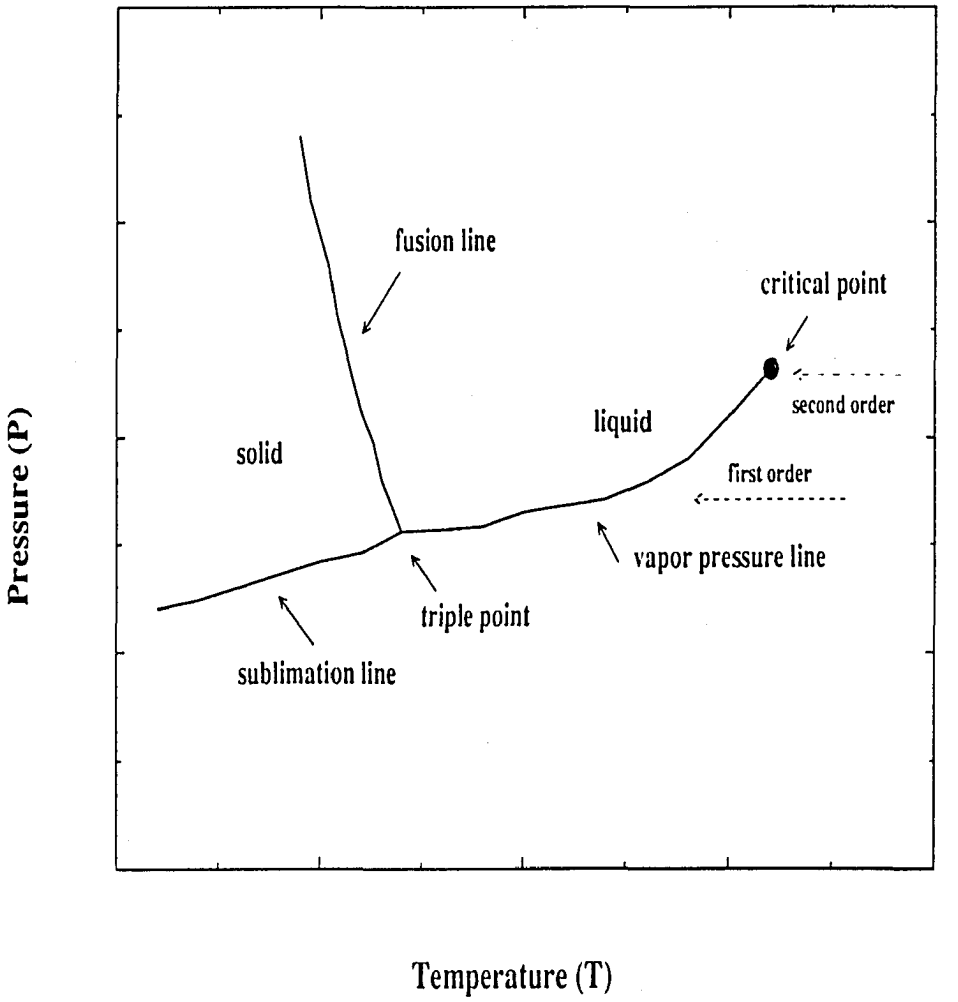


Figure 1: Phase diagram of water

*distance* between the state of the system and its critical state. As the system approaches a critical point this distance indicator vanishes smoothly. The choice of such an indicator varies from system to system. For water intuition directs us to use the difference between gas and liquid density. This quantity vanishes at the critical point of water, indicating no apparent distinction between the liquid and gas. This choice of a directly observable quantity as the order parameter should not be generalized because in many systems we do not impose any conditions on direct measurability when choosing an order parameter. Sometimes, an order parameter may not correspond to any physically measurable quantity. For example in the $He^4$ system, the order parameter is a complex field which is not directly measurable, and it is related to the superfluidity. In a superconductor, the order parameter is the amplitude of a Cooper pair. This quantity is also not directly observable.

Even though an order parameter may not be physically measurable, it plays a very important role in the theory of critical phenomena. The behavior of the order parameter and other thermodynamic quantities determines the critical behavior of a system. When a system approaches a critical point, many thermodynamic quantities have a singular behavior. For example, the order parameter in the liquid-gas system is proportional to $|T - T_c|^\beta$, where $T_c$ is the critical temperature. The exponent $\beta$ is known as the critical exponent for the order parameter, which characterizes the critical behavior. These critical exponents are a focal point of the theory of critical phenomena.

The first attempt to understand critical phenomena and to calculate critical exponents was made by Van der Waals. His theory of liquid and gas was the first mean field theory to calculate critical exponents. In this theory

averaged quantities such as temperature and pressure was utilized to describe the system; the utilization of these averaged quantities was to smooth out fluctuations. This method of smoothing out fluctuations by the process of averaging was carried over to other mean field theories and became a major feature of this type of theory. For example this technique was utilized in subsequent years by Weiss to formulate a theory for ferromagnetism[2]. To be more specific, consider the Ising model introduced by Wilhelm Lenz to explain magnetic systems[3]. In this model magnetic moments are localized on a lattice, and they interact with each other pairwise. The Hamiltonian of the system is given by

$$H = - \sum_{i,j=1 to N} J_{ij} S_i \cdot S_j \ , \tag{1}$$

where $S_i$ is the magnetic moment on the $i^{th}$ site, and $J_{ij}$ is a coupling constant. Weiss's theory replaces the effect of all moments on $S_i$ by an effective moment, which is taken to be the average of $S_j$. The advantage of this treatment is to simplify the interaction and render the problem solvable.

However, the price we pay in doing so is enormous; the accuracy of the critical exponents is directly affected by this averaging process. In general, these theories are far less accurate in predicting critical exponents. For example, the mean field theory of Weiss predicts 1/2 for the critical exponent of the order parameter as opposed to the measured value of $0.335 \pm 0.005$[4]. This discrepancy stems from the fundamental inadequacy of mean field technique as we will see later.

### 1.1.2 Modern Theory of Critical Phenomena

Since these early attempts to formulate a coherent theory of critical phenomena, the theory of phase transition and critical phenomena has grown into maturity in the pass fifty years beginning with a set of remarkable experiments done by Guggenheim. In the 1940s, Guggenheim[5] realized that the order parameter's dependence on temperature in a liquid-gas system is independent of the chemical composition. Fig. 2 implies that the order parameter $|\rho - \rho_c|$ of liquid-gas systems obeys a unique power law relation; the exponent $\beta$ of this power law is 1/3. Besides the liquid-gas system the order parameter of a magnetic system also obeys a power law relation with $\beta \approx 1/3$[4]. These experiments suggest that microscopic details are irrelevant in relation to critical behavior.

The discovery of the same critical exponent for the liquid-gas system and the magnetic system raised the speculation about a universal critical exponent for the order parameter. However, such a speculation was shown to be unfounded by a subsequent measurement of He transition by Roach[6], which gave a different exponent. Despite of the lack of a universal critical behavior, similarities of the transition were discovered among systems of diverse nature. These similarities offer the possibility of a narrower version of the universality, namely universality among a class of systems or a universality class. Within a class, each system exhibits a similar critical behavior, which is characterized by a common set of critical exponents, irrespective of the microscopic nature of the system.

At approximately the time Guggenheim made his discovery of universality, Onsager exactly solved the two-dimensional Ising model[7]. This exact solution demonstrated several important generic features of phase

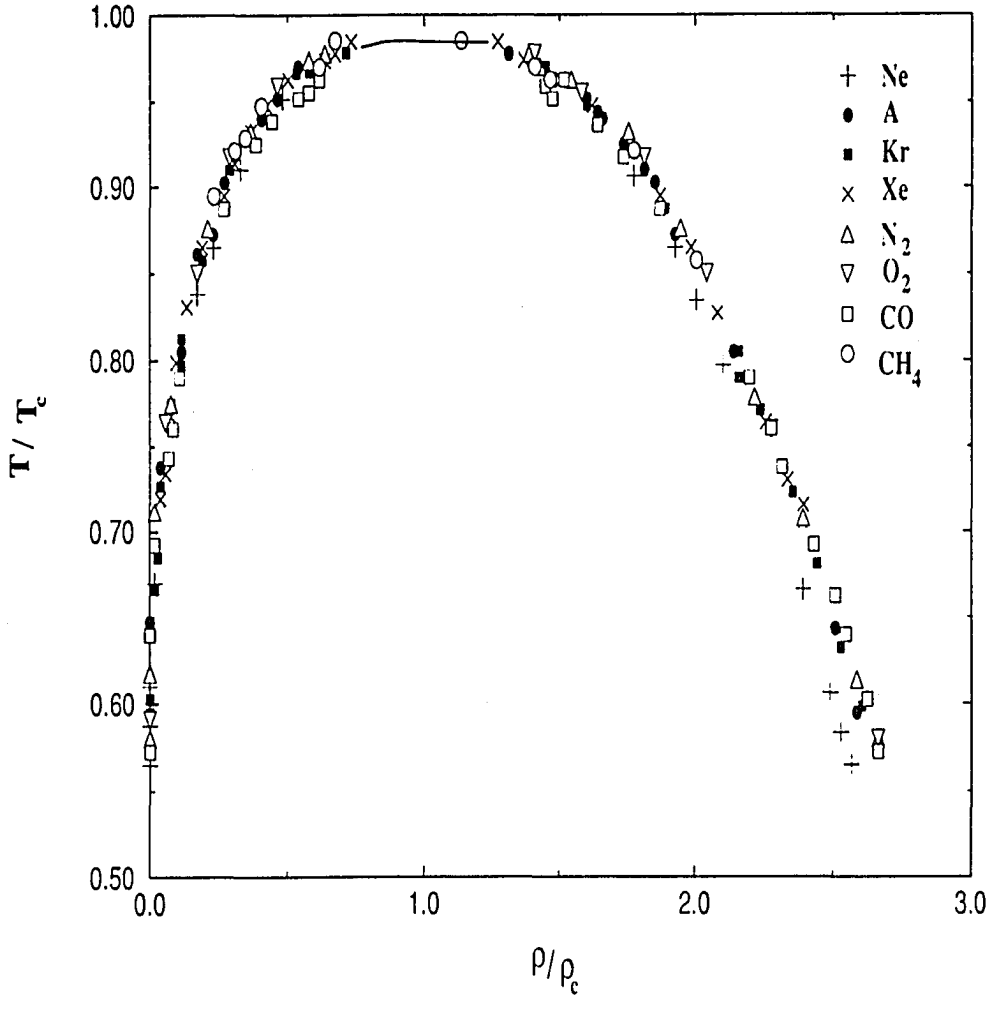


Figure 2: Universal behavior of different chemical compounds

transitions. First, the critical behavior of the one-dimensional Ising model differs dramatically from the two-dimensional model. No phase transition can occur in a one-dimensional model without an external magnetic field whereas a phase transition can occur at zero temperature with a finite field. The reason for the absence of a phase transition in a one-dimensional model with zero field can be attributed to large thermal fluctuations which destroy the long-range order, preventing the development of an ordered state. The destruction of the long-range order by large fluctuations is a rather generic feature of a one-dimensional system with a discrete symmetry. However in a two-dimensional model, phase transitions occur regardless of the external field. This result strongly indicates the fundamental importance of the dimensionality of a system in relation to its critical behavior.

Second as a system approaches its critical point, the correlation length of the system diverges. This correlation length $\xi$ is defined as

$$< M(r)M(0) > \propto e^{-r/\xi} , \qquad (2)$$

where M is some quantity of interests. To illustrate this point, we will considered a magnetic system. A ferromagnetic crystal such as iron has a nonzero magnetic field at zero temperature. At this temperature all atoms have their magnetic moments aligned forming an island of atoms with a particular spin orientation, say spin up. An increase of temperature produces a thermal excitation that tends to flip these spins; this tendency creates pockets of atoms with spin down. However below the critical temperature, we still have a big island of spin up atoms, suggesting the divergence of correlation length and existence of a long-range order. Above the critical temperature, the big island of spin up atoms is broken into small clusters, indicating the lack of long-range order and finiteness of the correlation length.

In addition to fluctuations and dimensionality, symmetry of the Hamiltonian also plays a crucial role in controlling the critical behavior. In the Ising model, the spin of each individual particle can assume a value of $\pm 1$. This system has a discrete inversion symmetry in spin space. For the XY model, the Hamiltonian is given by

$$H = -J \sum_{ij} (S_{ix} S_{jx} + S_{iy} S_{jy}) = -JS^2 \sum_{ij} cos(\phi_i - \phi_j) \,, \qquad (3)$$

which has a continuous symmetry in spin space. The critical behavior of XY model is different from the two-dimensional Ising model. Another example is the three-dimensional Heisenburg model; this model has a full three-dimensional rotation symmetry. This model has different critical behavior from three-dimensional Ising model.

In contrast to the importance of fluctuations, dimensionality, and symmetry, spatial geometry does not play a significant role in controlling the critical phenomenon. For example, the critical behavior of the Ising model on a triangular lattice and a square lattice is identical. Moreover, the range of interaction, as long as it is finite, does not alter critical behavior. This feature is illustrated by the identical critical behavior of the Ising model as long as the interaction involves only neighbors at a finite distance.

The discovery of the importance of these fundamental mechanisms in relation to critical phenomena has revolutionized the field of critical phenomena and phase transitions. A new picture of critical phenomena has emerged from this discovery. In this new picture microscopic details play no essential role while long wave fluctuations, dimensionality, and symmetry of the Hamiltonian control the critical behavior. Furthermore, the development of a long-range order and the divergence of correlation length demonstrate

the cooperative nature of critical phenomena. Consequently, studies of critical phenomena must take into account of this cooperative nature in order to describe the macroscopic behavior corrently. Moreover, it is also crucial to include fluctuations on length scale. Failure to do so will produce erroneous results. This point is best illustrated by the failure of mean field theory in predicting the critical behavior, which smooths out all fluctuations.

In order to consider the cooperative nature of a critical system, new techniques have to be developed. A conceptual treatment of this cooperative nature of the phenomenon is provided by the idea of scale invariance. An intuitive support for this idea was introduced originally by Kadanoff[8] and refined by Wilson and others into the powerful mathematical technique of the renormalization group[9]. The major advantage of this technique is in the preservation of essential ingredients such as fluctuations.

To illustrate the idea of Kadanoff, we consider the following picture. Beginning with small systems characterized by a set of quantities $a_i$, these systems are allowed to interact among themselves. These small systems can be transformed into a larger system characterized by a new set of quantities $b_i$. The construction of this larger system is accomplished by smoothing out irrelevant microscopic details. By allowing the larger block to interact with each other in a modified interaction, we can construct an even larger system. A repeated application of the above procedure creates a gigantic system that is insensitive to the microscopic details, yet it includes essential interactions on all length scales. This construction of a larger system by smoothing out irrelevant microscopic details is known as coarse–graining. At each level of the coarse–graining process, the functional form of all physical quantities remains unchanged except by a scaling factor. In addition, the

transformation is required to preserve the symmetry of the original system. The above intuitive argument of Kadanoff can be formulated into a scaling hypothesis for thermodynamic variables. The scaling hypothesis states that the thermodynamic potential is a homogeneous function of some variables[10]. For example, in a magnetic system, the singular part of the thermodynamic potential is a homogeneous function of both temperature and external field

$$LG(\epsilon, H) = G(\epsilon L^{a_1}, H L^{a_2}) , \tag{4}$$

where $\epsilon = | \frac{T-T_c}{T_c} |$; $L$ is the size of the system, and $a_1$ and $a_2$ are scaling parameters. Critical exponents for other thermodynamic quantities are obtainable from them. The magnetization, for example, is the derivative of G with respect to the external field H. It is given by

$$M(\epsilon, H) = L^{a_2-1} M(\epsilon L^{a_1}, H L^{a_2}) . \tag{5}$$

The critical exponent of the magnetization $\beta$ at zero field is obtained by setting $L^{-a_1} = \epsilon$

$$M(\epsilon, H) = \epsilon^{(1-a_2)/a_1} M(1, 0) , \tag{6}$$

This relation indicates that critical exponent $\beta = 1 - a_2/a_1$. Similarly, $a_1$ and $a_2$ also determine other critical exponents such as the exponent for the correlation length $\xi$. It is important to note that the scaling hypothesis only gives the form of a thermodynamic function; it does not provide any information on the scaling parameter $a_i$.

To implement the Kadanoff construction mathematically is the task of the renormalization procedure. For a thermodynamic system, we can construct a thermodynamic potential characterized by a set of parameters or coupling constants. The transformation of a small system into a larger

system is carried out mathematically by integrating out (coarse-graining) non-essential microscopic degrees of freedom. An appropriate rescaling of this coarse-grained potential produces the renormalized thermodynamic potential for a larger system characterized by a renormalized set of coupling constants. In other words, the renormalization process may be viewed as a process of transforming these coupling constants to represent a larger system. This mathematical operation forms a group or more precisely a semi-group because of the lack of an inverse operation. This process may eventually terminate when it reaches a stationary point of these coupling constants, known as a fixed point.

A simple way to visualize the renormalization process is to imagine a parameter space of coupling constants as shown in Fig. 3. These coupling constants are functions of some variables. For example, in a magnetic system, the coupling constants are functions of the temperature. Each point in this parameter space represents a system of certain temperature. For a second order transition, any point in the parameter space approaches the fixed point in every direction under the action of the renormalization group, except one direction known as the relevant direction. The rate at which the point moves away from the fixed point in the relevant direction can be related to the critical exponent. This is illustrated by the trajectory of point B in Fig. 3. This point represents a system away from the critical temperature. The renormalization group moves this point closer to the fixed point in the x and y direction but not in the z direction. However, there is a special portion of the parameter space known as the critical surface. The points on the surface represent systems at the critical temperature. A point on the critical surface will remain on the surface under the action of the

renormalization group until it reaches the fixed point. This is illustrated by point A in the Fig. 3.

A different way of viewing the above picture is to imagine a *hill* around the fixed point. The renormalization group moves a point uphill. The shape of the hill or the local surface topology of the fixed point determines the growth rate in the relevant direction. We can attribute the universal critical behavior to a unique local surface topology of the fixed point. However, in spite of constraints of the local topology on critical exponents, there are no similar constraints on critical points. Consequently, the location of critical points is a non-generic aspect of the critical phenomenon.

The landscape of the parameter space of a second order transition is the simplest of all. It is possible to have multiple fixed points in the parameter space. A tricritical point, as we may recall from the statistical mechanics, is a point where a first order transition line coalesces with a second order transition line. From a renormalization point of view, a tricritical point corresponds to an additional fixed point beside the one associated with the second order transition as shown in Fig. 4. For a point approaching the fixed point of the tricritical point, two relevant directions exist. One of these relevant directions points towards the second order fixed point. This direction *measures* the competition between the second order fixed point and the tricritical point. The point A in Fig. 4 represents a system at the tricritical point. The renormalization moves the system towards the fixed point of the tricritical point without the influence from the second order transition. This scenario is analogous to the above case of moving a point on the critical surface. With the influence from the second order transition suppressed, the system exhibits tricritical behavior.

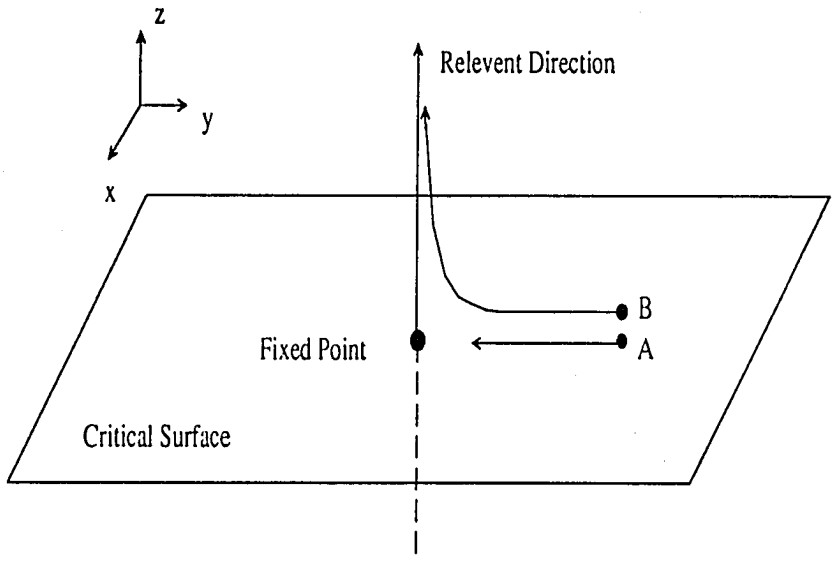


Figure 3: A pictorial illustration of the renormalization group

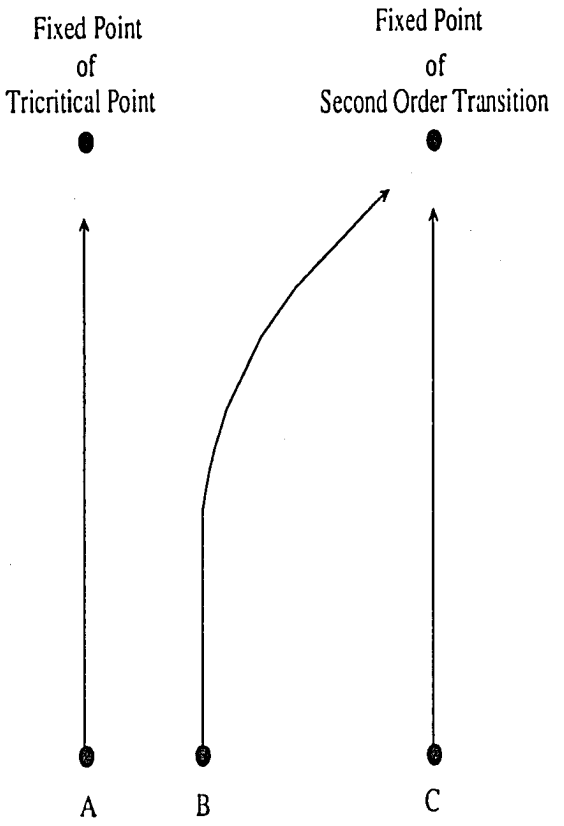


Figure 4: A pictorial illustration of the tricritical point and the crossover phenomenon

The inclusion of the influence from the fixed point of the second order transition produces a competition with the fixed point the tricritical point. This competitive nature of the fixed points can be visualized by considering the trajectory of a point initiated near the tricritical point such as the point B in Fig. 4. As this point approaching the fixed point of the tricritical point, it will sense the presence of the fixed point of the second order transition and eventually veer off towards the second order fixed point. In this region, a system has a complicated behavior that is influenced by both fixed points. This phenomenon is a so-called crossover phenomenon, meaning the system is crossing from one behavior to the other.

For a point such as point C, the critical behavior of the system is entirely that of second order. In summary, for a system with a tricritical point, three different regions may exist. In one of the regions, the critical behavior is dominated by the tricritical point with a set of exponents; the other is controlled by the second order transition with a different set of exponents; the third region is the crossover region in which the critical behavior is influenced by both fixed points.

## 1.2 Critical Phenomena of Nonequilibrium Systems

So far we have only discussed equilibrium systems. However, systems we observe in nature are frequently subject to the influence of external forces which prevent the attainment of thermal equilibrium. These systems are often nonlinear in character. Examples are exciton dynamics[11] and chemical reactions[12]. Under rather general conditions, these systems attain a steady state. The steady state of a nonequilibrium system may exhibit intriguing macroscopic structures such as spatial or temporal oscillation, chaotic

motion, and soliton propagation (non-dissipative waves with certain collision properties). These macroscopic structures are known collectively as dissipative structures. The formation of dissipative structures is a consequence of cooperative nature of a nonlinear system, known as self organization or synergetics[13].

Like equilibrium systems, second phase transitions of nonequilibrium systems exhibit enhanced fluctuation, growth of the correlation length and critical slowing down. Despite these similarities, the mechanism of a nonequilibrium phase transition is not well understood. The success of the theory of renormalization group in conjunction with the idea of long wave fluctuations and scale invariance has provided an elegant theory for the description of equilibrium phase transitions. The reproduction of such success for nonequilibrium transitions is still in doubt. Even though nonequilibrium systems exhibit behaviors similar to equilibrium systems, there are forces which are present only in a nonequilibrium system. Frequently these external forces play an essential role in creating dynamical fluctuations, thus, the character of these forces play an important part in controlling the critical behavior. The question we must address in the study of nonequilibrium phase transitions includes both static and dynamic behaviors. Similar to the study of equilibrium phase transitions, the objective of studying nonequilibrium phase transitions is to discover the fundamental mechanism governing dynamical transitions and search for universality classes.

Since there are many similarities between equilibrium and nonequilibrium systems, many of the concepts developed for an equilibrium phase transition may also apply to nonequilibrium systems. For example, we can continue to use the order parameter, assuming we can find one, to indicate

the closeness of the system from its critical point, and we can associate a critical exponent with the order parameter. We may continue to classify nonequilibrium transition according to its order; but Ehrenfest's definition of order is inappropriate because not every dynamical system can be described by a thermodynamic potential. Instead, we should choose some quantity that characterizes the system for the purpose of classifying the transition. If this quantity is continuous at the transition, the transition is referred to as a second order transition; if the quantity is discontinuous at the transition, this transition is first order.

So far we have only discussed first and second order transitions in nonequilibrium systems, and we have compared them with equilibrium systems. It is important to point out that first order and second order transitions are not the only forms of transitions which may occur in a nonequilibirum system. Other forms of nonequilibrium transitions such as pattern formation, and transition to oscillation and chaos may also occur in a nonequilibrium system. These types of transitions have no equilibirum analogue. It is appropriate at this point to provide some concrete examples of nonequilibrium transitions.

A first example is the well known Bernard instability. This is an example of pattern formation. A liquid layer is heated from below. If the temperature gradient is small, heat transport is in the form of conduction. When the temperature gradient exceeds some critical value, suddenly macroscopic motion occurs in the form of convective rolls; here the change of temperature creates a phase transition. A related phenomenon is the Taylor instability. A liquid is enclosed between two coaxial cylinders with the outer cylinder fixed and the inner one free to rotate. When the rotation reaches a

critical value, the liquid forms a macroscopic pattern known as Taylor vortices. Here the speed of the cylinder is the control parameter.

A third good example of a nonequilibrium phase transition is the laser. Lasers are produced by stimulating atoms, and these excited atoms emit light as they decay. The light emitted as the atoms decay is just incoherent light if the pumping power of a laser is below the laser threshold. Once the pumping power of the laser increases above the laser threshold, a sudden change in the light emission occurs. The light emitted changes from a low intensity, incoherent beam to a high intensity, coherent laser. As the pumping power goes even higher, the nature of light emission changes once again from a high intensity coherent laser to high intensity pulse laser. Therefore, the nature of light emitted from stimulated atoms changes dramatically as the pumping power varies. These excited atoms "self-organize" themselves from incoherent emission to coherent emission under the influence of the pumping power. In this example, the steady state exhibits temporal oscillation.

The last example is in developmental physiology. Cells can self-organize into distinguishable cell regions. Dictyostelium can spontaneously emit cAMP (cyclic Adenosin 3'5'Monophospate) in a form of pulse, which may be amplified by other Dictyostelium. This spontaneous and stimulated emission of chemicals (analogous to the spontaneous and stimulated emission of laser) produces a concentration gradient of cAMP. A single cell can detect the concentration gradient of cAMP and migrate towards the center to form a tissue.

In many instances, a dynamical system can be modelled by a class of nonequilibrium *toy* models. These models are simplified models for some real processes[11, 14]. These models are often subject to an external force

and characterized by an Markovian process. In other words, the evolution of a dynamical system is independent of its history. Frequently, a set of kinetic rules governing the dynamical evolution is given. These local rules describe a single step evolution of the local configuration of the system, and often violate detailed balance.

Examples of these models are Schlogl's autocatalytic models[15]. His models describe the autocatalytic generation and destruction of a species X. This system is characterized by the density of X. The evolution process of species X is governed by a single step transition rule. In his first model, the evolution process is given by:

$$X \longrightarrow 2X \tag{7}$$

$$X \longrightarrow 0. \tag{8}$$

The rate of change of X density is given by the following equation:

$$\frac{dn}{dt} = -n^2 + (1-\beta)n\ , \tag{9}$$

where $\beta$ is a parameter related to individual reaction rate, and $n$ is the density of X. Its steady state solution is given by

$$n = \begin{cases} 1-\beta & for\ \beta < 1 \\ 0 & for\ \beta > 1. \end{cases}$$

It is evident from the solution that this system has two different steady states as a function of $\beta$. As the $\beta$ varies, the system changes from a reactive steady state to a state with no X. This latter state is stable in the sense that no further reaction can occur once it is reached, and the system is trapped in this state permanently. This kind of state is often referred to as an absorbing state, for it acts as a *sink* in the configuration space. The absorbing state

corresponds to $X = 0$ state here, and the transition from a reactive steady state to this absorbing state is marked by a continuous variation in X density as shown by the solution. Therefore, this transition is second order in nature.

A variant model is the second model of Schlogl. In this model the auto-generation rule is given by

$$2X \longrightarrow 3X \tag{10}$$

$$X \longrightarrow 0. \tag{11}$$

The density of X at a steady state is governed by

$$\gamma = n^3 - 3n^2 + \beta n\ , \tag{12}$$

where $\gamma$ is a parameter related to individual reaction rate like $\beta$. This equation has three distinct solutions if $\beta < 3$. The steady states correspond to the largest and smallest $n$ are stable whereas the other steady state is unstable. The transition from one stable state to the other is marked by a discontinuous change in $n$, therefore a first order transition.

Another model is the *contact* process originally proposed by Harris[16]. This model simulates the spreading of a disease among cells. An infected cell is cured after a certain amount of time, and a cell is infected if its nearest neighbors are infected. This model has an absorbing state that corresponds to a population free from disease. Other examples of interacting particle systems include (D+1)-dimensional direct percolation and Reggeon Field Theory(RFT), the voter model, and various chemical systems[12, 17, 18, 19]. These models offer a way to study real systems by simplifying the problem while capturing the essence of the problem.

The study of nonequilibrium systems is more difficult to conduct due to the lack of a Hamiltonian formulation, therefore, traditional statistical

mechanics offers no assistance in studying these systems. In addition, these systems are often nonlinear in nature, and they frequently exhibit oscillatory or chaotic behavior as a function of time. These complicated phenomena are not fully understood despite many recent efforts. This lack of understanding stems from the inadequacy of the traditional method, such as linearizing a nonlinear equation, in predicting the global structure of a nonlinear system.

Apart from the difficulties associated with studying complicated transitions such as transition to chaos, a variety of tools are available for the study of nonequilibrium first or second order transitions. Because mechanisms which control the critical behavior such as fluctuations do not play a significant role in a first order transition, mean field theory remains a valuable tool. Complementing mean field theory, the renormalization approach may be a useful tool in studying critical behavior and calculate critical exponents. Another method of studying them utilizes the master equation. Since the master equation governs the time evolution of any statistical system, Hamiltonian or non-Hamiltonian, this approach has the advantage of being more generic. However, the disadvantage of this method is the difficulty in solving the equation due to the large degrees of freedom. A more phenomenological approach is Monte Carlo simulation. Critical behavior and exponents can be studied by various methods such as Monte Carlo renormalization or finite size scaling.

Monte Carlo has been utilized widely in studying statistical systems. We have utilized this technique extensively in this study, therefore, it is worth pointing out a generic feature in simulating systems with absorbing states such as Schlogl's models; if the size of these systems is finite, there is no true steady state except the absorbing states. However, there may exist a

metastable state in a finite size system; this state will eventually decay into one of the absorbing states if one waits long enough, but the time required for this to happen is a rapidly increasing function of the system size. In the limit of infinite volume, the system will be in the true steady state in the sense that it will not enter one of the absorbing states in a finite amount of time. This is the analogue of the absence of long-range order in a finite system in thermodynamic equilibrium.

The focus of this study is to characterize nonequilibrium phase trasnitions (first and second order transitions) and critical phenomena in a model proposed by Ziff, Gulari, and Barshad[19], which mimics the oxidation of CO on a square lattice. In addition, we will utilize the master equation to elucidate the mechanism for the dynamical phase transition and provide a connect to the transfer matrix technique. As a prelude to present our results, we will provide background information about the model in the next chapter.

# CHAPTER 2

# REVIEW OF CATALYTIC OXIDATION OF CO

## 2.1 Introduction

Dynamical systems frequently display a variety of fascinating behaviors that still elude our comprehension. Despite the complexity of these systems, progress has been made in understanding them. Prototype models, which simulate real processes, have been constructed to mimic real systems. An example would be a model which simulates the catalytic oxidation of CO. This nonequilibrium, open system is the subject of this study. Before proceeding, we will review some experimental results which are the basis for this model, and we will review some literatures on this model. Finally, we will provide the motivation for this study and an outline of this thesis.

## 2.2 Experimental Results of CO Oxidation

A catalyst is a substance which assists in a chemical reaction without a net change at the end of the reaction. The major effects of a catalyst in a chemical reaction are to reduce the energy barrier and to localize the reactants. Catalysts are commonly used in the commercial production of chemical products. One example is the use of catalytic converters in

automobiles to reduce air pollution by converting nitrogen compounds and carbon monoxide into less harmful products such as water and carbon dioxide.

### 2.2.1 Reaction Mechanism

The study of the catalytic oxidation of carbon monoxide dates back to Langmuir[20]. Even though this reaction is one of the longest known catalytic reactions, a detailed understanding of the process on microscopic scale is made possible only recently with the advent of surface-sensitive spectroscopies. Since the development of these new techniques in probing microscopic details, we have learned important information about the surface processes involved in the reaction.

There are two possible mechanisms for catalytic oxidations: Langmuir-Hinshelwood or Eley-Rideal. In the Langmuir-Hinshelwood mechanism, the CO and $O_2$ molecules form chemical bonds with a catalyst prior to the reaction, and oxidation occurs exclusively between chemisorbed CO and $O_2$. However, the Eley-Rideal mechanism only requires the chemisorption of $O_2$ with the oxidation occuring between gas phase CO and chemisorbed O. To determine which mechanism is responsible for the oxidation is a first step towards the understanding of this reaction.

Molecular beam relaxation spectroscopy (MBRS) is an excellent tool with which to probe reaction mechanisms. Consider a surface populated with adsorbed molecules; a beam of molecules is directed towards the surface. The adsorption and desorption process is given by

$$\frac{dN}{dt} = sI(t) - R_d N(t)\,, \tag{13}$$

where N(t) is the concentration of adsorbed molecules; I(t) is the flux of the molecular beam; s is the sticking coefficient, and $R_d$ is the desorption rate. The Fourier transform of this equation is

$$I_d(\omega) = R_d N_a(\omega) = \frac{sI(\omega)}{(1 + i\omega/R_d)} . \tag{14}$$

This equation provides a way to measure the residence time $\tau_r$, which is the reciprocal of the desorption rate. If a molecular beam with a frequency $\omega$ is directed at the surface, the measurement of desorbed molecules gives the necessary information to determine $\tau_r$.

Since the Langmuir-Hinshelwood mechanism involves surface processes such as $CO_2$ adsorption, this mechanism predicts a finite residence time $\tau_r$ while the Eley-Rideal mechanism predicts $\tau_r = 0$. The measurement of the residence time $\tau$ shows that $\tau_d = 6 \times 10^{-4} sec$[21]. This result suggests that the reaction occurs via Langmuir-Hinshelwood process.

More evidence came from the measurement of the activation energy. The catalytic oxidation of CO is an activated process. The reaction rate obeys an Arrhenius law

$$r_{LH} = \nu_1 e^{-E_1/RT} , \tag{15}$$

where R is the gas constant and $\nu_1 = 8.6 \times 10^9 s^{-1}$[22]. The activation energy has been measured by Engel[23, 24]. His result indicate an activation energy of 1.09eV. This result agrees with the activation energy 1.06eV calculated by assuming a Langmuir-Hinshelwood mechanism while it disagrees with 1.39eV predicted by the Eley-Rideal mechanism. It should be pointed out that this experiment was performed under high temperature at which CO desorption process dominates, therefore, the activation energy is that of CO desorption.

Since the oxidation is an activated process obeying Arrhenius law, the rate at which reaction occurs is temperature dependent. 500K is the temperature at which a significant number of experiments are performed; the reaction rate is about $6500s^{-1}$ at this temperature. It is necessary to point out that we have used an activation energy of 0.62eV in calculating the rate[22] because this value corresponds to the normal production of $CO_2$. This activation energy differs from the findings of Engel; this difference is due to experimental conditions such as surface CO density[25].

### 2.2.2 Adsorption and Desorption of CO

It has been shown that catalytic oxidation of CO occurs via the Langmuir-Hinshelwood mechanism. Prior to CO oxidation, O and CO molecules must first chemisorb; the question is how they are adsorbed. The adsorption of CO primarily occurs in a molecular form without dissociation[25]. The chemisorption of a CO molecule is generally accepted as through the carbon atom. Evidence of formation of M-CO bond comes from calculations of the binding energy which indicate that a M-CO bond is more energetically favorable[26, 27]. Ionic scattering experiment also suggests that the top layer of the adsorbate constitutes O adatoms exclusively[28]. Moreover, angular resolved photoelectron spectroscopy suggests that CO is perpendicularly chemisorbed[29, 30, 31, 32, 33]. While mechanism for the chemisorption was proposed by Blyholder for CO on nickel[34], there is theoretical as well as experimental evidence to suggest that the same mechanism applies to the adsorption of CO on Pd[35, 36]. In this mechanism, CO donates an electron in its $5\sigma$ orbital to a localized

orbital of the substrate while accepting an electron from the substrate into its $2\pi$ antibond.

Besides the chemisorption of CO, physisorption of CO also can occur, forming a so-called precursor state. Physisorption of CO occurs on top of a chemisorbed CO layer via Van der Waals interaction. This physisorbed CO can diffuse easily on top of the chemisorbed CO layer, due to the weakness of the Van der Waals interaction. As it diffuses, it may encounter a vacant site and chemisorption then occurs[37, 38, 39, 40].

While CO and metal substrate can bond to each other, the dissociation or desorption occurs at high temperature. The desorption process is also an activated process obeying an Arrhenius law. The activation energy for this process is 1.09eV with a prefactor of $4.35 \times 10^{13} sec$[22]. At $T = 500$, the desorption rate is about $1400 s^{-1}$, a much slower rate than the reaction process.

### 2.2.3 Adsorption and Desorption of O

The adsorption of oxygen is more complicated. At low temperature chemisorption of oxygen in the molecular form is possible[41, 42]. However at high temperature, oxygen is dissociated upon adsorption. This is the primary form of oxygen when the oxidation occurs. Oxygen may be chemisorbed on the metal or form oxide with the metal. An oxygen molecule which forms oxide on the metal surface is more inert in the oxidation process. However certain metal such as Pd, there is no oxide formation.

Thermal desorption of chemisorbed oxygen occurs in a similar fashion as CO. This process is also an activated process. The activation energy for

the desorption of oxygen is considerably higher than CO. At temperatures below 600K, experiments indicate that the desorption of $O_2$ is negligible[43].

### 2.2.4 Diffusion

Like the desorption process, surface diffusion of adatoms is also an activated process obeying an Arrhenius law. In general, the activation energy for diffusion is about 20% of the chemisorption energy. Therefore, the activation energy for CO and O is 0.2eV and 0.6eV, respectively. At temperature above 300 K, chemisorbed CO is relatively mobile[44] while O is still relatively immobile[43].

To summarize the above discussion, the oxidation of carbon monoxide occurs via the following steps in a Langmuir-Hinshelwood process. First, carbon monoxide and oxygen are chemisorbed on the catalytic surface. Carbon monoxide is adsorbed in a molecular form perpendicular to the metallic surface with the formation of M-C bond while chemisorbed oxygen dissolves into atomic oxygen with formation of M-O bond. Catalytic action reduces the energy barrier of the formation of $CO_2$. Consequently, the oxidation of CO adatom occurs, The end product of $CO_2$ is desorbed from the metal surface, and the reaction continues. In comparison with the reaction process, desorption is much slower processes, therefore, they play a lesser role. Surface diffusion of O can be neglected safely while CO diffusion may be important.

### 2.2.5 Experimental Phase Diagram

Even though the basic reaction mechanism of the oxidation process is known, a single theory capable of explaining every phenomenon observed

in experiments has yet to emerge. Under different external conditions, experiments indicate a wide range of phenomena. At low pressure($p \approx 10^{-5}$), the experimental phase diagram of the oxidation can be divided into three basic regions: high reactivity region; transition region; and low reactivity region[43]. This phase diagram is shown in Fig. 5; it is mapped out at temperature $T = 500$. In the high reactivity region, the normal catalytic process of converting CO into $CO_2$ occurs. The transition region marks the change in character of the reaction. In this region, the rate of formation of $CO_2$ abruptly drops. In the low reactivity region, the production of CO is inhibited. This region, characterized by a high concentration of CO on the surface, is known as a CO-poisoned phase. It is known that high coverage of CO on the surface will inhibit chemisorption of oxygen and poison the catalytic surface. However, no similar effect is observed for an oxygen covered surface; this is due to the fact that a considerable amount of CO still can be adsorbed by *compressing* chemisorbed oxygen[25].

If the experiment is performed under high pressure ($p > 10^{-5}$ Torr), the reaction rate exhibits oscillatory and chaotic behavior. This behavior is not limited only to the catalytic oxidation of CO. This phenomenon is almost a generic feature of catalytic reactions and occurs frequently in various types of catalytic oxidations such as that of $H_2$, $NH_3$, $C_2H_4$, $C_3H_6$, and $CH_3OH$[45].

The change of catalytic process with external conditions is closely related to surface processes such as surface reconstructions. To elucidate basic mechanisms responsible for these phenomena by including every surface process may not be enlightening due to the complexity. However, to study the fundamental processes that are responsible for the gross features of the reaction is essential towards understanding of the oxidation process. A first step

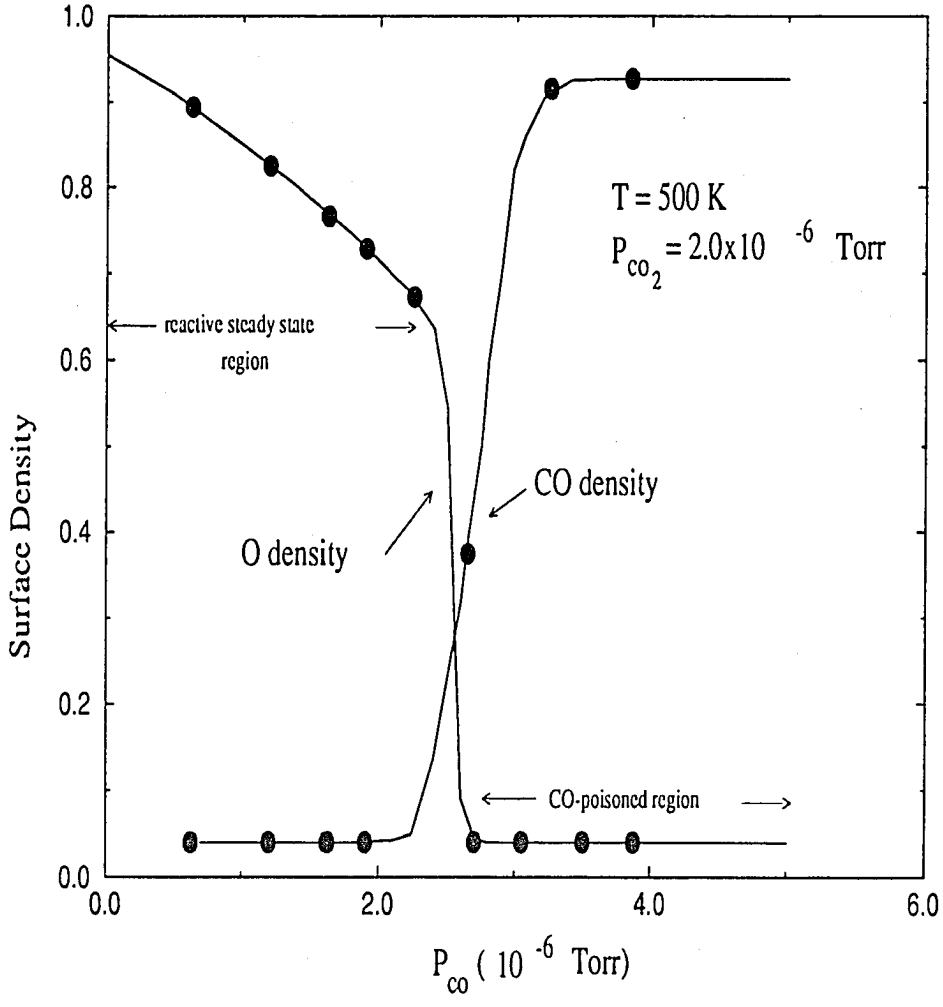


Figure 5: Experimental phase diagram of the ZGB model

in developing a conceptually simple model that accomplishes this objective was made by Ziff, Gulari, and Barshad[19].

## 2.3 The ZGB Model

The ZGB model[19] developed a two-component model, whose steady state is not described by thermodynamic equilibrium. The major advantage of the ZGB approach is its simplicity. The catalytic process is modelled by a set of kinetic rules, which describe a single step in the evolution of the state of the system, and we carry it out by Monte Carlo simulations.

### 2.3.1 Kinetic Rules

The kinetic rules utilized in the ZGB model are a simplification of the experimental observations using the Langmuir-Hinshelwood mechanism as the basic reaction mechanism. The catalytic surface is modelled by a square lattice of adsorption sites, for which CO and $O_2$ compete. A CO and O gas mixture is fed to the surface at a constant rate for oxidation. The relative concentration $y_{co}$ of CO and O in the gas mixture is fixed. The above discussion of the surface adsorption of CO and $O_2$ established that CC is chemisorbed through the C, while $O_2$ dissociates into two O adatoms as it chemisorbs. Therefore, the adsorption of CO requires only one active site while the adsorption of O needs two adjacent vacant sites. The adsorption and dissociation of $O_2$ are assumed to be independent of orientations. These observations and assumptions are incorporated into the model and translated into the following rules:

$$CO + vacant \longrightarrow C_{ad} \tag{16}$$

$$O_2 + vacant\ pair \longrightarrow 2\ O_{ad}. \tag{17}$$

Once CO and O are chemisorbed on the surface, the ZGB model assumes that immediate formation of $CO_2$ takes place. The oxidation process is assumed to occur only among nearest neighbor pairs. The end product of the oxidation is desorbed at once from the catalytic surface to allow for the next cycle of reaction. If the oxidation process is possible in several directions, the reaction occurs equally probable in each direction. This process is modelled by the following steps:

$$O_{ad} + CO_{ad} \longrightarrow CO_2 + vacant\ pair\ . \tag{18}$$

In this model, surface effects such as surface reconstruction and defect are ignored. No consideration is given to the possibility of anisotropy in the adsorption and reaction mechanisms. Furthermore, no attention is given to the diffusion and thermal desorption of reactants on the surface. Admittingly, these simplifications may produce a model that cannot exactly reproduce all the phenomena observed by experiments. However, it is not the objective of this model to exactly reproduce experimental results, rather, the only objective is to have a simple model which produces qualitative agreements with experiments as a first step towards understanding the oxidation. In addition, this model provides a nonequilibrium system with various phase transitions. Apart from oxidation considerations, these transitions are interesting from the perspective of critical phenomena.

### 2.3.2 Phase Diagram of the ZGB Model

The phase diagram of this model is presented in Fig. 6, showing the fractional coverage of O on the surface as a functino of $y_{co}$. This model has only one external parameter, which is the mixing ratio of CO and O concentration $y_{co}$. This parameter plays an analogous role in this model as the temperature in the magnetic system. Through simulations on a $128 \times 256$ lattice, Ziff *et al.*[19] found the following features: for $y_{co} < y_1 \approx 0.389$, the system reaches an absorbing state (states that cannot be left once they are entered) completely occupied by O; a similar CO occupied absorbing state occurs for $y_{co} > y_2 \approx 0.527$; between $y_1$ and $y_2$, a reactive steady state region exists where the surface is only partially occupied by CO and O, and the $CO_2$ formation rate assumes a non-zero value. The parameter $y_{co}$ determines the state of the system. As $y_{co}$ increases past $y_1$, the steady state changes from the O-saturated state to the reactive steady state via a second order phase transition. The reactive steady state is replaced by the CO-saturated state via a first order phase transition at $y_{co} = y_2$.

A comparison of this phase diagram with the experimental phase diagram reveals a general agreement between the two: a first order transition from the reactive steady state to CO-poisoned state is captured by the model; also this model indicates an O-poisoned phase, reminiscent of the O-rich phase in the real system. This model, however, indicates a feature that is not seen in the real system, namely the reactive steady state to O-poisoned transition (the second order transition). Irrespective of the oxidation process, this transition provides an excellent opportunity for the study of nonequilibrium critical phenomena.

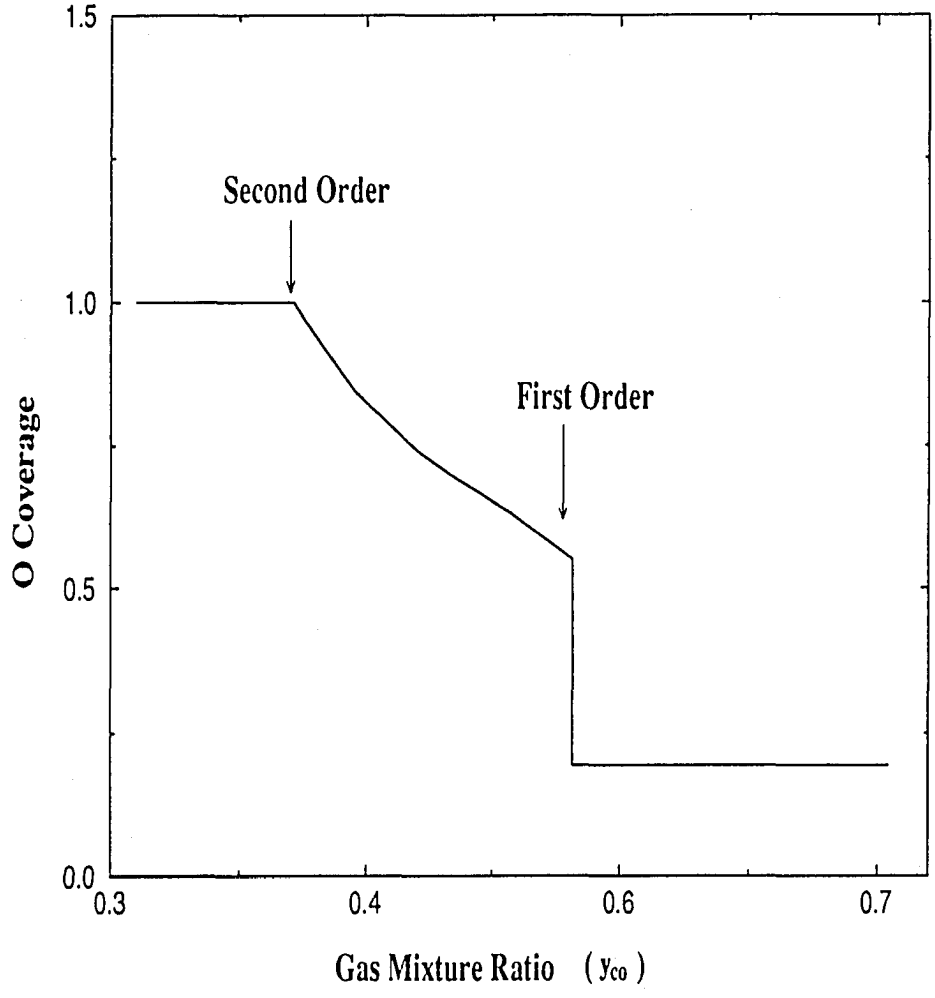


Figure 6: Phase diagram of the ZGB model

Besides the first and second order transitions, this model does not exhibit chaotic behavior. We attribute this lack of chaos to the fact that we have only two coupled degrees of freedom, namely CO and O density; this two degrees of freedom is below the minimum requirement for an autonomous system to exhibit chaos; more degrees of freedom are needed in producing chaos.

### 2.3.3 Review of Literature on the ZGB Model

The critical behavior and phase transition of this model have been the subject of extensive studies. The first order phase transition has been studied by Dickman using a mean field approach[46] that approximates the kinetic equations for the spatial correlations by truncating the correlations at a certain range. At the level of ignoring pair and higher order correlations, the equations are the same as the usual Langmuir adsorption equations with a Langmuir–Hinshelwood reaction term. This method correctly predicted the qualitative features of the phase diagram with two absorbing states and a reactive steady state, although the positions of transitions were somewhat in error. Dickman found better results by including nearest neighbor correlations, for which he found[46] a first order transition at $y_{co} = 0.56$ and a second order transition at $y_{co} = 0.25$.

Meakin and Scalapino[47] reproduced the ZGB simulation results with a larger square lattice of $512 \times 512$ and also on a hexagonal lattice of $512 \times 512$. The essential features of the phase diagram of square lattice remain unchanged in the hexagonal lattice, except that the first order phase transition occurs at $y_{co} = 0.561$ and the second order phase transition occurs at $y_{co} = 0.344$. Meakin and Scalapino[47] estimated that near the second

order transition the CO coverage varied as $n_{co} \propto (y - 0.344)^{\beta_{co}}$ with a critical exponent $\beta_{co} \approx 0.69$. Similarly they found the oxygen coverage obeyed $1 - n_o \propto (y - 0.344)^{\beta_O}$ with $\beta_O \approx 0.61$. From their work they could not rule out the possibility of the exponents being the same. Grinstein, Lai and Browne[48] argued from a simple renormalization group approach and some numerical simulations that the ZGB model belongs to the universality class of Reggeon field theory[18] and directed percolation[17], for which the critical exponent $\beta$ is 0.58. The continuous transition in a kinetic model to a noiseless (absorbing) state is generally believed[48, 49] to be in this universality class. Extensive simulations by Jensen, Fogedby, and Dickman[50] have confirmed that the dynamical behavior of the ZGB model belongs to universality class of Reggeon field theory and directed percolation.

The oxidation of CO has been studied extensively by experiments and has been the subject of numerous theoretical papers besides those mentioned above. Much recent work has been directed towards improving the mean field rate equations to account for the local correlations that are needed to describe correctly the $O_2$ adsorption and the $CO_2$ reaction. Dumont *et al.*[51] studied a model similar to the ZGB model but with a finite $CO_2$ production rate. They used simulations to correct the coverage dependence of the mean field adsorption and reaction rates. Their work was extended by Araya *et al.*[52] to include CO desorption and the effect of having several choices for potential partners to react with and having several neighboring vacancies when considering $O_2$ desorption. Their work was further extended by Ehsasi *et al.*[43] and by Kaukonen and Nieminen[53] to include CO diffusion. These latter authors also examined the influence of local adatom

interactions on changing the adsorption, desorption, reaction and diffusion rates.

The ZGB model with finite reaction rates was first considered by Considine *et al.*[54]. The finite reaction rate $r$ is defined as the probability of a reaction to occur in each Monte Carlo trial with adsorption occuring with probability 1-$r$. Unlike the case of the model with infinite reaction rates, each Monte Carlo trial can now be either an adsorption process or a reaction process. The simulation of Considine *et al.* was carried out on a 32x32 square lattice, starting from an initially blank surface. Results of their simulations revealed an additional feature in the phase diagram, namely a nonequilibrium tricritical point where a first order line coalesces with a second order line. The estimated position of this tricritical point is at $r = 0.14$ and $y_{co} = 0.28$[54].

Although simulations of Considine indicated the existence of a tricritical point, recent simulations done by Kohler *et al.* suggested a different result[55]. They claimed that no tricritical point exists at nonzero reaction rate; instead they found a narrow reactive steady state region. They employed a so called constant coverage method[56] in their work. The essence of this method is the following: the number of CO on the surface is maintained at a constant value. If the number of CO drops below this target value, the adsorption process is solely of CO. The $O_2$ adsorption process occurs only when the number of CO exceeds the target value. The value of $y_{co}$ is computed from these adsorption processes, and in the reactive steady state the value of $y_{co}$ will eventually converge. The ensemble so-generated is constant in CO coverage whereas the ensemble generated by the conventional Monte Carlo method is constant in $y_{co}$. This method has been utilized successfully

by Ziff[56] in elucidating metastable states that are otherwise undetected by the conventional method. Kohler *et al.* has gone a step further claiming this method is superior to the conventional method in detecting a narrow steady state region.

## 2.4 Objectives of This Study

Despite many studies done on the model, the effect of anisotropy has not yet been explored. Moreover, the question of tricritical point still needs further investigations. Furthermore, the dynamical process which is responsible for the critical behavior warrants study. It is the objective of this study to provide answers to these questions.

This work is composed of 6 chapters. In chapter 3, we will extend the ZGB model to include anisotropy. This extension is motivated largely by the structural anisotropy of Pd(110) surface. In this study, we will focus on the effect of spatial anisotropy on the phase diagram and the critical properties of the model. It is well established that the asymptotic critical behavior of a system in thermal equilibrium is not affected by spatial anisotropy, although it can lead to crossover effects close to the transition as the effective dimensionality of the critical fluctuations changes. We want to see if the same holds true in a nonequilibrium kinetic model.

In chapter 4, we extend the anisotropic model of ZGB to include finite reaction rates. The addition of finite reaction rates produces more complicated phase transitions such as tricritical points. However, this additional feature has been disputed by Kohler. In this chapter we will present some

evidence of a tricritical point in the anisotropic model based on a variety of considerations. In addition, we will study the effect of anisotropy and diffusion on the tricritical point.

In chapter 5, we investigate another simple model that simulates an one-dimensional chemical reaction. This model also belongs to the universality class of RFT and directed percolation. The objective of this study is to provide a clear physical picture of the underlying mechanism of a phase transition and to extract critical exponents from the master equation; this also represents an effort to develop an alternative way of calculating critical exponents. The method developed in this chapter may eventually be developed into a renormalization group approach for the calculation of critical exponents.

In chapter 6, we will summarize the entire work and outline feature directions. In the Appendix A, we will discuss certain aspects which are essential in performing a Monte Carlo simulation. Furthermore in the Appendix B, we will touch upon the generation of random numbers.

# CHAPTER 3

# ANISOTROPIC ZGB MODEL

## 3.1 Introduction

In this chapter, we will study an extension of the ZGB model that includes spatial anisotropy. We will map out the phase diagram, examine the effect of CO diffusion, and study two limiting cases of the model. Additionally, we will examine the critical behavior of the model. It is well established that the asymptotic critical behavior of a system in thermal equilibrium is not affected by spatial anisotropy, although it can lead to crossover effects close to the transition as the effective dimensionality of the critical fluctuations changes. We want to see if the same holds true in a nonequilibrium kinetic model. This chapter is organized in the following manner. In Section II we discuss the model and our simulation technique. The results we obtained for the phase diagram and the critical behavior are presented in Section III, and Section IV contains discussion and conclusions.

## 3.2 Description of Anisotropic Model

The present model was motivated largely by structural anisotropy of the (110) surface of Pd. Pd has a fcc crystal structure. If the crystal is cut along a (110) plane, the surface appears to have rows of elevated atoms in the $[1\bar{1}0]$ direction, as shown in Fig. 7. We will call the [001] and $[1\bar{1}0]$ directions the $\hat{x}$ and $\hat{y}$ directions respectively. Since the geometry in the two directions is different, it is reasonable to assume that adsorption and reaction processes will occur at different rates along each direction. Therefore, we incorporated

anisotropy into the kinetic rules to simulate the structural anisotropy. By studying the critical behavior of this anisotropic model, we will be able to determine whether anisotropy affects the universality class for the critical behavior of this nonequilibrium phase transition.

We introduced anisotropy into both adsorption and reaction rules. We assume that the adsorption of $O_2$ requires two adjacent sites, as in the ZGB model, but we will assume the $O_2$ molecule can be adsorbed only when oriented along the $\hat{y}$ direction(perpendicular to the troughs). No adsorption is permitted for molecules oriented along the trough even if two empty sites are available. The choice of the $\hat{y}$ direction for adsorption is completely arbitrary; the essential point is to permit adsorption only in one direction. We also will assume that the reaction of CO and O depends on whether the reactants are in the same trough on in adjacent troughs. We will call the probability to react in the same trough (perpendicular the $O_2$ adsorption direction) $R_x$, the probability of reacting when the reactants are in adjacent troughs is denoted $R_y = 1 - R_x$.

In our simulations, one Monte Carlo trial for the adsorption/reaction process is performed as follows. An empty site is chosen at random and then a molecule is chosen to adsorb, either a CO is chosen with probability $y_{co}$ or an $O_2$ with probability 1-$y_{co}$. If a CO is chosen, it will immediately react if any of the four neighboring sites are occupied by O. If the CO can react with more than one O, the reaction probability for a given direction ($\hat{x}$ or $\hat{y}$) is weighted by $R_x$ or $R_y$. Once the reacting partner is chosen, the reaction is instantaneous, and both the CO and O are removed from the surface. If the adsorbing molecule is $O_2$, one of the two nearest neighbors in $\hat{y}$ direction is chosen at random with equal probability. If this second site

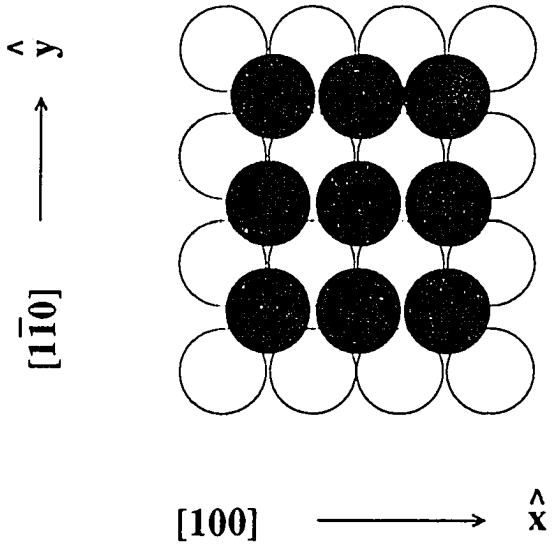


Figure 7: Structure of the (110) surface of a fcc crystal. The solid circles denote top layer atoms and the open circles show the locations of the second layer atoms.

is empty, the $O_2$ is adsorbed, and the six nearest neighbors are immediately searched for CO molecules to react with and the reaction proceeds in the same manner as described for CO adsorption events.

In order to model the system more realistically, we also considered the possibility of CO diffusion on the surface. We did not include oxygen diffusion because experiments show[44, 57] that it does not diffuse easily on the Pd surface due to its large binding energy. In each diffusion cycle, one CO is picked at random and one of its four nearest neighboring sites is chosen with equal probability. If the site chosen is empty, the CO is moved to that site and the three neighbors are checked to see if a reaction is possible according to the rules described above. If so, $CO_2$ is formed and removed from the surface. This cycle is repeated a total of $R_d$ times for each adsorption/reaction cycle, where $R_d$ is the diffusion rate. For example, if the diffusion rate is 10 times faster than the reaction rate, after each reaction cycle 10 CO molecules on the surface will be selected for diffusion. In the algorithm, it is possible for one CO to be picked repeatedly.

Except for the finite size scaling analysis described later, our simulations were done on a $100 \times 100$ square lattice starting from an empty lattice. The basic time unit in the simulation is 1 Monte Carlo Step(MCS), which is defined as one Monte Carlo trial for adsorption/reaction for every site of the lattice. We used a list of vacant sites to speed up the simulation. With the implementation of the list of vacant sites, the time step of each Monte Carlo trial is equivalent to the inverse of the number of vacant sites. In our simulation, each run was *thermalized* for 2000 MCS and data were taken for the following 3000 MCS to determine the steady state properties. In addition to the parameter $y_{co}$ in the ZGB model, we have as parameters the

reaction probability along the trough $R_x$, and the CO diffusion rate $R_d$. In this model, if we permitted $O_2$ adsorption in both directions, set $R_x = R_y$, and ignored diffusion, we would recover the ZGB model.

## 3.3 Results on the Anisotropic ZGB Model

### 3.3.1 Phase Diagram with no Diffusion

Fig. 8 shows the O coverage on the lattice *vs.* $y_{co}$ for various values of $R_x$ with no diffusion. The first and second order phase transitions present in the ZGB model appear here as well, although the position of the transition and the behavior of the coverage near it depends on $R_x$. In Fig. 8 there is no obvious shift of the first order transition with $R_x$, but a closer examination reveals a linear dependence of the transition point with $R_x$ as shown in Fig. 9. A least squares fit to the data gives a slope of $0.02 \pm 0.0008$.

On the other hand, the location of the second order phase transition is quite sensitive to the value of $R_x$. As $R_x$ increases, the position of the second order phase transition $y_1$ shifts to lower values, suggesting that the surface becomes harder to saturate with oxygen. The shift of $y_1$ does not obey the linear relationship seen for $y_2$. The second order transition disappears smoothly at $R_x = 0.742 \pm 0.002$, and for the larger values of $R_x$, the reactive steady state appears to be present for $0 < y_{co} < y_2$ as shown in Fig. 10.

Between the first and second order transitions, the phase diagram of Fig. 8 shows a reactive steady state similar to that seen in the ZGB model. For fixed $y_{co}$, the O coverage of the surface decreases with increasing $R_x$. The CO coverage stays very low throughout the reactive steady state region and the surface consists primarily of adsorbed O and vacancies.

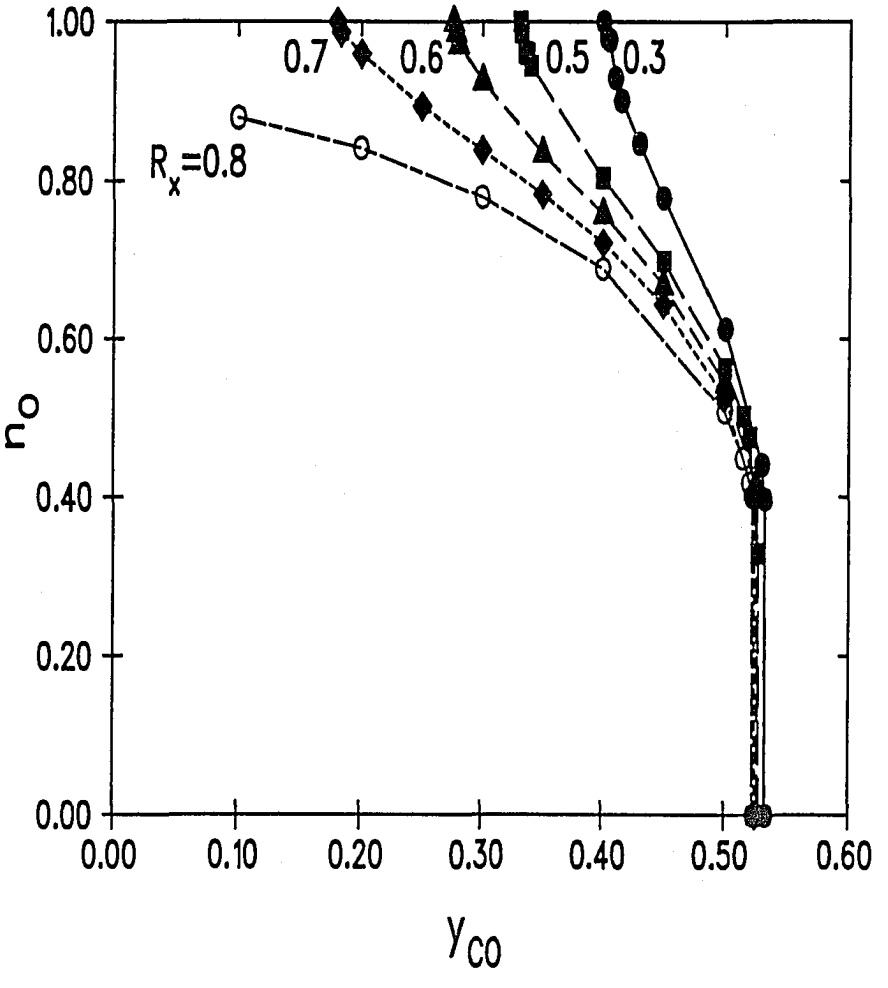


Figure 8: Oxygen coverage $n_O$ *vs.* $y_{co}$ for various values of $R_x$ for a 100×100 lattice. Note that while the position of the second order transition is very sensitive to the value of $R_x$, the first order transition moves very little.

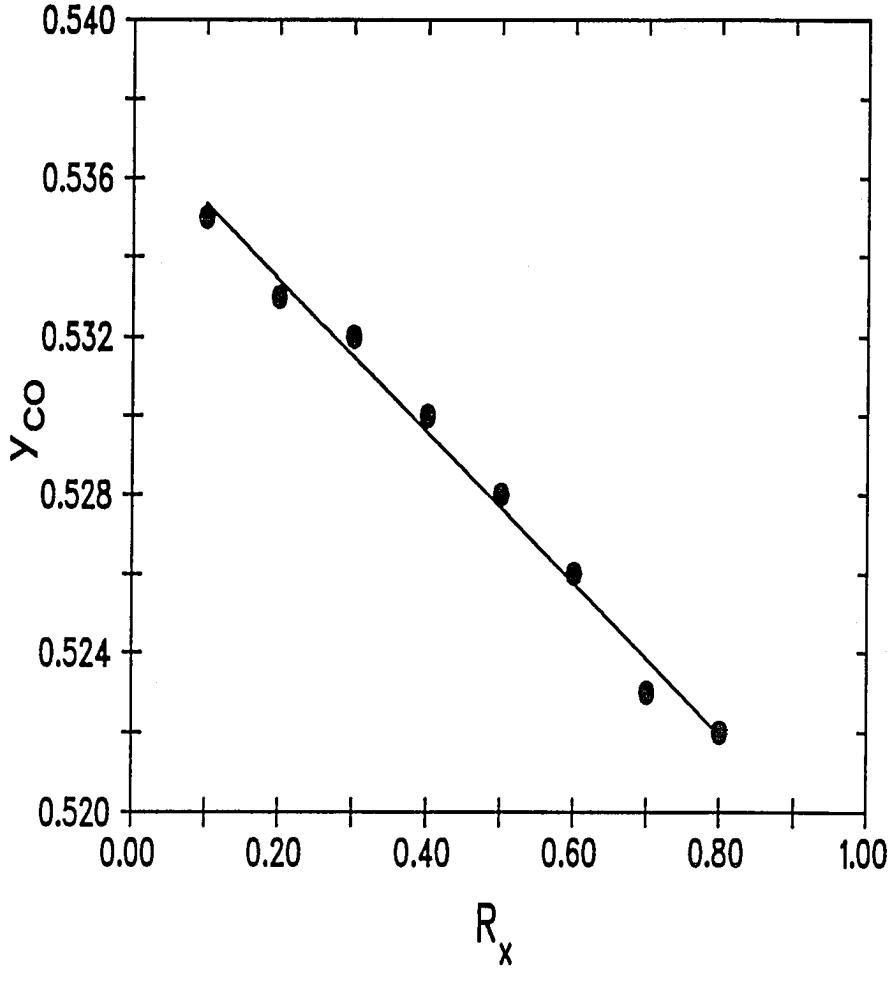


Figure 9: The location of the first order transition $y_2$ *vs.* $R_x$. Note the greatly expanded scale along the ordinate.

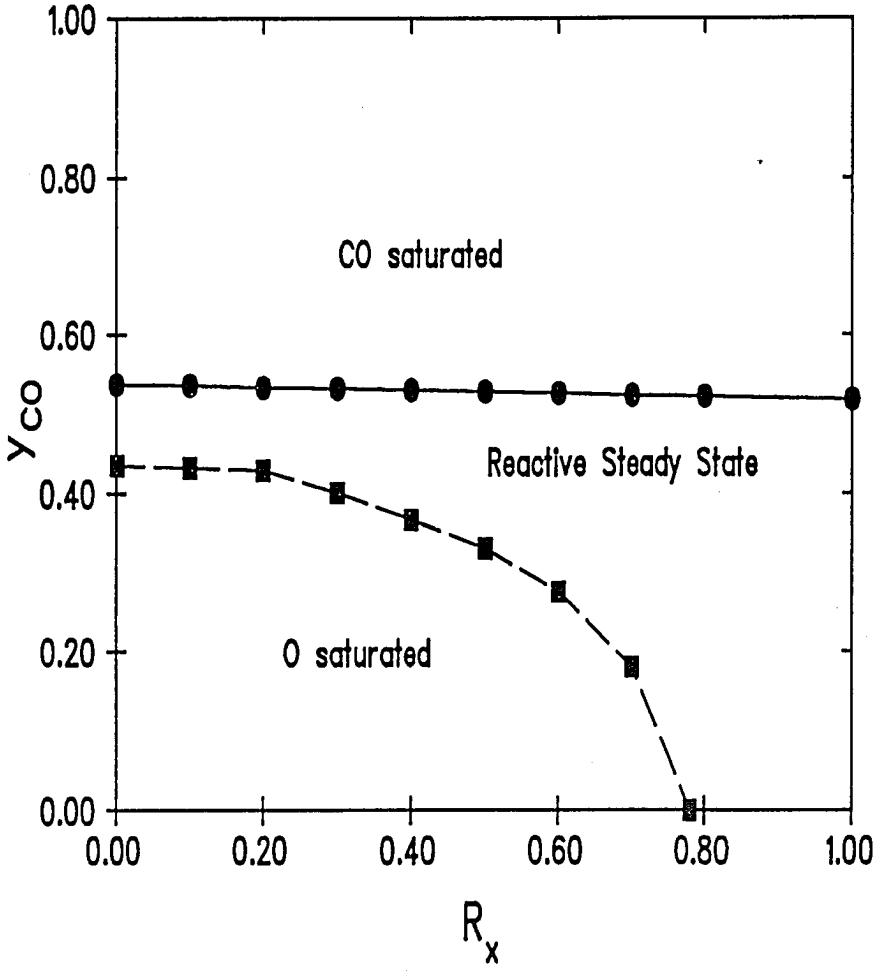


Figure 10: The phase diagram for the anisotropic model with no CO diffusion

Much of the behavior can be explained by recalling that in this model the $O_2$ can only be adsorbed in $\hat{y}$ direction. The reaction rate $R_y$ measures the rate for creating a pair of vacant sites along $\hat{y}$ direction; An $O_2$ can adsorb only on these sites. Near the second order phase transition, the surface is nearly completely covered by O and most vacant sites are isolated. In order for an isolated site to be occupied by $O_2$, a CO molecule must adsorb and react in $\hat{y}$ direction to create a pair of vacant sites for $O_2$ adsorption. If $R_y$ is large, it is quite likely that such a pair will be created, favoring $O_2$ adsorption. Therefore, the system is more easily saturated with oxygen, which is consistent with the phase diagram. As $R_x$ decreases ($R_y$ increases) the second order transition shifts towards higher values of $y_{co}$ (less $O_2$) indicating a larger CO adsorption rate is needed to prevent the surface from saturating with oxygen.

On the other hand, near the first order transition the lattice is almost half vacant, and many vertical pairs of vacant sites already exist. Increasing $R_y$ does not significantly increase the likelihood of $O_2$ adsorption through the process of creating pairs of vacant sites along $\hat{y}$ direction, hence increasing $R_y$ is not very effective in suppressing the saturation of the surface with CO and so $y_2$ only increases slightly as $R_y$ increases.

### 3.3.2 Behavior with Diffusion

Fig. 11 shows that for a given $R_x$, no significant shift of the first order transition point, $y_2$, occurs until the diffusion rate $R_d$ is comparable to the net reaction rate. For $R_d \geq 1$ $y_2$ shifts towards larger values of $y_{co}$. Diffusion not only affects $y_2$, it also changes the magnitude of the jump, which shrinks as the diffusion rate increases. This behavior was also noted in simulations

of the ZGB model with diffusion by Kaukonen and Nieminen[53] and by Ehsasi *et al.*[43].

The second order transition point $y_1$ is quite insensitive to the diffusion rate $R_d$ as shown in Fig. 11. This happens in part because each CO must be surrounded by 4 vacancies, but the vacancy fraction vanishes at the transition. In addition, diffusion of CO tends to make it more reactive by allowing it to move next to an O and react, which helps deplete the surface of CO. Hence there is no CO present to diffuse as $y_{co} \rightarrow y_1$. Further away from the second order transition, the diffusion does increase the steady state O coverage slightly, as the above argument would imply.

Near the first order phase transition, however, the CO concentration on the surface is much higher and small islands of CO appear on the surface. The diffusion of CO tends to break up these islands and prevent them from coalescing and eventually saturating the surface. A higher value of $y_{co}$ is needed to adsorb more CO to offset this dispersal process. Diffusion also makes the CO more reactive, by allowing it to move about and seek out an adsorbed oxygen to react with. This tends to reduce the steady state CO concentration on the surface for a given value of $y_{co}$. These effects must be offset by a higher $y_{co}$ in order to saturate the surface, therefore, the critical point $y_2$ shifts towards larger values.

### 3.3.3 Limiting Cases of ZGB Model

There are two limiting cases in which different rows of lattice are decoupled and the behavior on the two-dimensional lattice appears one-dimensional in character. The first case appears in the limit of $y_{co} \rightarrow 0$, in which no reaction occurs and the surface is randomly populated by $O_2$

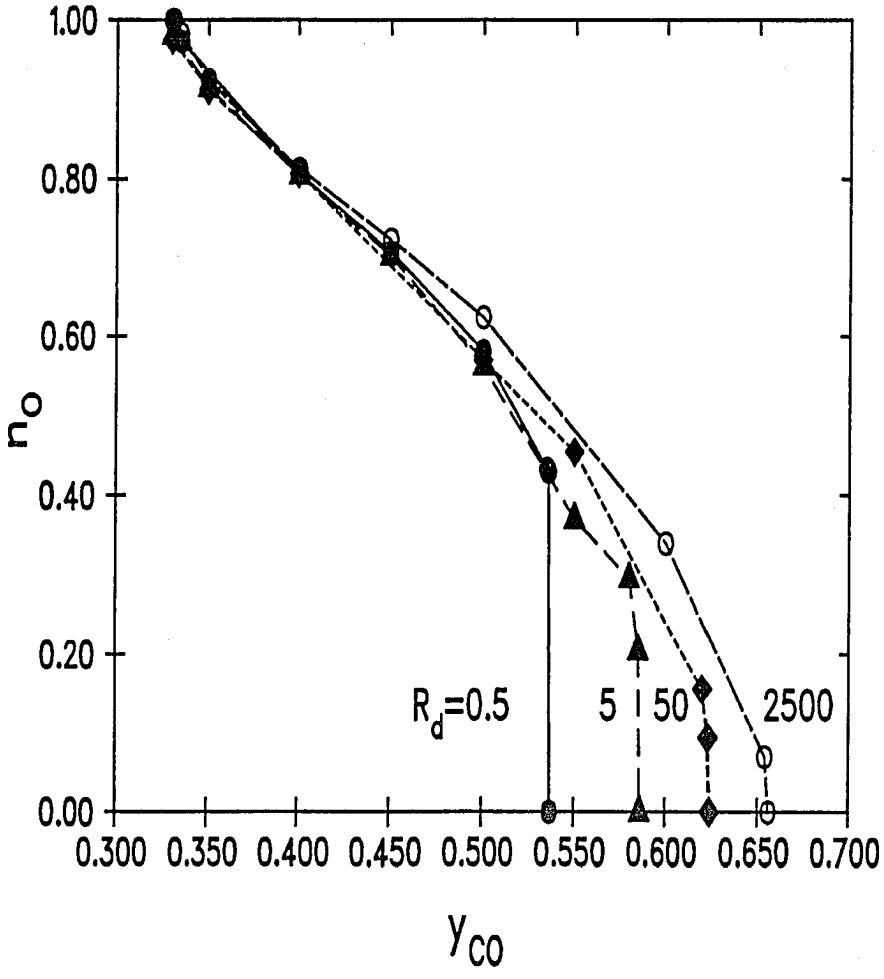


Figure 11: Oxygen coverage $n_O$ *vs.* $y_{co}$ for various diffusion rates with $R_x = 0.25$ on a 100x100 lattice.

molecules. Each row in the $\hat{y}$ direction is independent and the addition of $O_2$ molecules to a given row is equivalent to a model for random adsorption of dimers on a 1D chain. The dimer coverage for such a problem is known[58] to be $1 - e^{-2} = 0.864\,664\ldots$, and our simulation in this limit gave a result of 0.8636.

The other limiting case appears for $R_x \equiv 1$. Here there is no possibility of reaction between adjacent troughs to create the pairs of vacant sites that the oxygen molecules need to adsorb. We find that in this limit there is no reactive steady state; instead, two different absorbing states appear as $y_{co}$ changes. For $y_{co} > y_2$, where $y_2$ is the smoothly extrapolated value for $R_x \to 1$, the steady state consists of a surface saturated with CO as before. For $y_{co} < y_2$, this state is replaced with one that consists of rows of both CO and O oriented along the $\hat{x}$ direction, with all sites filled. In this steady state it is not possible for both species to coexist in the same trough, and the only stable configuration for a row is to be populated by a single species. This is akin to $A + B \to AB$ reactions in one dimension, which exhibits only $A$- or $B$-saturated states[19, 47]. As $y_{co}$ changes, the only possible change of configuration is to replace a row of one species with a row of another. In a finite system this leads to jumps in coverage as $y_{co}$ varies. The jumps disappear in the limit of an infinite system. Interestingly, we find there is no correlation in the spatial distribution of CO and O rows, even though the $O_2$ adsorption must occur in adjacent troughs. The third possibility, an O-saturated surface, is ruled out because it occurs only at $Y_{co} = 0$, which is the dimer-packing limit mentioned above.

### 3.3.4 Critical Behavior and Critical Exponents

As we noted earlier, there is considerable evidence[48, 50] that the critical behavior near the second order transition in the ZGB model belongs to the same universality class as Reggeon field theory and directed percolation. As we saw from the phase diagram in Fig. 10, the position of the second order phase transition depends upon $R_x$. For $R_x \geq 0.742$, the second order transition disappears. This behavior is akin to a shift in transition temperature in an equilibrium system with anisotropy. It is interesting therefore to ask whether the critical behavior is also affected by anisotropy.

We investigated the critical behavior of the second order phase transition by using finite size scaling to obtain the critical exponents. In the present study we examined two exponents, one for the static behavior and one for the dynamics.

For the static behavior we studied the critical exponent $\beta$ that describes the behavior of the "order parameter" $\psi$, which we chose to be the fraction of sites not occupied by O atoms: $\psi = 1 - n_O$. Because of the very low CO coverage, this order parameter really measures the vacancy fraction. This choice was taken in light of the work in Ref. 47 which showed that the CO serves primarily as an agent to keep the reaction going and is not an important component of the critical fluctuations. In the O saturated state this order parameter obviously vanishes, and near the transition point $y_1$ in an infinite system we expect a dependence of the form

$$\psi(y_{co}) \propto (y_{co} - y_1)^{\beta} . \tag{19}$$

We assume that near the second order transition that $\psi$ obeys a finite size

scaling form

$$\psi(y_{co}, L) = L^{-\beta/\nu} F(|y_{co} - y_1|L^{1/\nu}) , \tag{20}$$

where $\nu$ measures the growth of the correlation length, $\xi$, near the transition, $\xi \propto |y_{co} - y_1|^{-\nu}$, and $F(x) \propto x^{\beta}$ for large $x$ so that Eqn. (19) obtains for $L \rightarrow \infty$.

We also calculated the dynamical exponent $z$ by finite size scaling, where $z$ describes the critical slowing down of the fluctuations near the transition. If $\tau$ measures the time scale for relaxation, we expect

$$\tau \propto \xi^z \propto |y_{co} - y_1|^{-z\nu} . \tag{21}$$

For our simulations, we define a characteristic time $\tau$ for the system to become poisoned[59] as:

$$\tau = \frac{\sum_t t\ \psi(t)}{\sum_t \psi(t)} , \tag{22}$$

where the sum is over the simulation time in MCS and $\psi(t)$ is the number of sites not occupied by oxygen atoms at time $t$. Below $y_1$, we expect $\tau$ will grow exponentially with the system size, while above $y_1$ we expect $\tau$ to have the finite size scaling form

$$\tau(y_{co}, L) = L^z G(|y_{co} - y_1|L^{1/\nu}) , \tag{23}$$

where $G(x) \propto x^{-z\nu}$ for large $x$.

The simulations for the finite size scaling analysis were done using a variety of lattice sizes, from $7 \times 7$ to $100 \times 100$, starting with an empty lattice and sampling the state of the system regularly until the surface was saturated. The average of these samples gave the values of $\psi$ and $\tau$ for that run. For each $L$, we made several hundred independent runs and averaged $\psi$ and $\tau$ to find the characteristic values for the given lattice size.

From Eqn. (20), $\psi$ is proportional to $L^{-\beta/\nu}$ at the critical point $y_1$. A log-log plot of $\psi$ *vs.* $L$ at $y_1$ should give a straight line with slope $-\beta/\nu$. Similarly, a log-log plot of $\tau$ *vs.* $L$ at $y_1$ should give a straight line with slope $z$. In Fig. 12, we plot $\tau$ *vs.* $L$ in a log-log plot for $L$ = 7, 12, 16, 20, 24, 32, 64 for $R_x = 0.2$. We determined the value of $y_{co}$ from the $\log(\tau)$ *vs.* $\log(L)$ graph, since its curvature is more sensitive to value of $y_1$ than the plot $\log(\psi)$ *vs.* $\log(L)$ in the critical region, and thus gives a more accurate determination of $y_1$. We have therefore omitted a plot of $\psi$ *vs.* $L$, but we stress that the two values of $y_1$ determined from both the static and dynamic scaling analysis are consistent.

If $\psi L^{\beta/\nu}$ is plotted against $|y_{co} - y_1|L^{1/\nu}$, curves with different $L$ values should collapse to a single curve for the correct choice for $\beta$ and $\nu$. Our results are shown in Fig. 13, which shows data from $L$ = 16, 32, 64, 100 on a single curve. Table 1 lists the values for $\beta$ and $\nu$ determined in this manner for three different choices of $R_x$. The error bars for $\beta$ are determined by varying $\beta$ until the curves fail to collapse well to the eye. Similarly, if $\tau L^{-z}$ is plotted against $|y_{co} - y_1|L^{1/\nu}$, curves with different $L$ values should collapse to a single curve. We collapsed data with $L$ = 40, 64, 80, 100 onto a single curve with fixed $\nu$. Table 2 gives the values of $\nu$ obtained in this fashion. The error bars for $\nu$ are obtained in the similar fashion as for $\beta$. As we observe, the value of $\nu$ obtained by two different methods are consistent within the error bars. We should point out that the curve for $R_x = 0.70$ does not collapse as well as for smaller values of $R_x$. We suspect that the

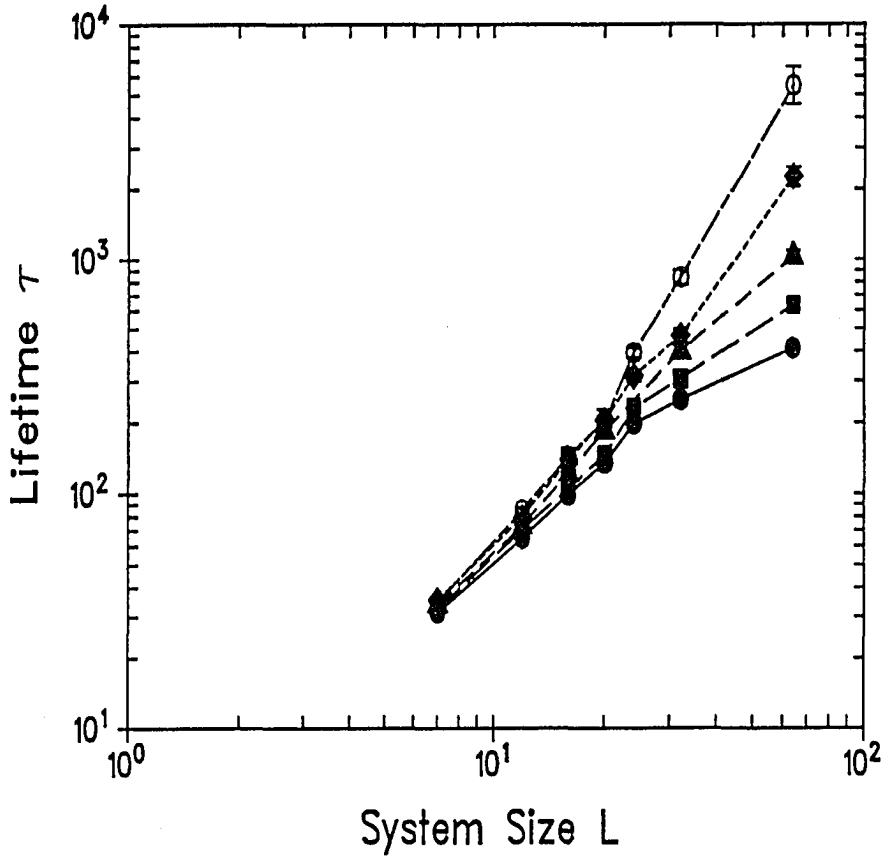


Figure 12: The mean lifetime $\tau$ as defined in Eqn. (22) *vs.* system size $L$ for various choices of $y_{co}$. The symbols for various $y_{co}$ are $y_{co} = 0.426$: solid circles, $y_{co} = 0.428$: squares, $y_{co} = 0.430$: triangles, $y_{co} = 0.432$: diamonds, and $y_{co} = 0.434$: circles. The straightest curve yields a value of $y_1 = 0.430$.

finite size scaling assumption is only approximately valid there due to the fact that $R_x$ is close to the value of 0.742 at which second order transition disappears.

Table 1: Critical exponents from static scaling for various anisotropy $R_x$.

| $R_x$ | $y_1$ | $\beta/\nu$ | $\beta$ | $\nu$ |
|---|---|---|---|---|
| 0.70 | $0.196 \pm 0.002$ | $0.75 \pm 0.02$ | $0.59 \pm 0.02$ | $0.74 \pm 0.04$ |
| 0.50 | $0.332 \pm 0.001$ | $0.77 \pm 0.01$ | $0.65 \pm 0.06$ | $0.82 \pm 0.07$ |
| 0.20 | $0.4305 \pm 0.0005$ | $0.78 \pm 0.01$ | $0.64 \pm 0.04$ | $0.83 \pm 0.05$ |

Table 2: Critical exponents from dynamical scaling for various anisotropy $R_x$.

| $R_x$ | $y_1$ | $\nu$ | $z$ |
|---|---|---|---|
| 0.70 | $0.196 \pm 0.002$ | $0.64 \pm 0.14$ | $1.70 \pm 0.06$ |
| 0.50 | $0.332 \pm 0.001$ | $0.70 \pm 0.10$ | $1.67 \pm 0.06$ |
| 0.20 | $0.4305 \pm 0.0005$ | $0.75 \pm 0.10$ | $1.64 \pm 0.03$ |

We believe that our model belongs to the directed percolation universality class[17, 48, 50], even though the critical exponent $\beta$ is consistently larger than the value of 0.58 found for directed percolation in (2+1) dimensions[18]. The reason we believe this is that if one examines the $\beta/\nu$ values for various $R_x$, they are all roughly 0.77, which is the value of $\beta/\nu$ for (2+1)D directed percolation[17]. We suspect that our value of $\beta$ is larger than that found in directed percolation, because of systematic errors in determining $\nu$ from the

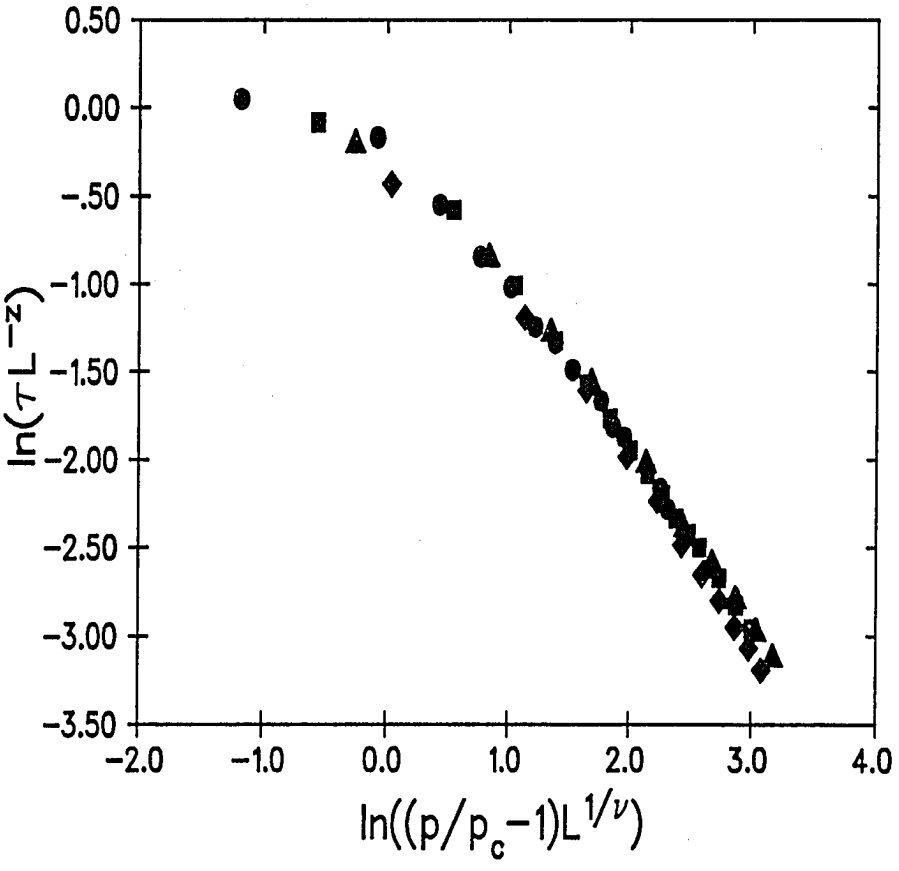


Figure 13: A scaling plot of $\log(\psi L^{\beta/\nu})$ *vs.* $\log(|y_{co}/y_1 - 1|L^{1/\nu})$ for various system sizes with $R_x = 0.2$. The fact that all the data collapse onto a single curve justifies the scaling relationship postulated in Eqn. (22). The symbols for the different system sizes are: $L = 40$: circles, $L = 64$: squares, $L = 80$: triangles and $L = 100$: diamonds.

collapsing of the data for different $L$. This collapsing process also requires a good estimate of $y_1$, while $\beta/\nu$ is less sensitive to our determination of $y_1$. We have no independent way of calculating $\nu$ other than to infer it by collapsing the data, so we cannot rule out systematic error. Therefore, we believe $\beta/\nu$ is a much better indicator than $\beta$ itself; further evidence that suggests directed percolation comes from the dynamical exponent $z$, which agrees with the directed percolation value of 1.69[17].

## 3.4 Conclusion

Here we have studied a kinetic model for CO oxidation on an anisotropic catalytic surface. This model exhibits transitions similar to that in the ZGB model. However, in this model the second order critical point varies as a function of reaction rate $R_x$ and can actually disappear if $R_x$ is large enough, while the first order transition point is almost unaffected. For $R_x \equiv 1$, the reactive steady state is replaced by a saturated surface of random rows of pure O or pure CO. Diffusion changes the phase diagram only when the diffusion rate exceeds the reaction rate. It affects primarily the first order transition by shifting the transition point to larger $y_{co}$ and reducing the jump in concentration.

From a finite size scaling analysis, we obtained the critical exponents $\beta$, $\nu$, and $\tau$ for various degrees of anisotropy. Our results indicate that spatial anisotropy, just as in case of an equilibrium system, does not affect the critical behavior of a nonequilibrium system. Furthermore, our results

suggest that this model belongs to the universality class of Reggeon field theory and directly percolation, which lends support to the hypothesis that the critical behavior in any transition to a noiseless state should be in the Reggeon field theory universality class[48, 49].

# CHAPTER 4

# ZGB MODEL WITH FINITE REACTION RATE

## 4.1 Introduction

The aim of this chapter is to investigate the effect of finite reaction rates on anisotropic ZGB model. As we have mentioned, the existence of a tricritical point has been questioned. We will present some evidences that support the existence of a tricritical point. This chapter is organized as follows: section II compares the finite reaction rate model with infinite reaction rate model; section III presents our evidence of a tricritical point; and section IV summarizes our findings.

## 4.2 Comparison of the Models

The model we will investigate is the extension of the anisotropic model studied in the previous chapter modified to include a finite reaction rate. In the model studied in the previous chapter, we have two parameters: $y_{co}$ and $R_x$. Modification of our model to incorporate finite reaction rate gives an additional parameter, the finite reaction rate $r$.

We used a 64x64 square lattice in our simulations. A typical run was carried out to 100,000 MCS. We carried out simulations for various anisotropy $R_x$ and reaction rate $r$ and mapped out the phase diagram of the system as shown Fig. 14-Fig. 15.

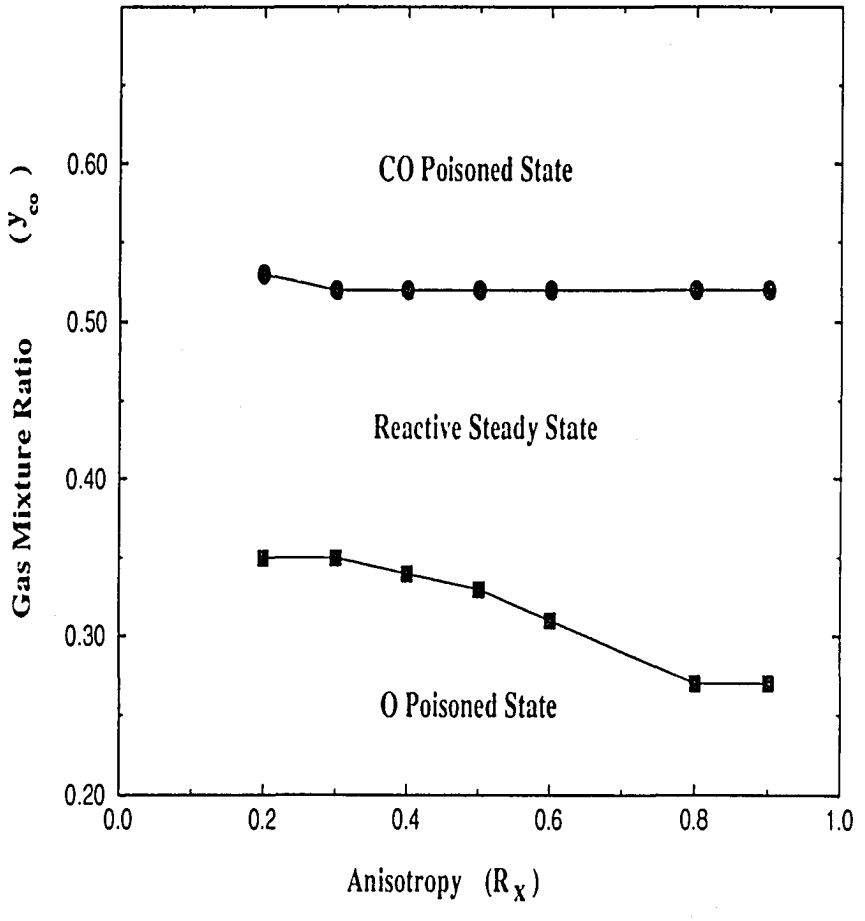


Figure 14: First order and second order transition points *vs.* anisotropy $R_x$ at $r = 0.9$. Circles represent first order transitions, and squares are second order transitions

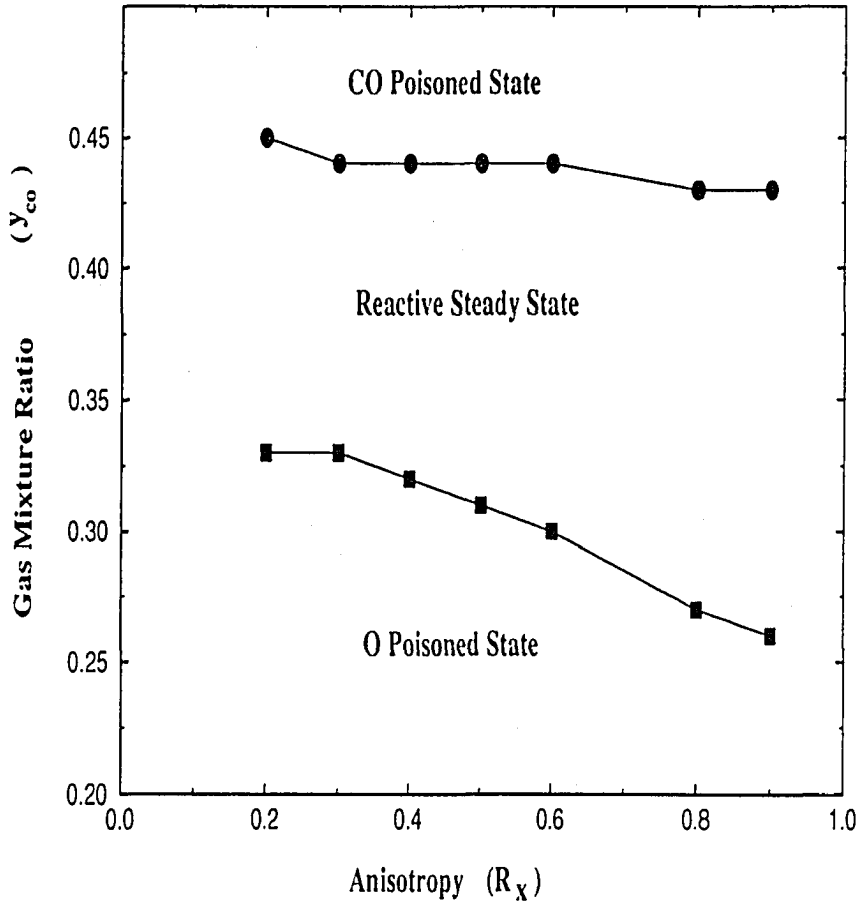


Figure 15: First order and second order transition points *vs.* anisotropy $R_x$ at $r = 0.4$. Circles represent first order transitions, and squares are second order transitions

As these phase diagrams demonstrated, the effects of anisotropy on both first and second order transitions are similar to the infinite reaction model. Anisotropy has more profound impact on the second order transitions, whereas the first order transitions are relatively unaffected by it; however, the effects of finite reaction rate are entirely different. Fig. 16 is a slice of the phase diagram along the direction of finite reaction rate. It is evident from these figures that the second order transition is relatively insensitive to the change of reaction rates, contrasting with the first order transition.

We may understand these trends if we considered the adsorption and reaction processes. Recall that the adsorption of $O_2$ requires two adjacent vertical sites; the metastable state of the second order transition only has a small number of vacant pairs that are favorable for $O_2$ adsorption. The creation of these pairs, and consequently their concentration, is solely controlled by the anisotropy parameter. Therefore over a wide range of reaction rate, the second order point is relatively constant. A slight decrease of the second order point is a reflection of the enhancement of CO adsorption at low reaction rate due to the increase of adsorption rate. Fig. 17 is a plot of CO concentration as a function of the reaction rate at second order transitions; the CO concentration is much higher at low reaction rates as shown. Consequently, more $O_2$ molecules are required to offset this adsorption enhancement, a fact accounts for the trend in second order transition points.

The enhancement of CO adsorption is further reflected in the shift of first order transitions towards lower $y_{co}$ values. This trend is indicative of higher CO concentration resulting from the adsorption enhancement. The transition to a CO-poisoned state becomes much easier due to a higher

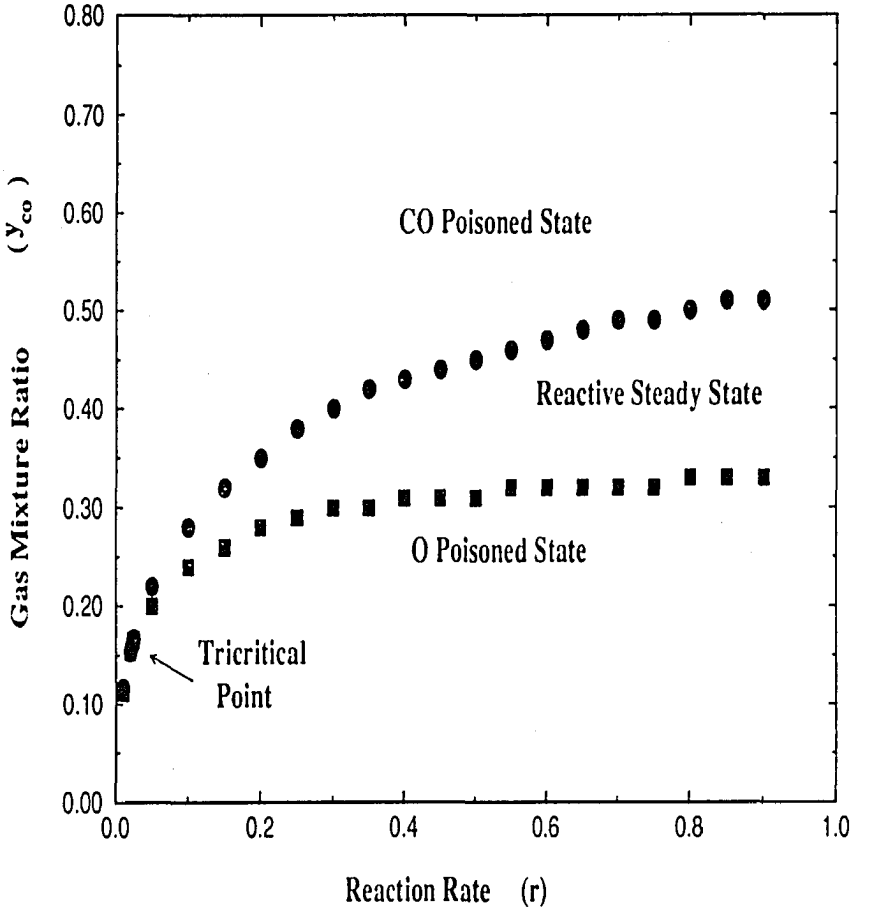


Figure 16: First order and second order transition points *vs.* reaction rate at $R_x = 0.5$. Circles represent first order transitions, and squares are second order transitions

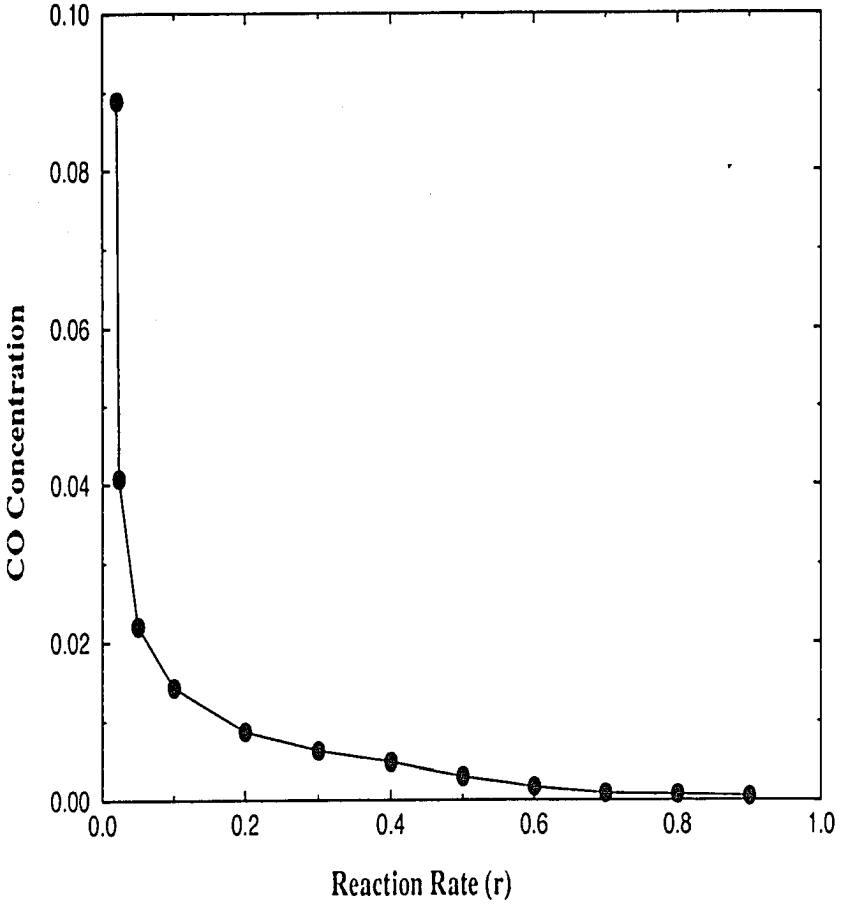


Figure 17: Steady state CO concentration as a function of reaction rate at $R_x = 0.5$

CO concentration on the lattice. As a result, lower CO concentration in relation to O in the gas mixture may still result in poisoning the system. This reduction of CO in the gas content translates into a lower $y_{co}$ value for the first order transition as indicated by the phase diagram. This trend accounts for the narrowing of the reactive steady state region and ultimately the formation of a tricritical point as shown in Fig. 18.

## 4.3 Tricritical Point

Even though the existence of the tricritical point shown by Considine[54] has been questioned by Kohler[55], further investigation is still needed due to the following reasons. While the constant coverage method has been successful in elucidating the metastable region, its utility in demonstrating a steady state region is less evident. As has been shown by Ziff[56], this method is capable of elucidating both the steady and metastable states of the conventional method. But this method does not provide any indications as to whether the apparent steady state of the constant coverage is a metastable or a stable state in the conventional method.

Ziff[56] has pointed out that there is a critical CO coverage above which the apparent steady state of the constant coverage method is unstable in the conventional sense. The support for this assertion comes from the decay of this apparent steady state evolving by the conventional method. Moreover, if this apparent steady state is below the critical value, the conventional method will destroy CO clusters, and this state will decay into a reactive steady state sustained by vacancies. However, this scenario is changed dramatically near the tricritical point. Because of high adsorption rates, CO adsorption is enhanced. This enhancement destroys vacancies in favor of

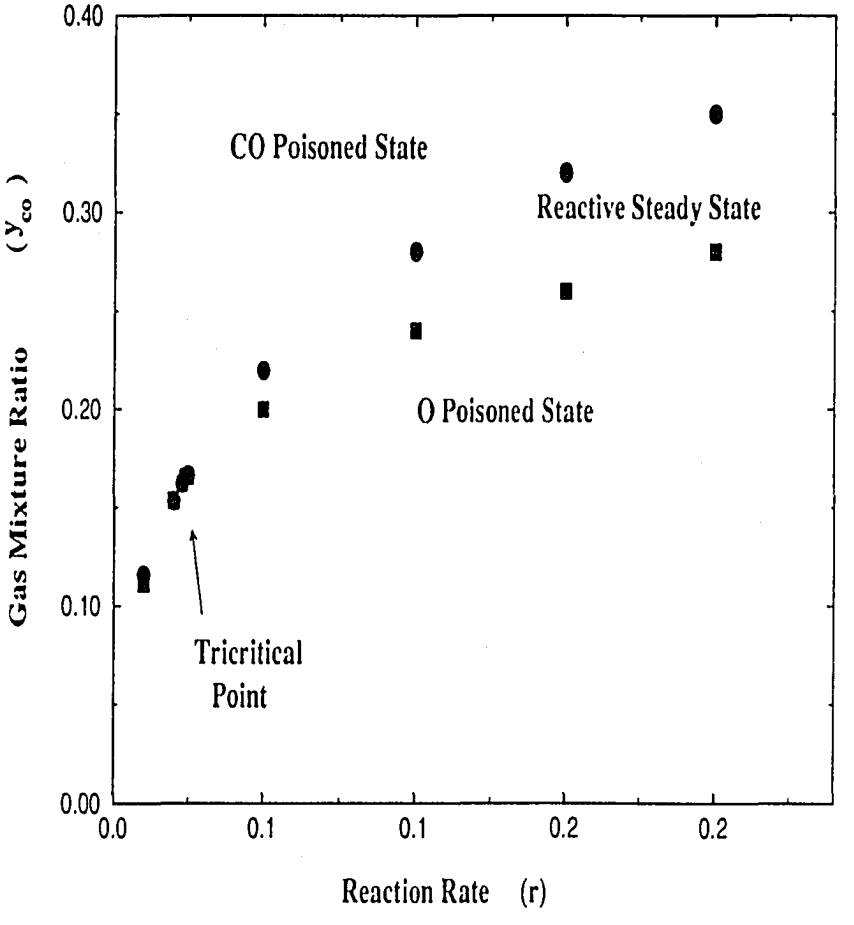


Figure 18: Magnification of the tricritical region. Circles represent first order transitions, and squares are second order transitions

CO. As a result, very few vacant sites are present, and they play the role of a spectator as shown in Fig 19. Consequently, there is no analogous reactive steady state sustained by vacant sites. The shrinkage of CO will force the system into the O-poisoned state. The constant coverage method may produce an apparent steady state that is metastable in the conventional sense in analogy with the situation above the critical CO value.

The character of the reactive steady state changes as a function of the reaction rate. Far from the tricritical point, O atoms dominate the reactive steady state with some vacant sites, and the presence of CO is entirely negligible as shown in Fig. 20. In this steady state the competition is between O and vacancy. In contrast, small clusters of CO begin to form in the steady state of the first order transition Fig. 21. In addition, the steady state has significantly more CO and fewer O atoms. The steady state of the tricritical point incorporates features of the steady states of both first and second order transitions as shown in Fig. 22. This steady state of the tricritical point has relatively fewer isolated vacant sites together with a large number of O atoms, reminiscent of the steady state of the second order transition. Islands of CO are also present in the reactive steady state in resemblance to that of the first order transition. In this reactive steady state, islands of CO and O atoms are compact objects with few vacant sites residing between CO and O interfaces, suggesting that reactions occur only on the edges of clusters. Therefore, transition to CO- or O- poisoned state is characterized by the competition between CO and O atoms while vacant sites are merely spectators. The appearance of the tricritical point is a consequence of this change in competing partners from vacant sites to CO in the transition to O-poisoned state.

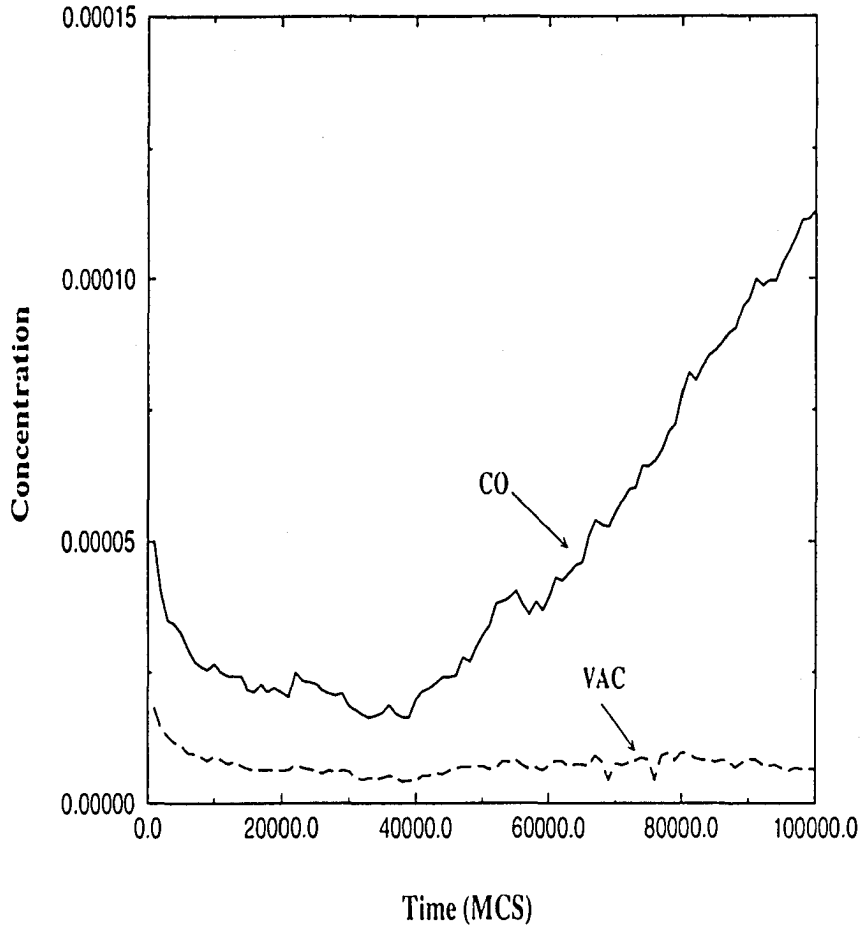


Figure 19: Concentration of CO and vacancies as a function of time

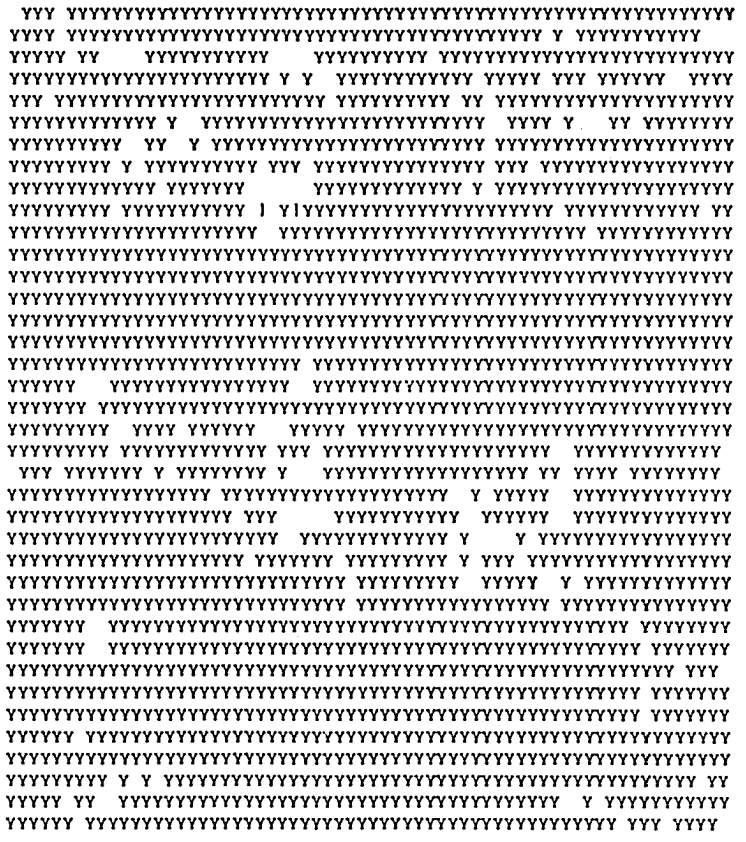

Figure 20: A typical steady state at the second order transition. CO is represented by I, and O is by Y

Figure 21: A typical steady state at the first order transition. CO is represented by I, and O is by Y

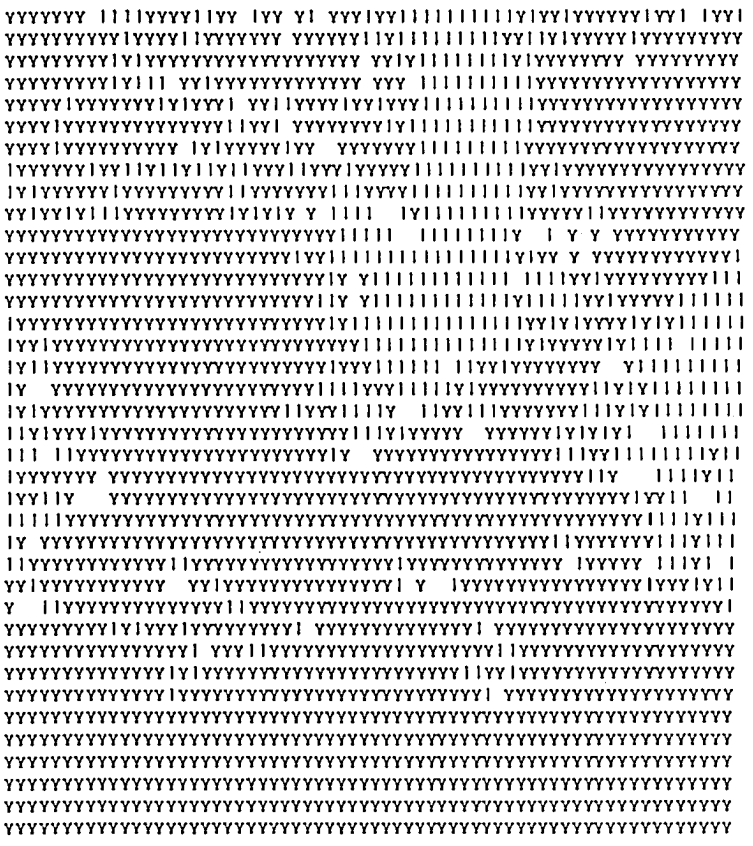

Figure 22: A typical steady state at the tricritical point. CO is represented by I, and O is by Y

Here we will present evidence which supports a tricritical point in a slightly different model. The appearance of the tricritical point, from the renormalization point of view, corresponds to an additional relevant direction. In this context, the critical behavior of the system is entirely different at the tricritical point or away from it. An indication of this difference is the critical exponents, which assume distinctive values in different regions with a crossover phenomenon marking the transition from one region to the other. Beside this change, a distinction in the decay characteristics of the unstable state in the poisoned regions and the steady state region also exists. Moreover, the nature of the O-poisoned transition above and below the tricritical point are dramatically different in the sense that the second order transition is no longer a second order transition below the tricritical point, due to the lack of a reactive steady state. Consequently, we do not expect to observe many characteristics of a second order transition such as significant growth in susceptibility.

In short if a tricritical point exists, the critical behavior, characteristic time scale and susceptibility should indicate its existence. In the following, these aspects will be examined carefully to provide evidence of its existence. Because of the lack of analytical understanding of the model, this evidence should not be construed as a conclusive answer to the question of the tricritical point. Rather, it should be viewed only as evidence which is incompatible with the expectations one may have for a narrow reactive steady state. Furthermore, it should be noted that differences exist between our model and Cardy-Sugar's. Although we do not expect significant changes in the phase structure, nevertheless, cautions should be applied in extending results from one model to the other.

### 4.3.1 Characteristic Time Scale and Susceptibility

First we studied the characteristic time $\tau$. When the system is far away from the tricritical point, we expect the characteristic time to behave differently in various regions, and the transition points mark a significant change in the characteristic time. Consequently, its derivative with respect to $y_{co}$ should reflect this change. Fig. 23 reveals three different regions, corresponding to two poisoned regions and a reactive steady state region. The two peaks in the derivative (Fig. 24) mark the transition points; clearly, they are separated by a reactive steady state region. Accompanying the increase of the reaction rate, the peak separation narrows, indicating the narrowing of the reactive steady state as shown in Fig. 25 and Fig. 26. Eventually, this peak separation is indistinguishable as shown in Fig. 27 and Fig. 28 within the resolution at $r = 0.01$, suggesting the lack of a steady state region.

In addition to the fact that various regions of the phase diagram are marked by enormous differences in the characteristic time, vacancy susceptibility also shows that transitions are of a different nature above and below the tricritical point. Above the tricritical point, the vacancy susceptibility is expected to grow in a finite size system as it approaches the second order transition point. This increase of susceptibility is indicative of large fluctuations at a critical point, and is an analogue of the divergence of susceptibility in an infinite volume system. Below the tricritical point, the reactive steady state region is absent, and the transition is of a different nature compared with the second order transition. Therefore, we do not expect large fluctuations associated with a second order transition; in turn, the vacancy susceptibility is not expected to grow significantly as the transition point is approached. Fig. 29 is the susceptibility vs. $y_{co}$ for various reaction rates.

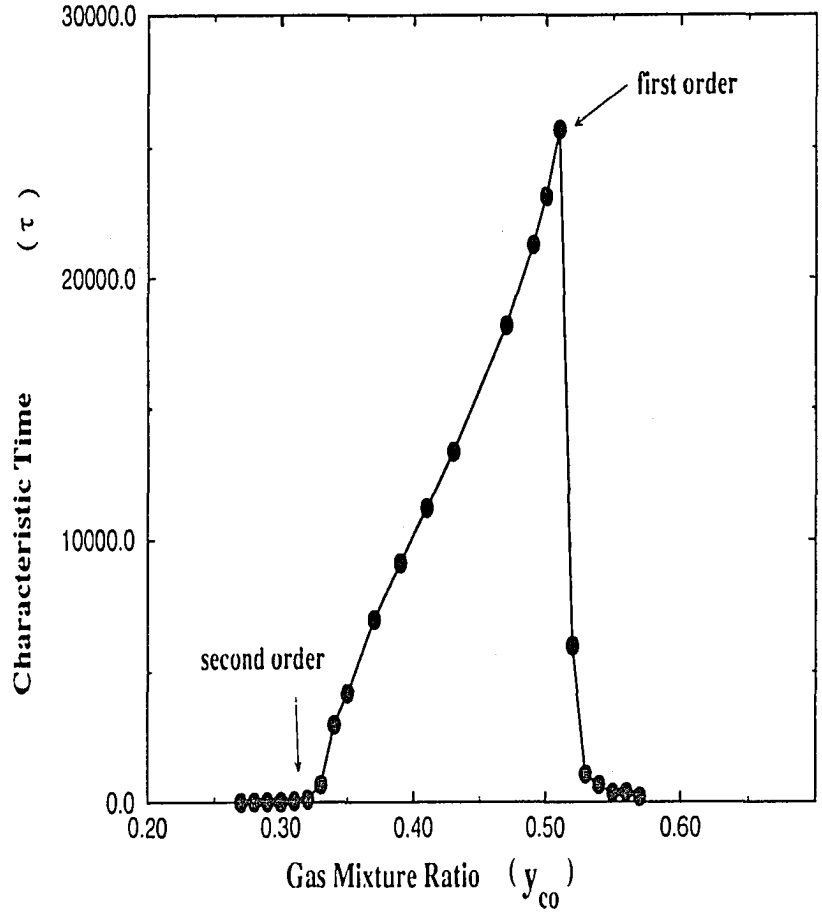


Figure 23: Characteristic time $\tau$ *vs.* $y_{co}$ at $r = 0.9$ and $R_x = 0.5$

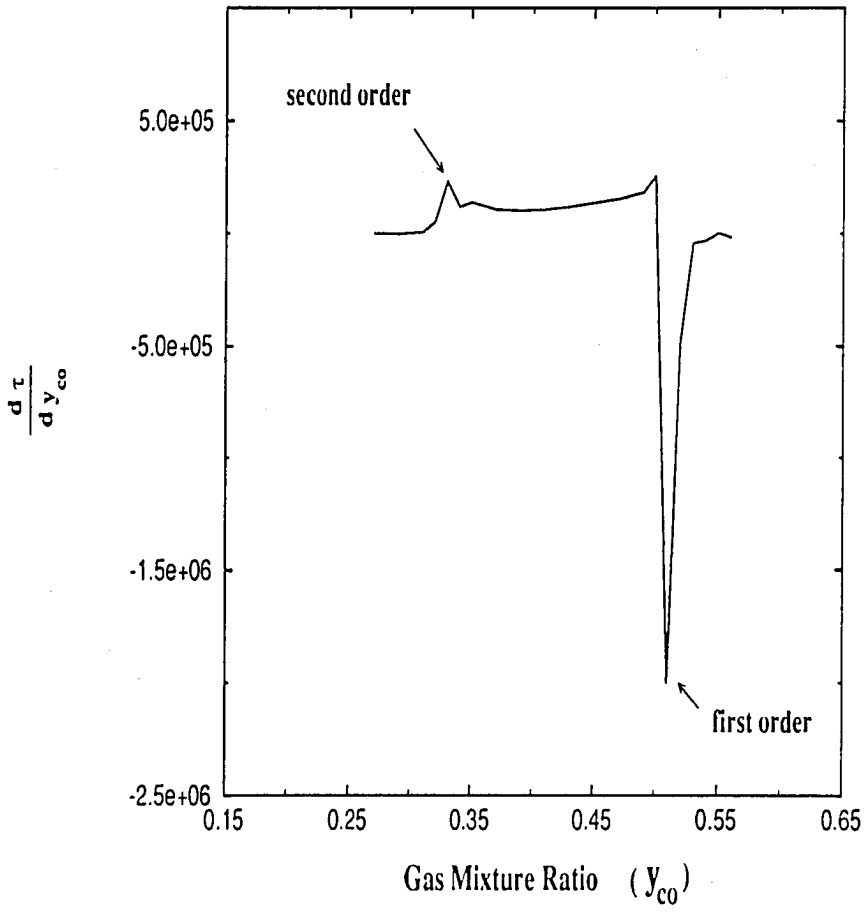


Figure 24: Derivative of characteristic time $\tau$ *vs.* $y_{co}$ at $r = 0.9$ and $R_x = 0.5$

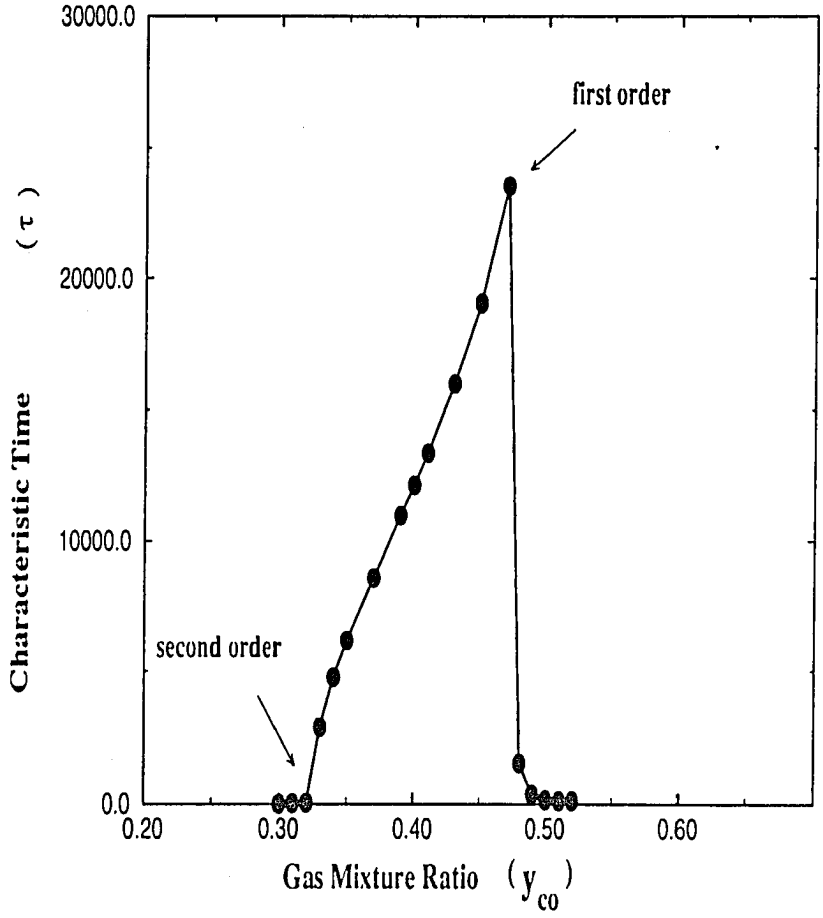


Figure 25: Characteristic time $\tau$ *vs.* $y_{co}$ at $r = 0.6$ and $R_x = 0.5$

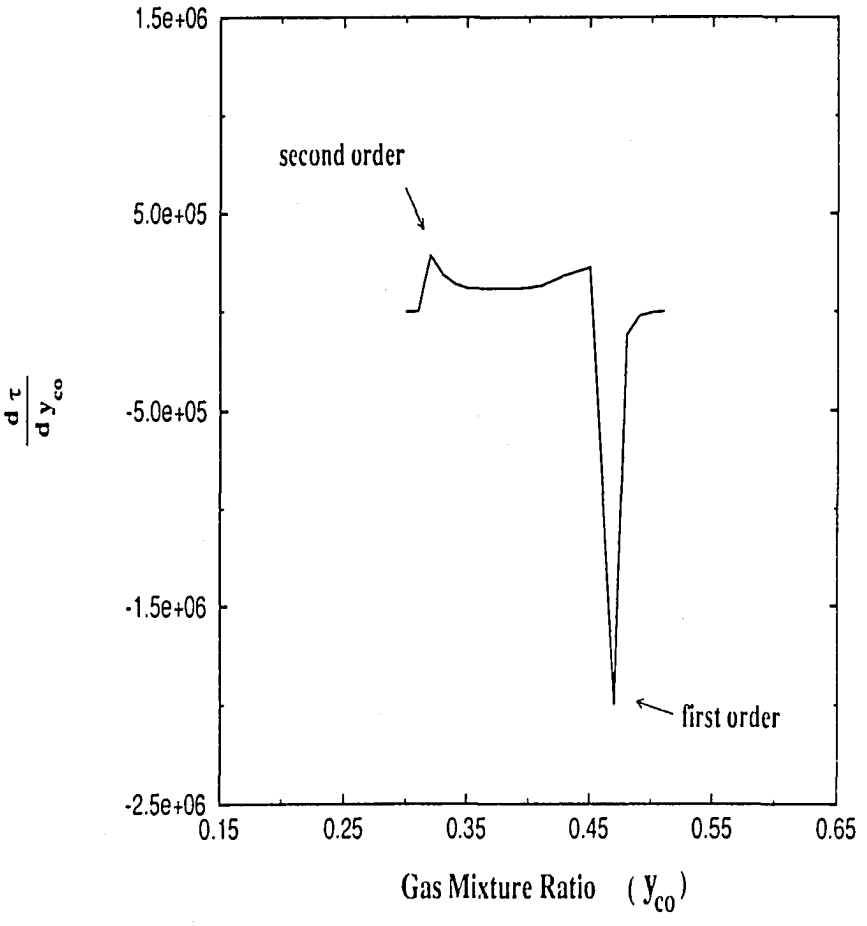


Figure 26: Derivative of characteristic time $\tau$ *vs.* $y_{co}$ at $r = 0.6$ and $R_x = 0.5$

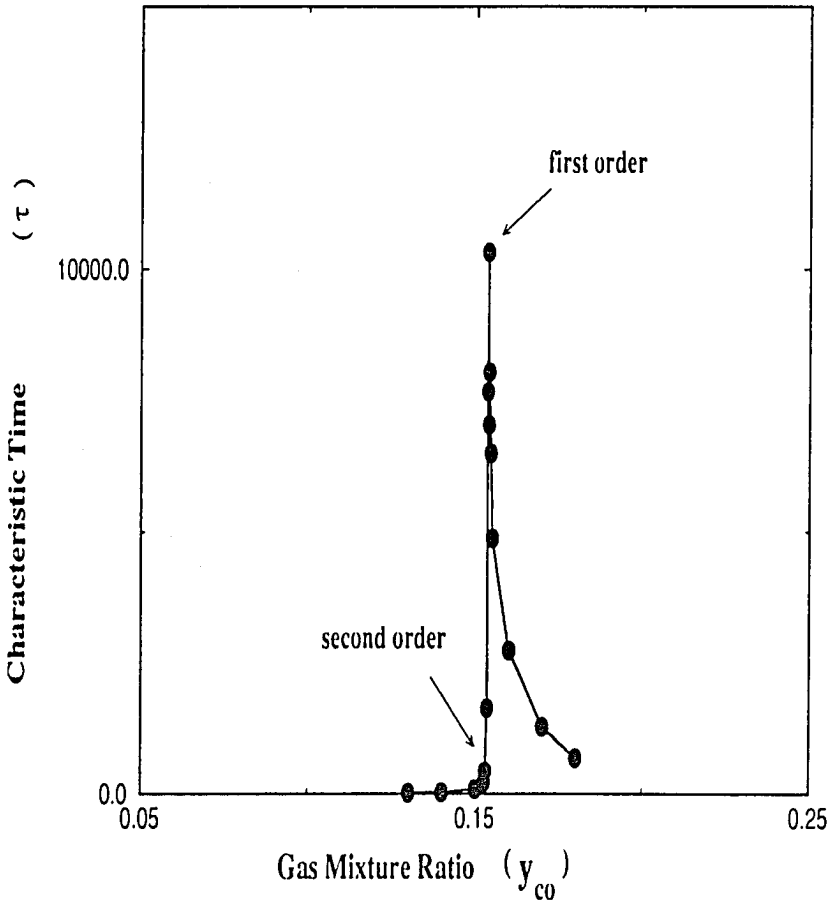


Figure 27: Characteristic time $\tau$ *vs.* $y_{co}$ at $r = 0.01$ and $R_x = 0.5$

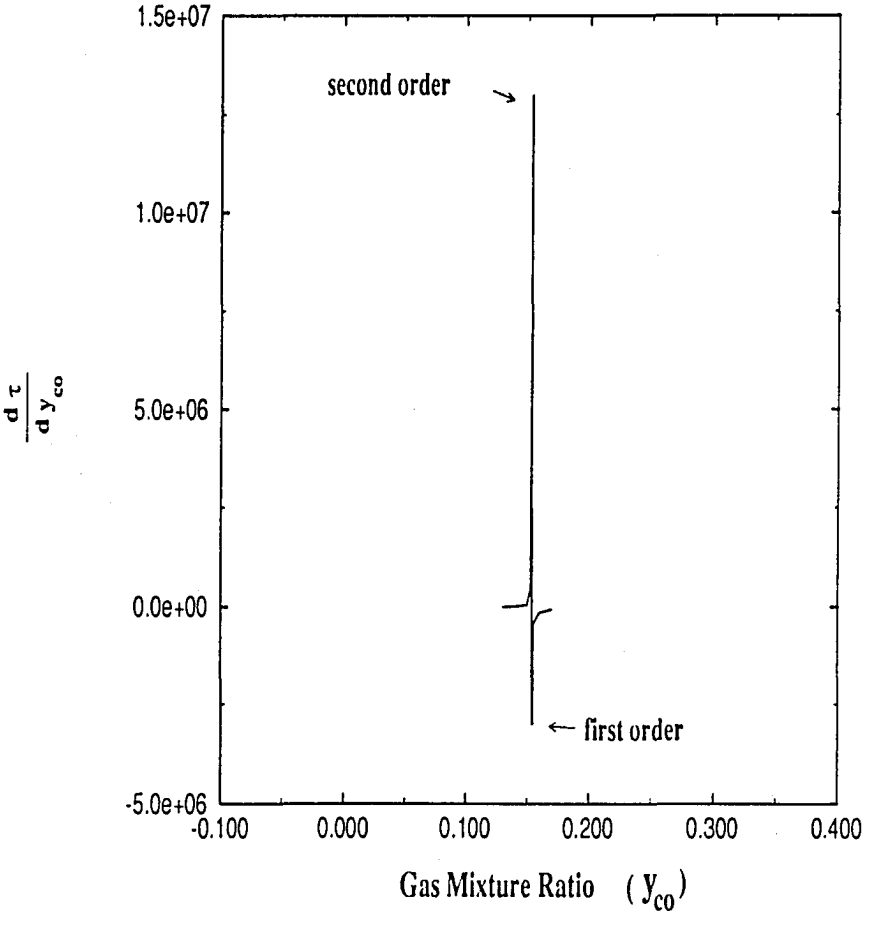


Figure 28: Derivative of characteristic time $\tau$ *vs.* $y_{co}$ at $r = 0.01$ and $R_x = 0.5$

It is evident from this figure that the growth of susceptibility is significantly curtailed beyond the tricritical point, indicative of a first order transition and the lack of a narrow reactive steady state region. More evidence of the tricritical point comes from the critical behavior and critical exponents.

### 4.3.2 Critical Behavior and Critical Exponents

Before we proceed further, we will consider an *epidemic model* approach in the study of dynamical systems[49, 60]. A conceptual understanding of this method is simple. Imagine a group of people; some of these people are healthy, and others are infected with a curable disease. The spreading of this non-lethal disease to a healthy person and the subsequent cure from this disease is a dynamic process. The absorbing state of this dynamical process corresponds to a disease free society. The number of people with the disease at any given time depends upon the rate at which the disease spreads through the population. The dynamic information about this phase transition from an infected world to a disease-free world can be learned by monitoring the number of infected people. We can exact a complete analogy between this scenario and our model. In the same way as the spreading of an epidemic, we consider the spread of vacant sites and CO molecules in time. In this epidemic model approach, we embedded vacant sites in a sea of O molecules. We monitored the growth of these vacant sites and CO molecules by computing its statistical average over a large ensemble, which includes configurations that have been poisoned prior to the computation of the average.

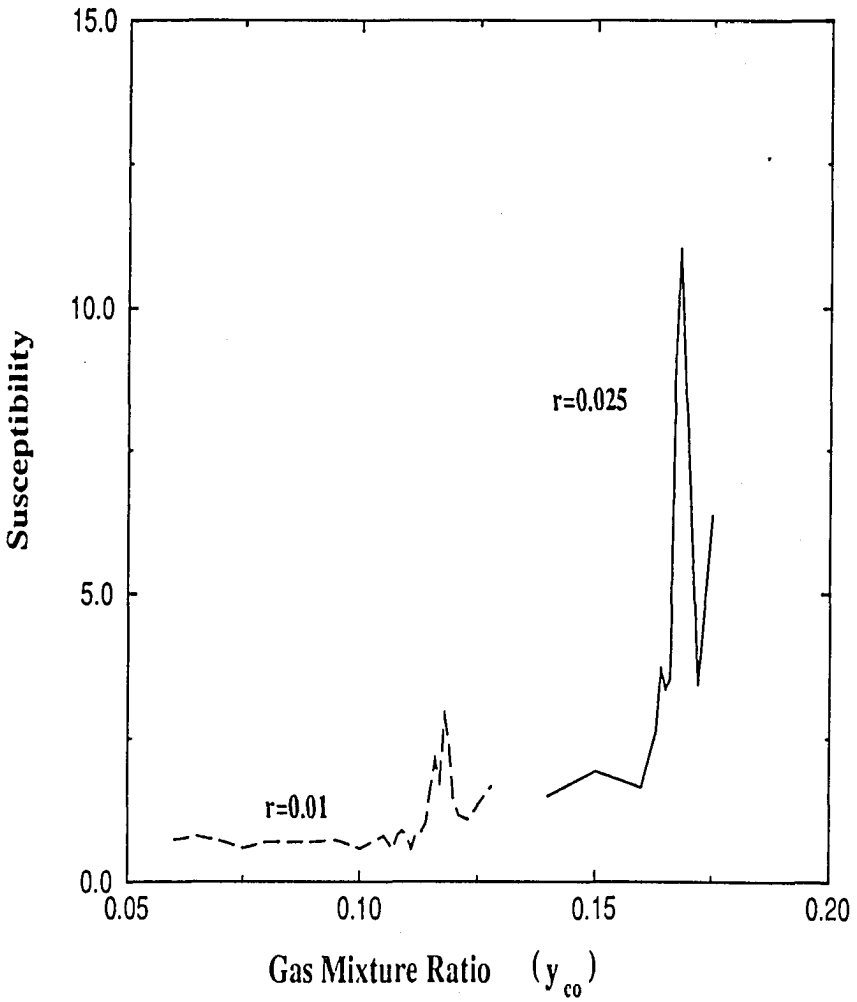


Figure 29: Vacancy susceptibility as a function of $y_{co}$ at $R_x = 0.5$. The symbol for the reaction rate are: $r = 0.025$, solid line and $r = 0.01$, dash line

If we start from a configuration of two vacant sites in a sea of O atoms initially, CO plays no essential role at a high reaction rate as seen from Fig. 30. The CO eventually decays to some constant background while the number of vacant sites increases in time. The essential dynamics is controlled by vacant sites. This result is consistent with the findings of chapter 1. As the adsorption rate increases, both CO and O increase over time as seen in Fig. 31. This increase of CO over time is a result of enhanced CO adsorption. Consequently, CO no longer plays the role of a spectator. Further increase of the adsorption rate results in a dramatic decrease of vacant sites over time as shown in Fig. 32. Because of this decrease, vacant sites become spectators, reminiscent of the role played by CO at high reaction rates, and CO dominates the dynamical behavior as shown in Fig. 32. This reversal of fortune further indicates the competition in the tricritcal region is between CO and O.

To characterize the dynamic behavior of the transition, we monitor the number of CO atoms and vacancies, $N_{co+vac}$, on the surface. We can define a growth rate exponent $\eta$ as

$$N_{co+vac}(t) \propto t^{-\eta} . \tag{24}$$

Additional dynamical information can be obtained by computing survival probability at a given time. We define the survival probability at a given time as the fraction of total independent runs which survived till this time. Similarly, we can define an exponent $\delta$ for the survival probability $P(t)$

$$P(t) \propto t^{-\delta} . \tag{25}$$

We expect both $P(t)$ and $N_{co+vac}(t)$ to be a homogeneous function,

$$f(\mu_1 L, tL^{a_1}) = L^{a_c} f(\mu_1, t) , \tag{26}$$

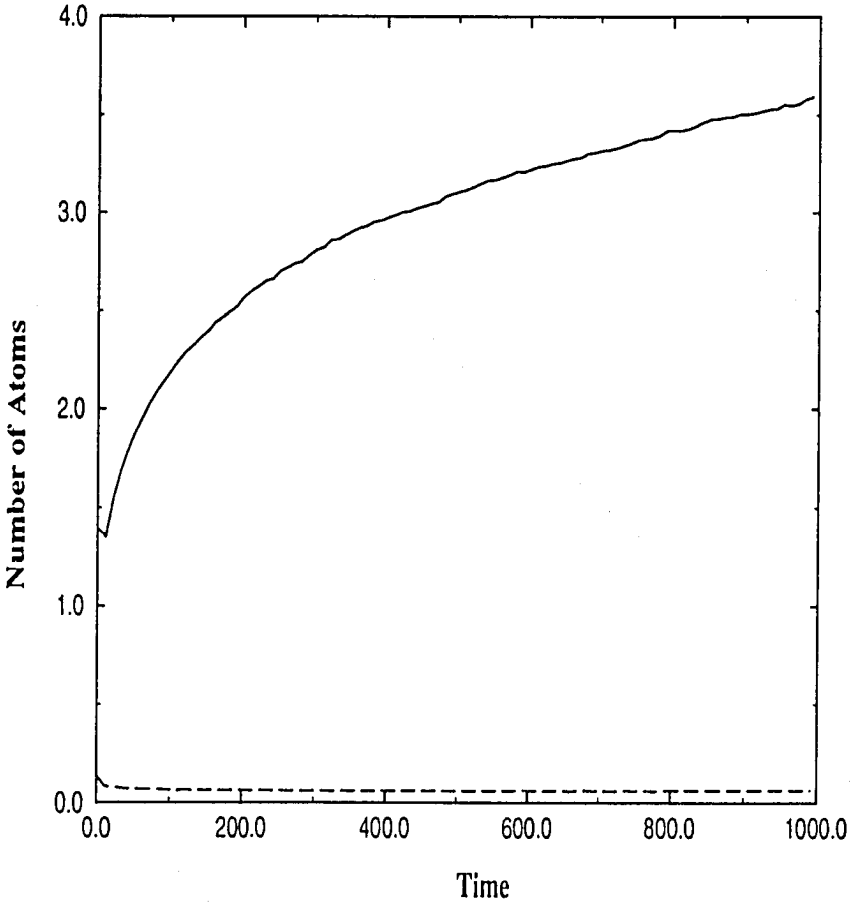


Figure 30: CO and vacant sites on the surface as a function of time at $r = 0.9$ and $R_x = 0.5$. The solid represents vacancy. The dash line represents CO.

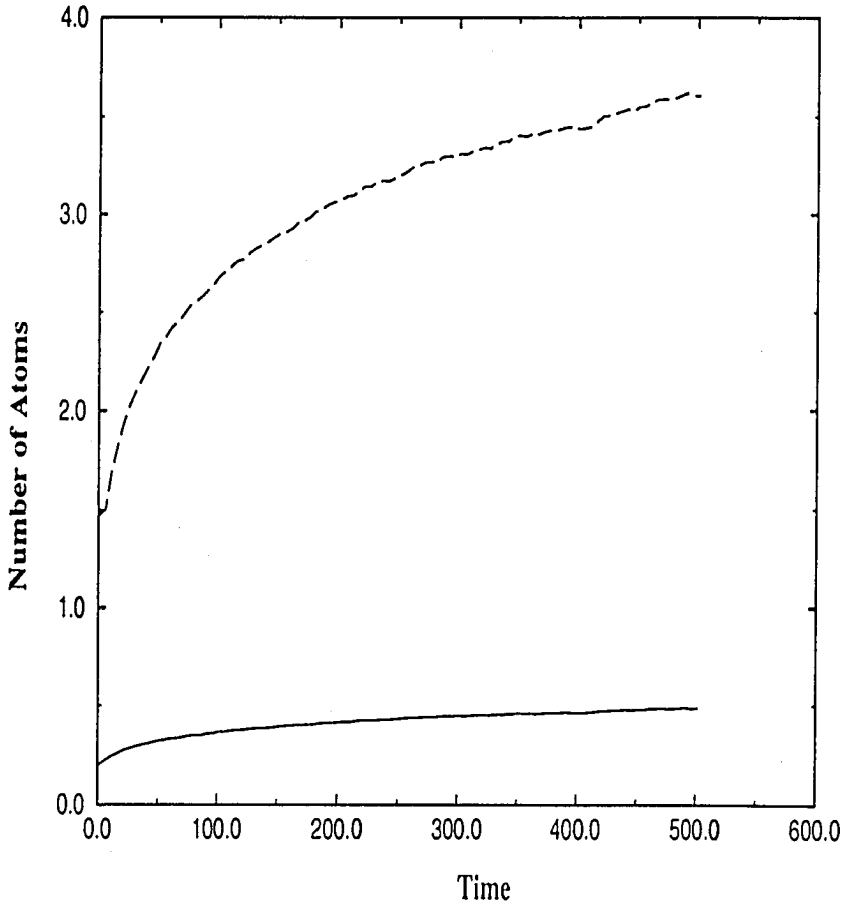


Figure 31: CO and vacant sites on the surface as a function of time at $r = 0.4$ and $R_x = 0.5$. The solid represents vacancy. The dash line represents CO.

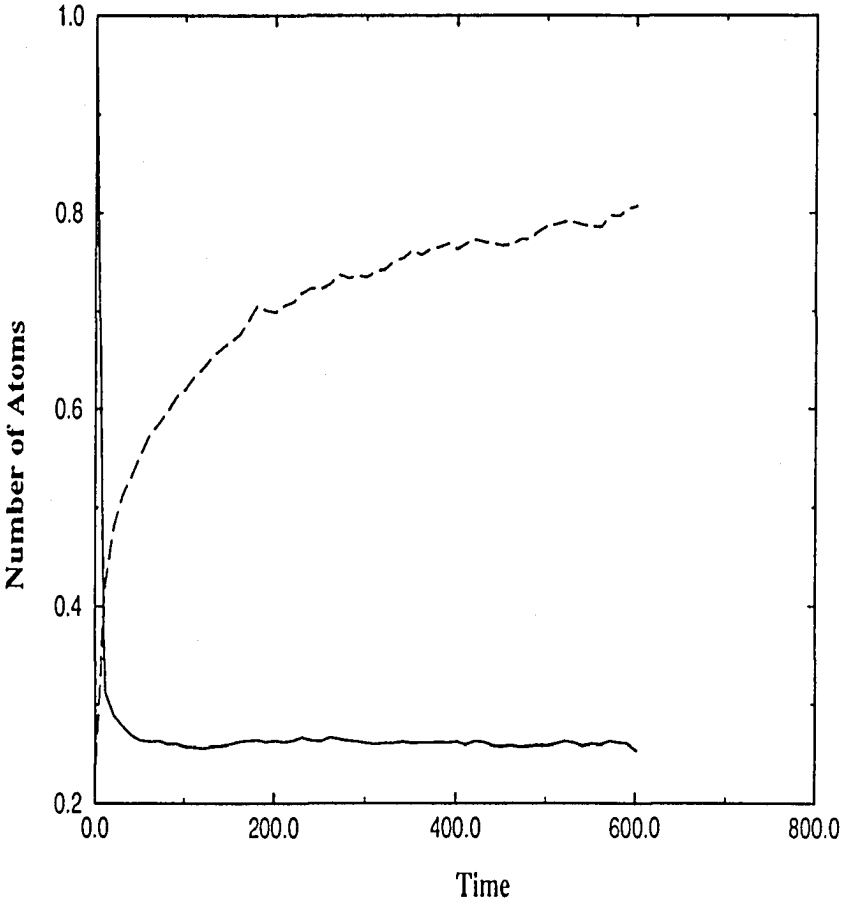


Figure 32: CO and vacant sites on the surface as a function of time at $r = 0.02$ and $R_x = 0.5$. The solid represents vacancy. The dash line represents CO.

where $\mu_1 = y_{co} - y_{co_c}$. We can obtain the scaling behavior of this function by setting $t = L^{-1/a_1}$, and we have

$$f(\mu_1, t) = t^{a_c/a_1} f(\mu_1 t^{-1/a_1}) . \tag{27}$$

At critical point, we expect this function to obey a power law relation:

$$f(t) = t^{a_c/a_1} . \tag{28}$$

At a tricritical point, we expect to have an additional variable in the homogenous function, indicating the existence of a second relevant direction from a renormalization point of view[61, 62, 63]

$$f(\mu_1 L, \mu_2 L^{\theta}, t L^{a_1}) = L^{a_t} f(\mu_1, \mu_2, t) , \tag{29}$$

where $\mu_2 = r - r_t$ and $\theta$ is the cross over exponent. In analogy with critical point scaling, we expect a power law dependence at a tricritical point

$$f(t) = t^{a_t/a_1} , \tag{30}$$

but having a different exponent from that of a second order transition.

Fig. 33 is a log-log plot of the number of vacant sites plus CO ($N_{co+vac}$) *vs.* time. The straight line shows the critical point, and the slope is the exponent $\eta$. To locate the critical point more accurately, we compute the local slope, which is defined as

$$\eta(t) = \frac{\log[N_{co+vac}(t)/N_{co+vac}(t/8)]}{\log 8} . \tag{31}$$

According to Grassburger, the local slope obeys the following relationship:

$$\eta(t) = \eta + \frac{a}{t} + \frac{\eta' b}{t^{\eta'}} + \ldots . \tag{32}$$

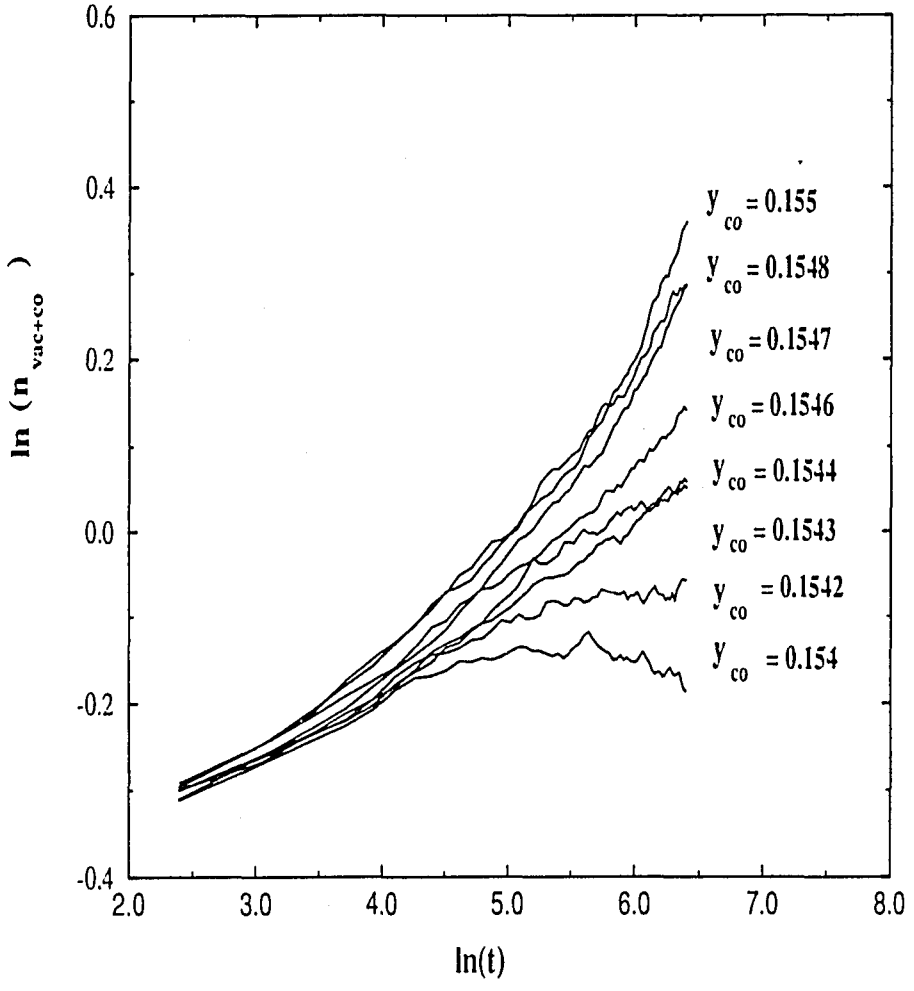


Figure 33: $\log(n_{vac+co})$ *vs.* $\log(L)$ at $r = 0.02$ and $R_x = 0.5$

Fig. 34 shows the local slope vs. the reciprocal time. A linear relation indicates the critical point, and the intersection is the critical exponent. The exponent $\delta$ can be obtained similarly. The results for $\eta$ and $\delta$ are summarized in Table. 3. The static exponents, $\mu$ and $\beta$, and dynamical exponent, $\tau$, are obtained via the method of finite size scaling as we have done in the previous chapter.

Table 3: Dynamical and static critical exponents at $R_x = 0.5$

| $r$ | 0.9 | 0.40 | 0.025 | 0.02 |
|---|---|---|---|---|
| $y_1$ | $0.3307 \pm 0.0005$ | $0.3080 \pm 0.0002$ | $0.1666 \pm 0.0002$ | $0.1544 \pm 0.0002$ |
| $\beta/\nu$ | $0.78 \pm 0.03$ | $0.768 \pm 0.003$ | $0.65 \pm 0.05$ | $0.61 \pm 0.05$ |
| $\beta$ | $0.62 \pm 0.05$ | $0.65 \pm 0.05$ | *none* | *none* |
| $\nu$ | $0.80 \pm 0.05$ | $0.85 \pm 0.05$ | *none* | *none* |
| $\tau$ | $1.75 \pm 0.10$ | $1.75 \pm 0.10$ | $1.70 \pm 0.10$ | $1.45 \pm 0.10$ |
| $\eta$ | $0.22 \pm 0.01$ | $0.22 \pm 0.02$ | $0.17 \pm 0.02$ | $0.14 \pm 0.03$ |
| $\delta$ | $0.45 \pm 0.02$ | $0.44 \pm 0.01$ | $0.65 \pm 0.01$ | $0.65 \pm 0.01$ |

In this finite size scaling, we have used a lattice of 8x8, 16x16, 32x32, 64x64. In Fig. 35, we plotted log of the order parameter *vs.* log of the system size at critical points, located by the straightest line in $\log(\tau)$ *vs.* $\log(L)$ plot as shown in Fig. 36. The slope of Fig. 35 determines the critical exponent $\beta/\mu$. Similarly, the slope of Fig. 36 gives the dynamical exponent $\tau$. To extract the information about the critical exponent of the order parameter $\beta$ and static correlation length $\nu$, we collapsed data from a variety of lattice size on a log-log plot of $\psi L^{-\beta/\nu}$ vs. $\mid p - p_c \mid L^{1/\nu}$. It is shown in Fig. 37. We have summarized these results in Table 3.

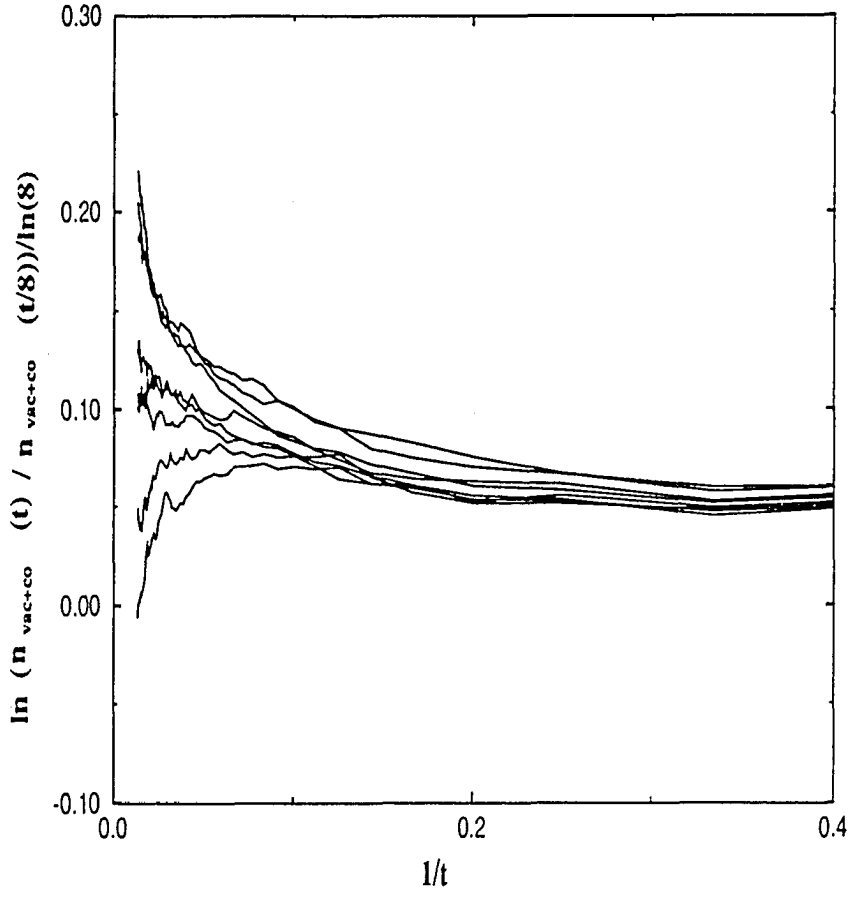


Figure 34: Local slope of the growth rate *vs.* the reciprocal time at $r = 0.02$ and $R_x = 0.5$

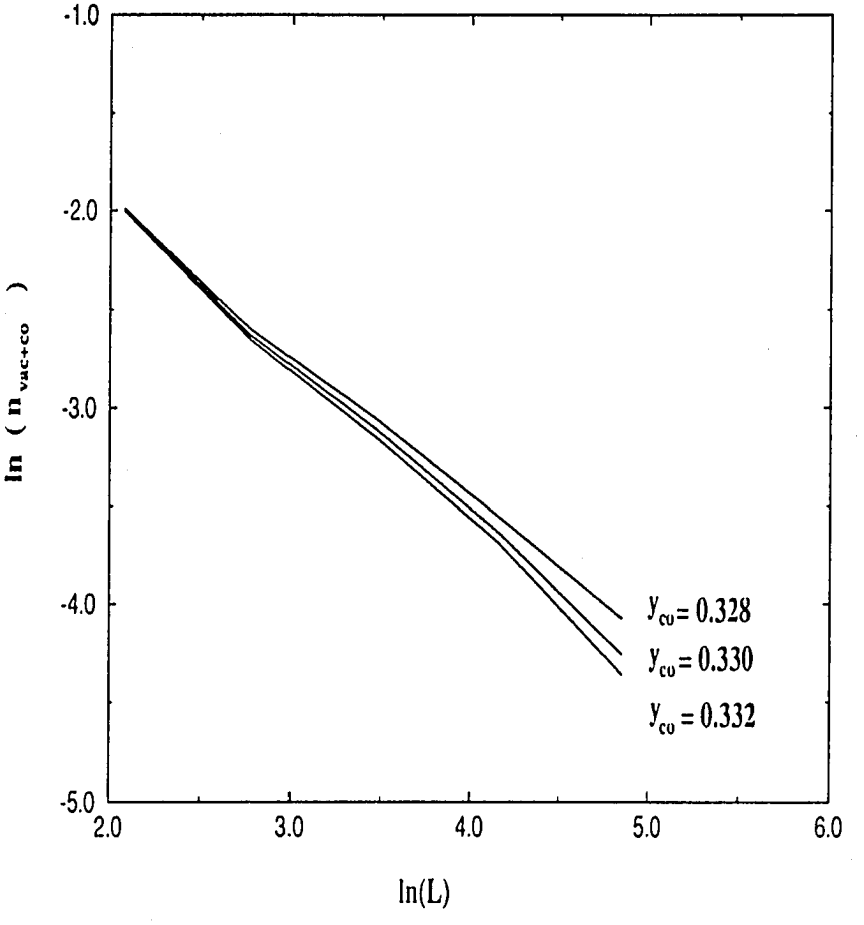


Figure 35: $\log(n_{vac+co})$ *vs.* $\log(L)$ at $r = 0.9$ and $R_x = 0.5$

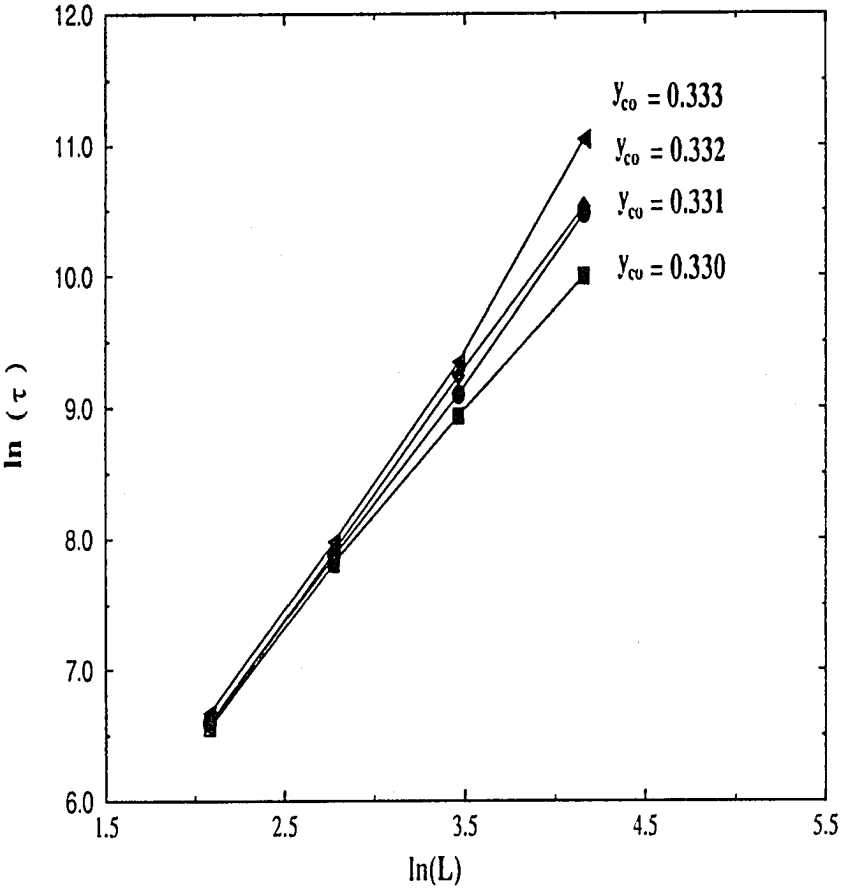


Figure 36: $\log(\tau)$ *vs.* $\log(L)$ at $r = 0.9$ and $R_x = 0.5$

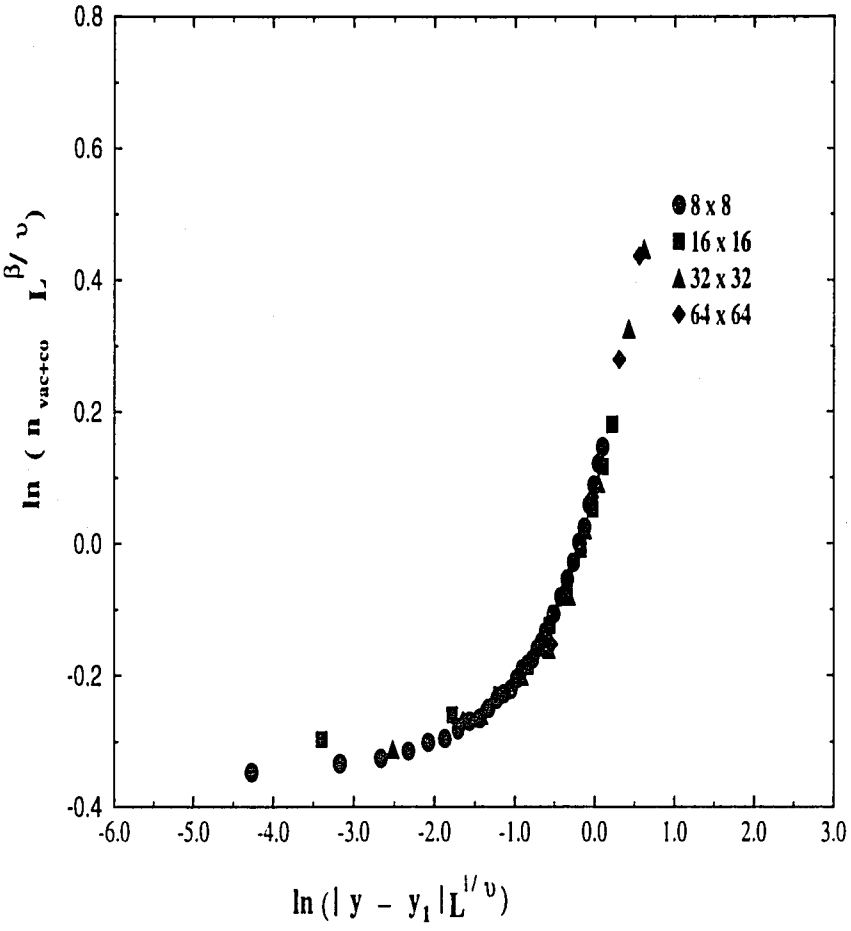


Figure 37: A scaling plot of $\log(n_{co+vac}L^{\beta/\nu})$ *vs.* $\log(|y_{CO}/y_1 - 1|L^{1/\nu})$ for various system sizes with $r = 0.9$ and $R_x = 0.5$

As we may have observed in Table 3, the reaction rate $r$ has virtually no effects on both static and dynamical behaviors. The critical exponents ($\beta$, $\nu$, $\beta/\nu$, and $\tau$), which are indicative of the critical behavior of both static and dynamical in nature, remain unaffected by the variation of the reaction rate except near the tricritical point. It is this insensitivity of these critical exponents as a function of the reaction rate which suggests the robustness of the universality class of RFT and directed percolation.

In spite of the robustness of the RFT and directed percolation, a different critical behavior is seen near the tricritical point, as suggested by the phase diagram. As have discussed earlier, we expect to observe two different critical behaviors plus crossover phenomena. Our results seem to be compatible with these expectations except a clear indication of the crossover phenomena. We have observed a marked charge in character of the steady state near the presumed tricritical point. Furthermore, we have observed a slight variation of the critical exponents near the tricritical point. Admittingly, this small variation may well be a consequence of statistical error. Nevertheless, we cannot exclude this from the possibility of being a crossover phenomenon; in a crossover region, the behavior of the system will be marked by two different exponents; to discern these two exponents amidst statistical noises is highly non-trivial. What we expect to observe under the circumstance is an averaged exponent ranging between the tricritical exponent, and RFT and directed percolation exponent; this expectation is compatible with our results. Moreover, all exponents deviate significantly from that of RFT and directed percolation; there are two possibilities to account for this fact. One is that we have two different second order transitions. In the language of renormalization, each one corresponds to a different fixed point; as the

reaction rate changes, one fixed point loses its dominance to the other, causing crossover phenomenon and the eventual change of critical exponents. However, this scenario is unlikely, because of the susceptibility of vacant sites ceases to develop after certain reaction rates, indicating a lack of reactive steady states. Further evidence comes from parameters that are crucial in settling the question of the tricritical point. In the following, we will formulate a theory of tricritical point. The parameters that indicate the tricritical point emerge naturally from this theory.

### 4.3.3 A Theory of the Tricritical Point

Before we turn our attention to formulate the theory, we will digress slightly to discuss tricritical phenomena in the Blume-Emery-Griffth model and the Landau-Ginzburg model. This discussion will provide us with insight into various aspects that are necessary in developing a theory which may encompass a tricritical point.

The Blume-Emery-Griffth model is a classic example of a thermodynamic system, which exhibits a tricritical point. This is a system of $He^3 - He^4$; Fig. 38 depicts a phase diagram of this system. When the temperature is above the tricritical point of the system, the transition is second order. It is just the ordinary $\lambda$ transition from a fluid state to a superfluid state. If $He^3$ is added to the system, the transition temperature is lowered. When the concentration of $He^3$ reaches 0.67, the transition from $He^4$-richer superfluid state to $He^3$-richer normal state is discontinuous. The dividing point of first and second order transitions is the tricritical point of the system; many other systems, such as $NH_4Cl$ and $FeCl_2$, also have tricritical points[64].

In addition to the temperature, which indicates the $\lambda$ point of normal superfluidity transition, an additional parameter(known as non-order parameter) has to be introduced into this system to locate the tricritical point; here it is the $He^3$ concentration. This feature of a two-parameter system is generic to all systems that have a tricritical point. In our model, we have two parameter: $y_{co}$ and r. From the perspective of the renormalization group, this two-parameter requirement shows the existence of two relevant directions; in order to construct a theory which encompasses a tricritical point, it must meet this requirement. The most general theory which encompasses static critical phenomena of every kind was formulated by Landau-Ginzburg.

In the Landau-Ginzburg model, the thermodynamic free energy is expressed in terms of a power series of an order parameter near critical points. This theory assumes the free energy has inversion symmetry in the order parameter, therefore, no odd terms in the series expansion may occur.

$$G(m,T) = a(T) + \frac{1}{2}b(T)m^2 + \frac{1}{4}c(T)m^4 + \frac{1}{6}d(T)m^6 + \dots , \qquad (33)$$

where the coefficients are functions of the temperature. To avoid extensive discussion of Landau-Ginzburg model, we will only briefly show the important aspects of the model in producing phase transitions.

The creation of phase transitions in the Landau-Ginzburg model is base on the behavior of various coefficients as a function of T. For example, to produce a second order transition from the theory, it is assumed that coefficients c and d are always positive; the coefficient b changes its sign at the critical point. Moreover, to produce a first order transition, c has to change its sign at the transition point while d must always be positive and b has to be a decreasing function of T. To incorporate tricritical points into

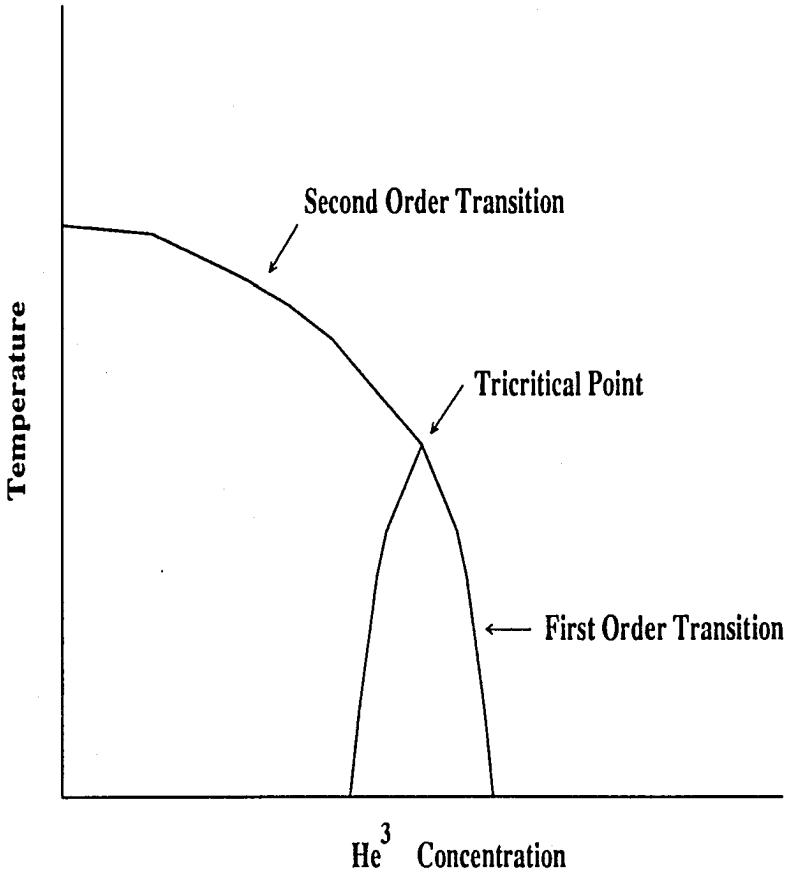


Figure 38: $He^3 - He^4$ phase diagram

the theory, these coefficients are also functions of the non-order parameter. The thermodynamical function becomes

$$G(m,\delta,T) = a(T,\delta) + \frac{1}{2}b(T,\delta)m^2 + \frac{1}{4}c(T,\delta)m^4 + \frac{1}{6}d(T,\delta)m^6 + \ldots . \quad (34)$$

From the above discussion, it is clear that $b(T,\delta) = 0$ gives a line of continuous transitions, whereas $c(T,\delta) = 0$ defines a line of discontinuous transitions. A tricritical point, which is the point of convergence of the continuous and discontinuous transitions, is defined by $b(T,\delta) = c(T,\delta) = 0$. From this example, it is evident that two major features are critical in producing tricritical behavior. First, an additional non-order parameter is necessary besides the temperature. Furthermore, different types of phase transitions are related to the behavior of various coefficients.

As we have mentioned earlier, a theory of tricritical points must contain two parameters; moreover, the example of Landau-Ginzburg model elucidates the relationship between critical points and these parameters. With these points in mind, we will formulate our theory. In this formulation, we will use a mean field theory approach. Since the objective of this theory is to provide an explanation of the phase boundary rather than extract critical exponents, the inadequacy of smoothing out fluctuations inherited in a mean field theory may not be profound. It may be argued that critical points are less influenced by fluctuations, dimensionality, and symmetries. If the influence of these factors is strong, the location of critical points will be generic in each universality class, reminiscent of critical exponents. The lack of such generic behavior suggests a weaker dependence of critical points on these factors. Further evidence supporting the use of a mean field approach comes from the study of Dickman, who has employed a mean field approach studying the ZGB model[46]. Some of his results are in very good

agreement with simulations. In view of these arguments, we may expect a mean field type approach will yield a satisfactory result in predicting phase boundary.

To facilitate a dynamical description of the evolution, we construct the evolution equation for CO and O. The exclusion of vacant sites from the consideration is a consequence of its dependence on CO and O. Therefore, evolution of CO and O encompasses the entire system. In this description, dynamical equations are functions of $y_{co}$ and $r$, written as

$$\frac{dx_o}{dt} = 2(1 - y_{co})(1 - r)x_{bb} - x_{co-o}r \tag{35}$$

$$\frac{dx_{co}}{dt} = y_{co}(1 - r)x_b - x_{co-o}r, \ , \tag{36}$$

where $x_{co}$, $x_o$, and $x_b$ are the concentration of CO, O, and vacant sites, respectively; $x_{bb}$ is the concentration of vacant pairs that have a suitable orientation for $O_2$ adsorption. The first term of the two equations represents the adsorption process, and the second term describes reaction. The factor of 2 in the first term of the first equation accounts for the pair adsorption of oxygen. If we subtract Eq. 35 from Eq. 36, at steady state we have

$$2(1 - y_co)x_{bb} - y_{co}x_b = 0 \ . \tag{37}$$

It has been argued by Considine[54] that the concentration of vacant pairs $x_{bb}$ can be expressed as a series expansion in terms of the concentration of single vacant site. In the second order approximation, the vacant pair concentration can be expressed as

$$x_{bb} = c_1 x_b + c_2 {x_b}^2 \ . \tag{38}$$

Furthermore, the coefficients $c_1$ and $c_2$ in the expansion are functions of

reaction rate, and they can be written as

$$c_1 = g_0 + g_1 r + g_2 r^2 + g_3 r^3 \ldots \tag{39}$$

$$c_2 = h_1 r + h_2 r^2 + h_3 r^3 + h_4 r^4 \ldots . \tag{40}$$

If we use these expansions of c's in $x_{bb}$ and substitute it into the steady state condition Eq. 37, after a little algebra we obtain a quadratic equation of the following form

$$\frac{d(x_o - x_{co})}{dt} = as^2 - (a+b)s + b\,, \tag{41}$$

where $s = x_{co} + x_o$, $a = 2(1 - y_{co})(1 - r)c_2$, and $b = [2 * (1 - y_{co})(c_1 + c_2) - y_{co}](1 - r)$. It should be noted that parameter a is always positive.

The solution to this equation is simply given by the quadratic formula. One solution is $s = 1$. Physically, this solution indicates a steady state with no vacant sites on the lattice. This is evidently unphysical for a reactive steady state since vacant sites are always present in a reactive steady state. Therefore, this solution corresponds to either a CO-covered or an O -covered surface. This solution occurs when $b = a$, $b = 0$ and $a \neq 0$, or $a = -b$. To further distinguish a CO-poisoned state from an O-poisoned state, we consider each case separately. For $b = a$, the dynamical evolution equation of $x_o - x_{co}$ is

$$\frac{d(x_o - x_{co})}{dt} = a(s^2 - 2s + 1) = a(s-1)^2\,. \tag{42}$$

Since the quantity on the right is positive, the difference in O and CO concentration increases as a function of time, and the surface will have more O than CO. The system eventually reaches an O-poisoned state. This conclusion is further confirmed by numerically evolving the dynamical equations with an initially empty surface.

If $b = 0$ and $a \neq 0$, Eq. 41 reduces to

$$\frac{d(x_o - x_{co})}{dt} = as(s-1)\,. \tag{43}$$

This equation is always nonpositive. Therefore, O density is always decreasing in relation to CO density until the system reaches CO-poisoned state. This conclusion is verified by numerical evolution of the equations. Similar conclusion can be reached for the case $a = -b$.

The other solution to the quadratic equation is $s = b/a$. Evidently, a physically realizable solution is $b < a$, which corresponds to the steady state. Besides these combinations of a and b that give physically realizable states, other combinations are forbidden on the physical ground. In short, the parameter space bounded $a$-axis and $a = b$ line corresponds to the reactive steady state region. The CO poisoned state occurs on the a-axis, whereas the 45 degree line defines the O poisoned state. The tricritical point occurs where the first order and the second order transition converges, and it is the origin of the parameter space. Fig. 39 graphically summarizes these results.

As Fig. 39 indicated, the region where $a \geq b$ marks the O-poisoned state and reactive steady state. This result provides a condition for calculating the second order transition points

$$y_{co} - 2(1 - y_{co})c_1 \geq 0\,. \tag{44}$$

Solving this equation for $y_{co}$, we obtained the condition for second order transition and reactive steady state

$$y_1 = \frac{2c_1}{1 + 2c_1}\,. \tag{45}$$

This result shows the reactive state occurs when $y_{co}$ is greater than $y_1$ while the system attains an O-poisoned state if $y_{co}$ is less than $y_1$.

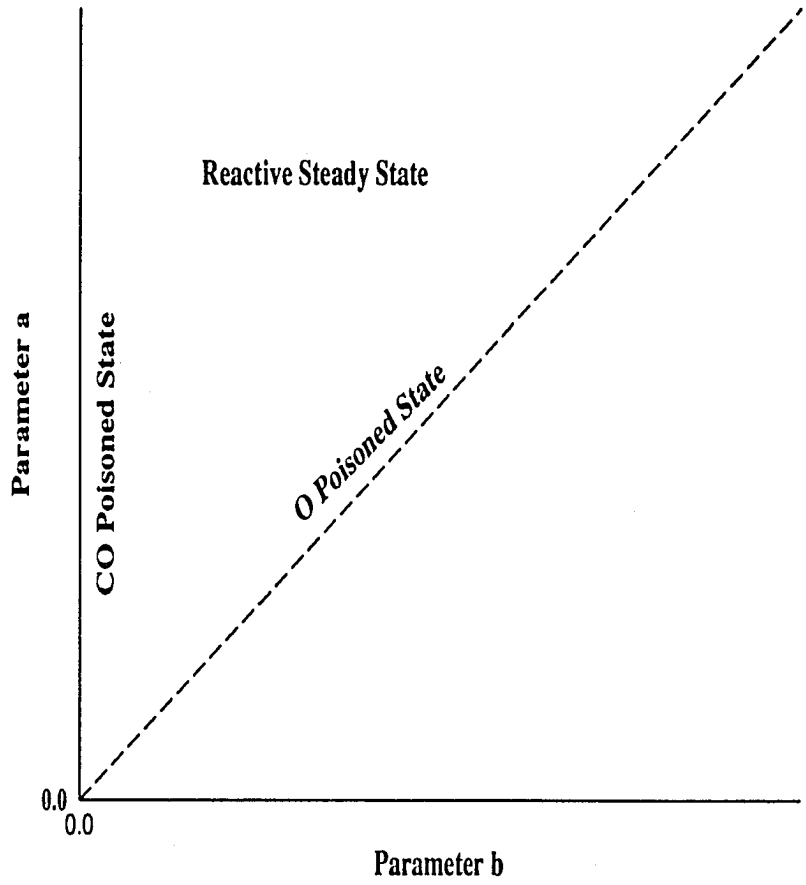


Figure 39: Phase boundary in a-b space. The $a$-axis corresponds to CO-poisoned state; $a = b$ line is the O-poisoned state. Steady state region is between $a$-axis and $a = b$ line. The origin corresponds to the tricritical point

Similarly, the condition $b = 0$ provides a means to locate the first order transition points

$$2(1 - y_{co})(c_1 + c_2) - y_{co} = 0 \,. \tag{46}$$

Solving this equation for $y_{co}$, we obtained the first order transition points

$$y_2 = \frac{2(c_1 + c_2)}{1 + 2(c_1 + c_2)} \,. \tag{47}$$

This result shows the system reaches CO-poisoned state if $y_{co}$ is greater than $y_2$. Additionally, the condition $a = -b$ gives a CO-poisoned state; the transition points are given by

$$y_2' = \frac{(2c_1 + 4c_2)}{1 + (2c_1 + 4c_2)} \,. \tag{48}$$

Since this $y_2'$ is greater than $y_2$, the boundary of the CO-poisoned phase occurs at $y_2$.

A comparison of $y_2$ and $y_1$ reveals that $y_2$ is greater than $y_1$; This result indicates that the O-poisoned phase occurs at lower $y_{co}$ values than the CO-poisoned phase; the reactive steady state occurs between $y_1$ and $y_2$. This phase diagram is consistent with the phase diagram from the simulation. As we have seen, a tricritical point is where first order and second order transitions converge, that is $y_1 = y_2$. This observation lead to the conclusion that the tricritical point occurs at $c_2 = 0$.

From the series expansion for $c_2$, it is clear a critical point exists at zero reaction rate. However, other zeros of $c_2$ may also exist for nonzero reaction rate. These zeros produce a tricritical point at a finite reaction rate, therefore, the search of a tricritical point at a finite reaction rate is to search for zero's of $c_2$. In addition to $c_2 = 0$ at the tricritical point, Eq. 46 implies $c_1 = y_{co}/2y_o$. Since the exact form of $c_1$ and $c_2$ is unknown and

nontrivial to derive, we will extract them from the phase diagram. In this extraction, we retained the fourth order term in the expansion of $c_2$ and the third order term in $c_1$.

Fig. 40 illustrated the form of $c_2$ near the tricritical point. It is clear that $c_2$ has a zero at approximately $r = 0.02$; further evidence of $c_2 = 0$ is provided by the extracted value of $c_1$, which has a value of 0.091. Assuming $c_2 = 0$, Eq. 46 gives a calculated value of 0.091 for $c_1$, which is in good agreement with the extracted value. This agreement is indeed consistent with the expectation of $c_2 = 0$. Fig. 41 shows a phase diagram from simulations and a calculated phase diagram using extracted $c_1$ and $c_2$. As we have seen, the results are in very good agreement with simulations. Besides curve fitting, further evidence that $c_2 = 0$ comes from the relationship between the concentration of CO-O pairs and vacant sites.

The equilibrium condition requires

$$x_{co-o} = \frac{(1-r)}{2r}(y_{co}x_b + 2y_o c_1 x_b + 2y_o c_2 {x_b}^2) \,. \tag{49}$$

Using the values for $c_1$ and $c_2$ at the tricritical point, the equilibrium concentration of $x_{co-o}$ at the tricritical point is given by

$$x_{co-o} = \frac{(1-r)}{r} y_{co} x_b \,. \tag{50}$$

In Fig. 42-Fig. 44, we plotted CO-O pair density from simulations and calculated values of CO-O pair density with the assumption that $c_2 = 0$ for various $y_{co}$. We observe that simulated CO-O pair density curve does not cross that of the calculated curve for $r > 0.018$, implying $c_2$ is nonzero. At $r = 0.018 \pm 0.001$, $c_2$ vanishes, suggesting a tricritical point.

In view of these facts, we may conclude that a tricritical point may in fact exist in the model. However, to make a conclusive answer based upon

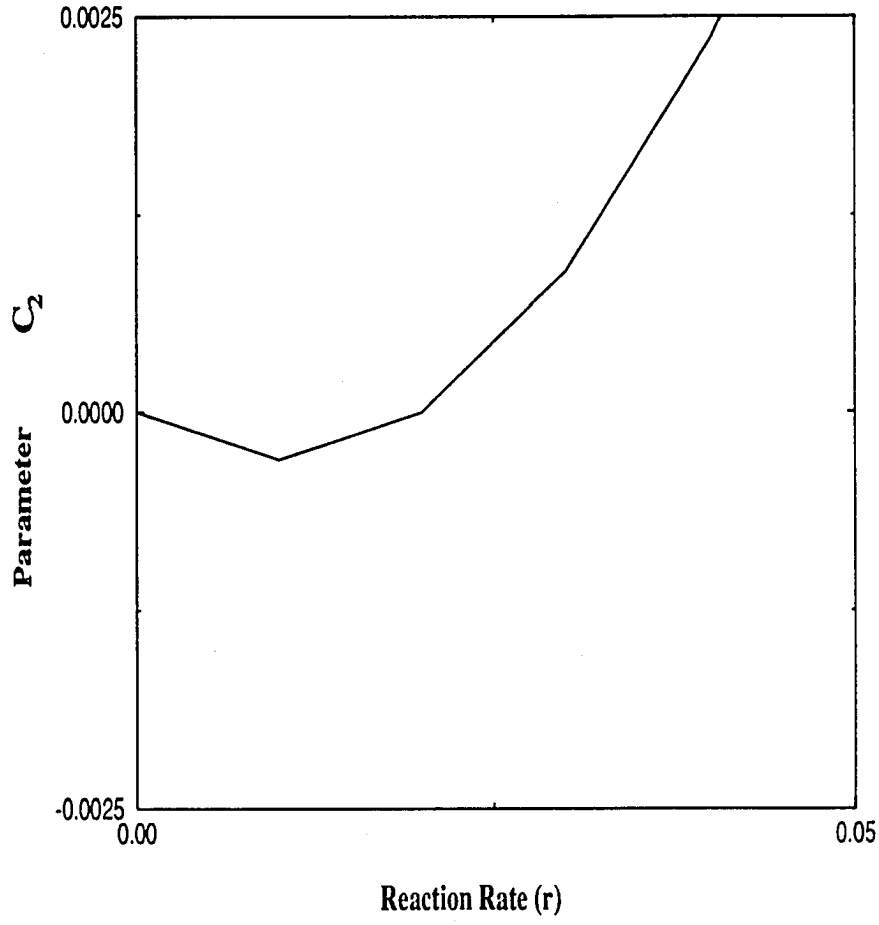


Figure 40: $c_2$ as a function of reaction rate at $R_x = 0.5$

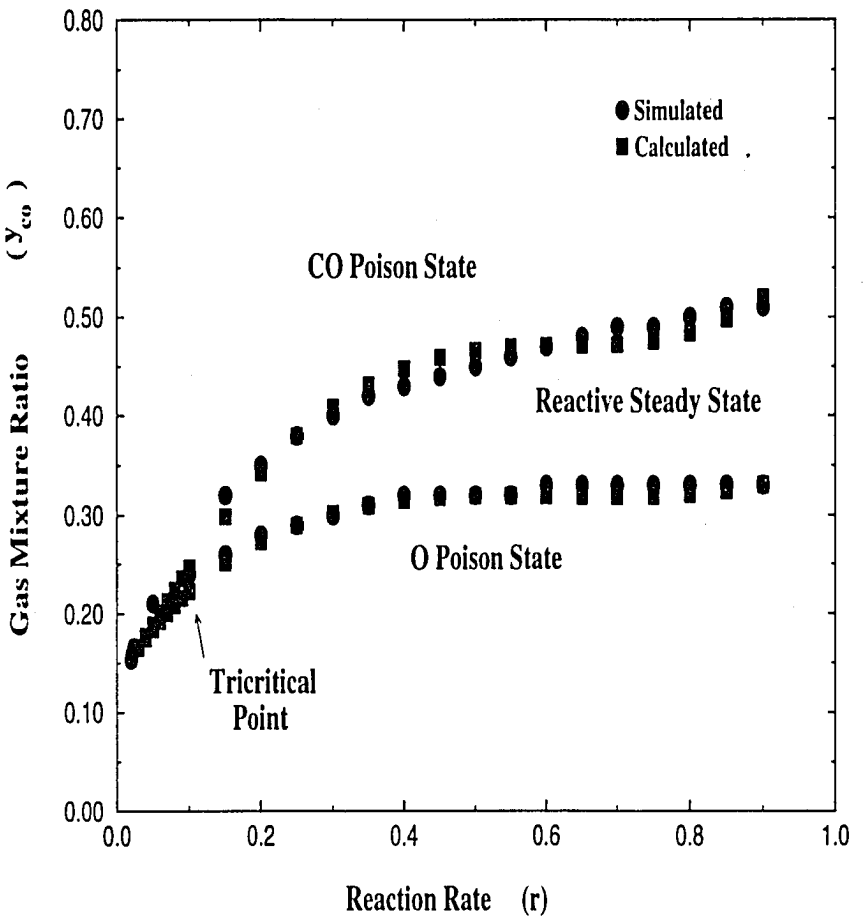


Figure 41: Phase diagram computed using extracted $c_2$ at $R_x = 0.5$

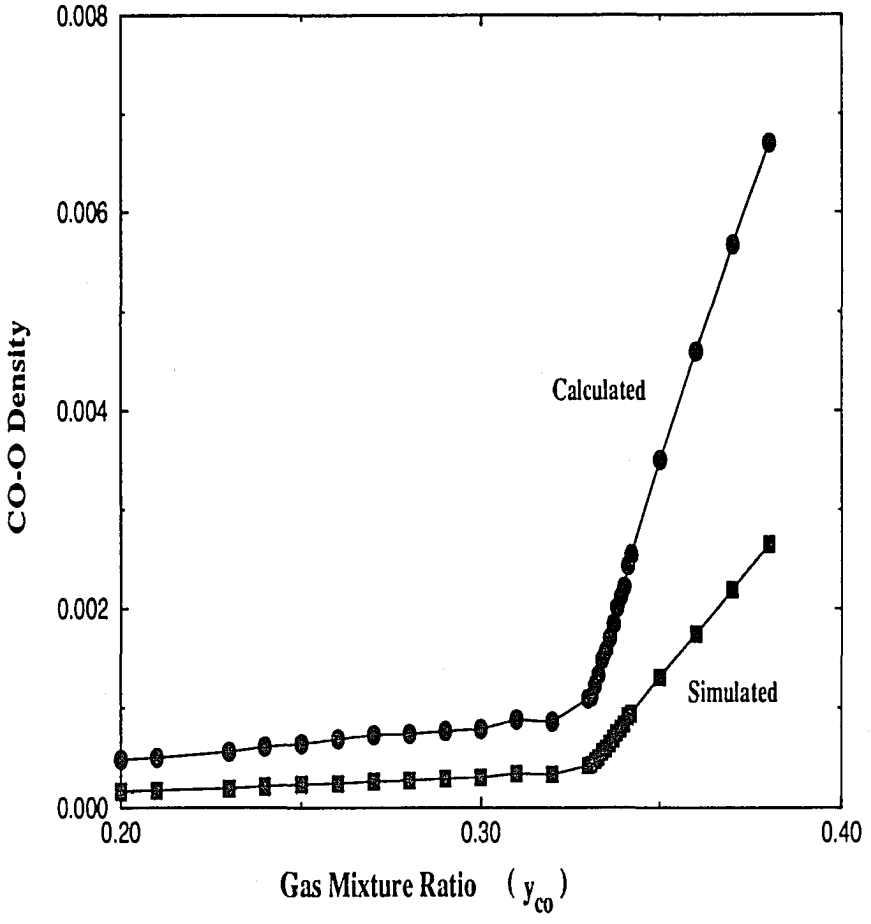


Figure 42: CO-O concentration from simulation and calculation assuming $c_2 = 0$ and $r = 0.9$

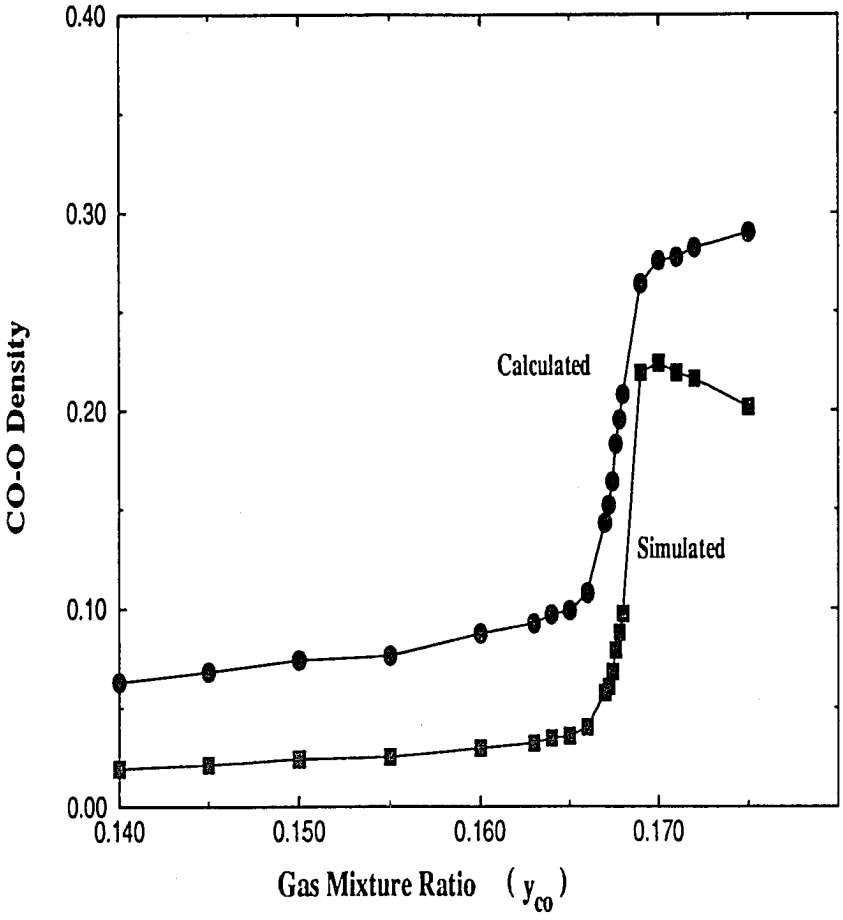


Figure 43: CO-O concentration from simulation and calculation assuming $c_2 = 0$ and $r = 0.025$

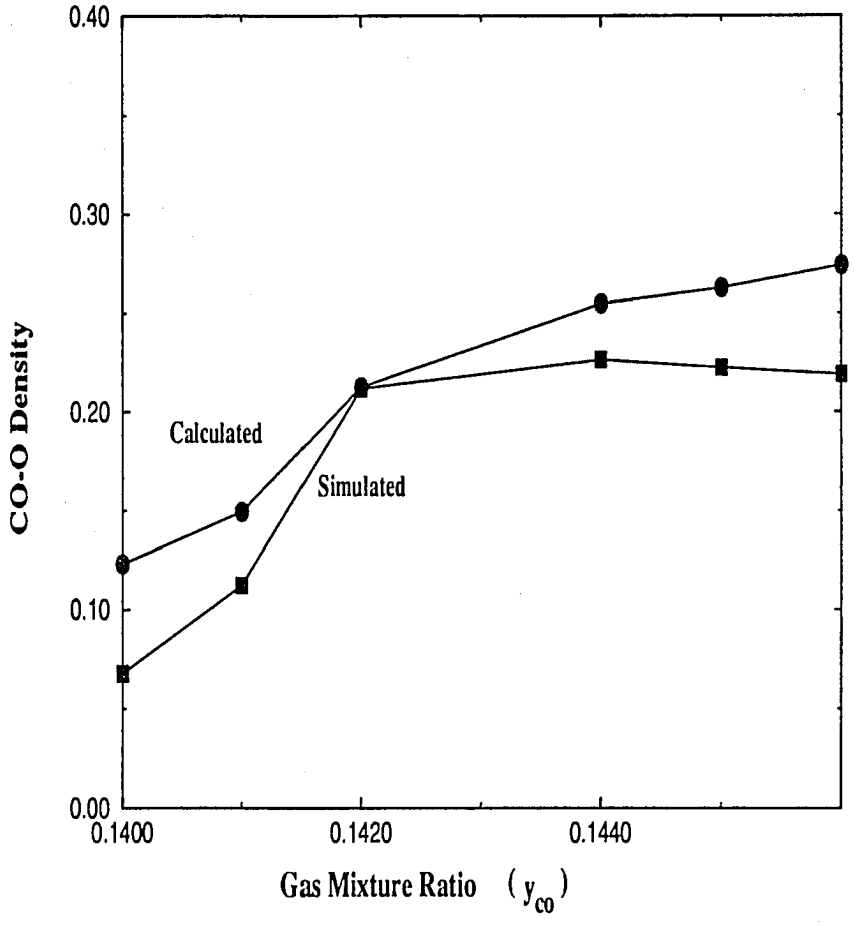


Figure 44: CO-O concentration from simulation and calculation assuming $c_2 = 0$ and $r = 0.018$

numerical calculation alone is rather premature. Further analytical studies are needed in order to answer the question with certainty.

### 4.3.4 Effects of Anisotropy and Diffusion on Tricritical Points

Before we conclude this chapter, we will briefly consider the effect of anisotropy and diffusion on the tricritical point. Fig. 45 and Fig. 46 are projections of the tricritical line onto $R_x - r$ and $R_x - y_{co}$ planes, respectively. Projections of the tricritical line onto these planes reveal a minimal dependence of $r_t$ on anisotropy, yet a stronger dependence of $y_{co_t}$ on anisotropy is seen. The dependence of $y_{co_t}$ on anisotropy and adsorption rate is consistent with the trend of first order points. An increase of the anisotropy parameter $R_x$ results in the shift of the second order points towards smaller $y_{co}$ values. To compensate this shift, a higher adsorption rate is necessary to shift the first order transition points towards lower $y_{co}$ values as shown by Fig. 46.

As we found in the previous chapter, diffusion has little influence on the second order transition because of the low concentration of CO. However, the first order transition point is highly sensitive to diffusion. An increase of diffusion rates results in moving the first order transition point towards a higher value of $y_{co}$. In the present case, we expect CO diffusion to become more important in the region of high adsorption rate due to higher CO concentration. Fig. 17 shows the trend of CO concentration towards high adsorption rates. It is evident from this figure that the enhancement of CO adsorption results in higher CO concentration at second order transition. Therefore, we expect the effect of diffusion on the second order transition will be more profound. Consequently, the tricritical point will become unstable. Fig. 47 shows the phase diagram with a variety of diffusion rate; the result of

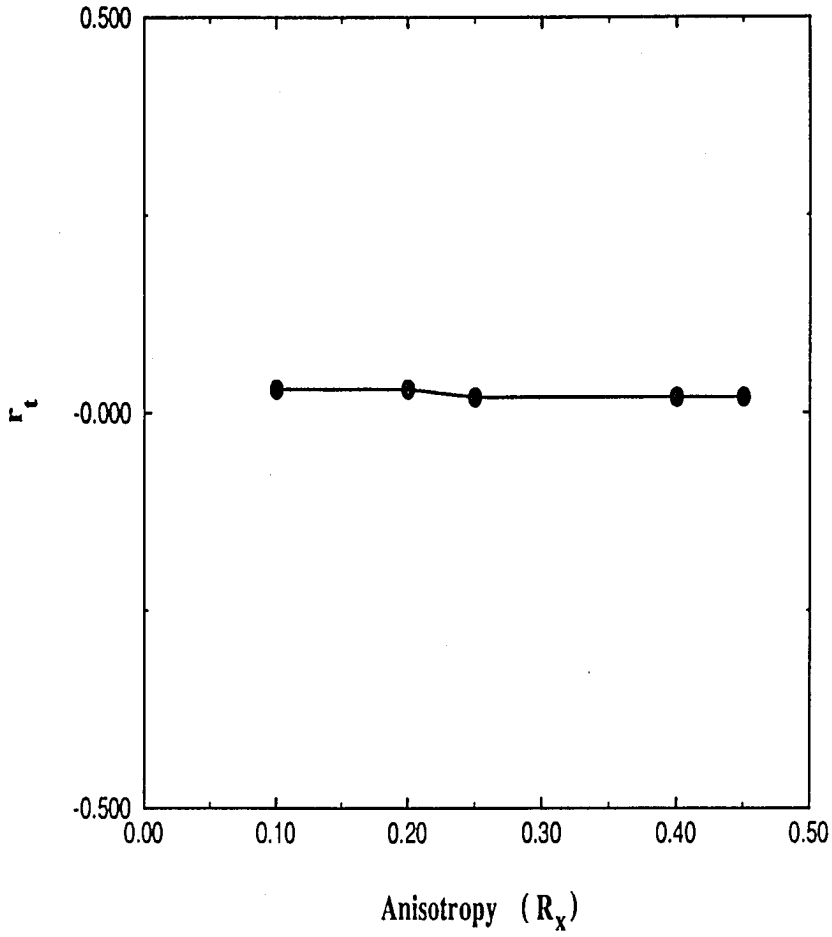


Figure 45: Projections of the tricritical line onto $R_x - r$ plane

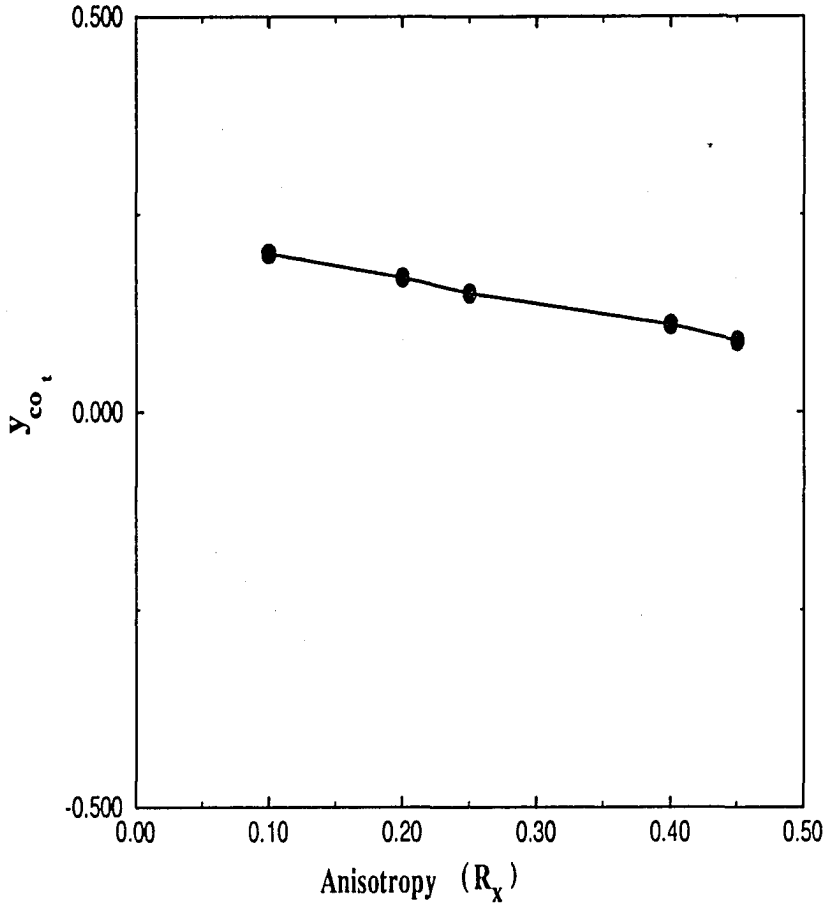


Figure 46: Projections of the tricritical line onto $R_x - y_{co}$ plane

a slow diffusion moves the tricritical point $yco_t$ to a higher value of $y_{co}$, and a fast diffusion reintroduces steady state and destroys the tricritical point. This can be understood in terms of the effective reaction rate. The diffusion process, as we have seen in the previous chapter, increases the effectiveness of CO to react. Therefore, the system behaves as a system with a high reaction rate, and the reactive steady state reemerged as a result.

## 4.5 Conclusion

In conclusion, we have studied a variant of ZGB model with finite reaction rates. We have mapped out phase diagrams via Monte Carlo simulations. Our results indicate that anisotropy has a minimal impact on the discontinuous transition, whereas more profound effects are seen on the continuous transition in reminiscent of the model with infinite reaction rate. In contrast to this behavior, finite reaction rate has more profound impact on the discontinuous transitions than on continuous transitions. Moreover, Our simulations as well as those of Considines[54] suggest the existence of a tricritical point. Further evidences of its existence are shown by the critical exponents, susceptibility, characteristic time scale, and parameters $c_1$ and $c_2$. As we have mentioned earlier, our results strongly indicate the possibility of a tricritical point in this model. However, a conclusive answer can be reached only by analytical means, therefore, further analytical study of the tricritical point may be warranted. Besides the evidence we provided for the possibility of a tricritical point, we have also examined the effect of diffusion on the tricritical point. It has been shown that fast diffusion tends to destroy the tricritical point in the region we surveyed.

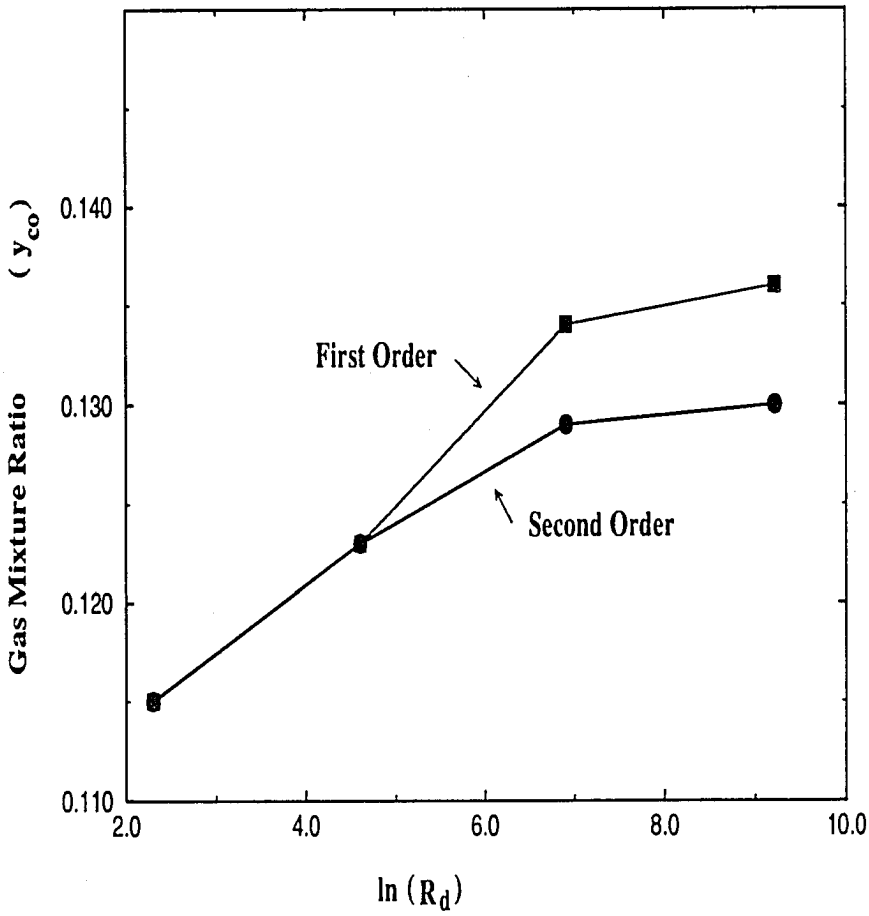


Figure 47: Effect of diffusion on the tricritical point at $r = 0.01$

# CHAPTER 5

# MECHANISM OF DYNAMICAL PHASE TRANSITION

## 5.1 Introduction

In recent years much work has been devoted to understanding the behavior of nonequilibrium systems. Various methods, such as mean field theory and series expansion technique, have been employed in the pass to study nonequilibrium phase transitions. We will study nonequilibrium systems from a different perspective, which has the advantage of being more generic. Frequently, a nonequilibrium system is governed by a set of dynamical rules, which describe the statistical evolution of the system. The ZGB and Schlogl models are examples of such a statistical system. A Hamiltonian description of such a system is difficult to obtain due to the lack of an energy function. Therefore, it is natural to employ a statistical description. In this chapter we develop a method for studying dynamical system, utilizing this statistical description. We organized this chapter as follows: section II describes the approach and presents a physical mechanism of dynamical transitions; section III compares this approach with the transfer matrix method; section IV explores the importance of noise in controlling critical behavior. Finally, we will illustrate this method with a simple example.

## 5.2 A Master Equation Approach

A master equation is a kinetic equation describing the evolution of a statistical system based on transition probabilities. The solution to this equation provides us with complete information concerning the statistical nature of the system, and in principle it affords the calculation of any quantity of interests. For a nonequilibrium system undergoing a kinetic phase transition, the most important characterization of the transition is its critical exponents, which determine the universality class. To learn the critical behavior from the master equation, it is essential to understand the basic mechanism of the dynamical transition.

The fundamental dynamical process of a nonequilibrium system is typically Markoffian. In other words, the dynamical evolution of the system is independent of its history. The temporal trajectory of the system in configuration space is expressed in terms of transition probabilities. The master equation

$$\frac{dP_i}{dt} = \sum_j (W_{ij}P_j - W_{ji}P_i) \tag{51}$$

is the mathematical realization of this fact. Here $P_i$ is the probability for the system to be in a particular configuration $i$, and $W_{ji}$ is the transition probability from one state $i$ to the another state $j$. The solution to this equation provides the probability for the statistical realization of various configurations. With a suitable combination of these configurations, a dynamical system can be decomposed into various independent dynamical processes. This decomposition procedure is equivalent to diagonalizing the master equation. In this context, we can view the evolution of the dynamical system as the evolution of the normal modes, and the eigenvalues of the

master equation are the decay rates of these normal modes. These eigenvalues define the characteristic time scale of the decay process. Evidently, the long-time behavior is entirely controlled by those modes with a slow relaxation rate. In the vicinity of a phase transition, these slow modes play a crucial role in controlling the critical behavior. The dynamical phase transition, a profound change in the macroscopic character of the steady state, must be a consequence of some changes in these slow modes. The simplest way to achieve this in the infinite volume limit is to have additional steady states emerging from these slow modes.

In this scenario the nonequilibrium phase transition occurs via the appearance of additional steady states. In the vicinity of a phase transition, the character of a slow mode does not change dramatically, rather it is the dependence of the relaxation rate on system size that changes. Thus the essential critical behavior of the system is controlled by those modes that metamorphose into steady states in the infinite volume limit. All other modes act only as spectators in the transition. Furthermore, we expect these modes that become steady states, in the infinite volume limit, to be controlled by the symmetries of the kinetic rules and the spatial dimensionality in reminiscent of equilibrium systems. The emergence of new steady states and the degeneracy of these steady states in the limit of infinite volume are closely related to the transfer matrix technique.

## 5.3 The Master Equation as a Transfer Matrix

The transfer matrix technique has been used in the study of Ising model[7, 65, 66, 67, 68] and directed percolation systems[69, 70, 71]. More recently, there has been studies of global features of the spectrum[72, 73].

To show the essence of the transfer matrix technique, we will present a simple example in the form of one-dimensional linear Ising model[74]. However, this method is not only limited to a one-dimensional system. For a one-dimensional Ising system, which is a system composed of interacting magnetic moments of two different orientations, the partition function of this system is

$$Z_N = \sum_{\mu} \exp(\nu \sum_{i=1 to N} \mu_i \mu_{i+1} + B \sum_{i=1 to N} \mu_i), \tag{52}$$

and it can be recast into a matrix form

$$\begin{aligned} Z_N &= \sum_{\mu_i=\pm 1} L(\mu_1,\mu_2)L(\mu_2,\mu_3)\ldots L(\mu_{N-1},\mu_N)L(\mu_N,\mu_1) \\ &= \sum_{\mu_1=\pm 1} L^N(\mu_1,\mu_1) = Tr(L^N)\,, \end{aligned} \tag{53}$$

where $L(\mu_i,\mu_{i+1}) = \exp[\nu\mu_i\mu_{i+1} + \frac{B}{2}(\mu_i + \mu_{i+1})]$ is the transfer matrix.

The major advantage of this matrix representation of the partition function lies in the fact that an increase in the length of the chain corresponds merely to a multiplication of the transfer matrix. The partition function can be calculated from the trace of this transfer matrix. Consequently, the study of the Ising model becomes an eigenvalue problem, which can be easily studied. One of the generic results of this method is the relationship between the correlation length and these eigenvalues. For an infinite volume system, the correlation length is proportional to the logarithm of the ratio of the two largest eigenvalues[75]. The larger eigenvalues may become degenerate in the limit of infinite volume. This asymptotic degeneracy was discovered in the 1940s[7], and equilibrium phase transition was attributed to this degeneracy[76].

The connection between the master equation and transfer matrix becomes apparent if we consider the evolution of a dynamic system as a one-dimensional *chain* in the temporal direction. The master equation, in this context, is effectively a transfer matrix. In the language of transfer matrix, the characteristic time scale of a dynamic system can be viewed as a correlation length in the temporal direction for dynamic modes. With this interpretation, we are able to relate the characteristic time to the largest eigenvalues of the master equation. Asymptotic degeneracy of eigenvalues contributes to the divergence of the characteristic time scale; this divergence is the mechanism of phase transitions and the reason behind critical slow down in the critical region. We can draw a close connection between asymptotic degeneracy and our mechanism of phase transitions. The appearance of new steady states in an infinite volume system is equivalent to asymptotic degeneracy of eigenvalues. In our picture, we attribute phase transitions to the emergence of new steady states, whereas in the language of the transfer matrix, degeneracy of the eigenvalues of these steady states is attributed as the cause of phase transitions. Therefore, these two views are equivalent.

For a finite size system belonging to the universality class of RFT and directed percolation, the only stable state of this class of systems is the absorbing state. Since the mode corresponding to the steady state has unit probability of one configuration only, there is no statistical noise in this steady state. However, all other modes of the master equation have nonzero probability for different configurations that are not related by translational invariance. Thus there is some statistical noise in all these states. As a function of some control parameter $p$, there may be a critical value $p = p_c$ where for $p < p_c$ the relaxation rate $\gamma$ of this mode into the absorbing state

remains nonzero for large systems and for $p \geq p_c$ the relaxation rate of one of these modes vanishes in the limit of infinite system size. This mode then becomes the effective steady state for the system and the system changes from a noiseless absorbing steady state to a noisy steady state. Because these systems have no symmetry other than translational invariance, we expect that only one mode will become critical at $p_c$. This is the scenario which occurs for models which show critical behavior characteristic of directed percolation[48, 49]

## 5.4 Noise and Universality Class

In a dynamic system, the noise plays an essential role in determining the universality class. This can be demonstrated by the time-dependent Landau-Ginzburg model[77], which bears a strong resemblance to the model of RFT and directed percolation[48]. However, this model is in a different universality class due to a different noise characteristics.

In the Landau-Ginzburg model, the dynamical equation for a field $\phi(x,t)$ is

$$\frac{\partial \phi}{\partial t} = r\phi - u\phi^2 + D\nabla^2\phi + \cdots + \eta(x,t)\,. \tag{54}$$

The random noise $\eta(x,t)$, assumed Gaussian, obeys

$$\langle \eta(x,t)\eta(x',t')\rangle = \Gamma(x,x',\phi)\delta(t-t')\,, \tag{55}$$

where $\Gamma$ measures the noise amplitude. Grassberger[49] and Grinstein *et al.*[48] point out that the transition from a noisy configuration to an absorbing, noiseless state in this class of nonequilibrium models obeys a very similar kind of equation, with one important difference. The amplitude of the random noise in the time dependent Landau-Ginzburg model is a

constant, which is independent of the field variable $\phi(x,t)$. The amplitude of the random noise in the RFT and directed percolation models is coupled to the field variable; moreover, it is proportional to the field variable. It is this difference which contributes to the different universality class of these two models.

Even though a closer scrutiny of the evolution equations of Landau-Ginzburg may reveal an essential difference in the quantity that these equations represent, nevertheless, an argument of equivalence may be made. The Landau-Ginzburg model describes the evolution of an order parameter while the master equation represents the evolution of configurations. However, if one recognizes the fact that an order parameter is an average quantity taken over all the possible configurations,

$$\phi = Tr[\phi_i P_i(t)] \,. \tag{56}$$

one may effect an argument of equivalence. At steady state the dominate contribution to this average derives from the slowest mode. Any quantities of interests, which includes the order parameter, are in essence a disguised measurement of this slowest mode; therefore, the Landau-Ginzburg equation, in this sense, represents the evolution of the slowest mode. In this context, these two equations represent different quantities of the same dynamic process. It is this equivalence that affords the above comparisons although the two equations characterize different quantities of a dynamic system.

## 5.5 A Case Study

To demonstrate the above mechanism of kinetic phase transitions, we studied a simple model which simulates a catalytic reaction on a linear lattice. The critical exponents of this model have been extensively studied by Monte Carlo simulations and renormalization approach. The results from the renormalization study and general arguments on transitions in models with absorbing states suggest that this particular model belongs to the universality class of RFT and directed percolation. The choice of this model is based on its simplicity and the feasibility of numerically analyzing the model with available resources.

The model which we have studied simulates a catalytic reaction on a linear lattice. Random adsorption and reaction occur on the lattice according to a given set of kinematic rules. A site is chosen at random for adsorption. If the two nearest neighbors are vacant, the atom is adsorbed to that site. If any one of the nearest neighbor is occupied by an atom, it is either adsorbed by the lattice with the probability $p$, or reaction occurs with the probability $1-p$. The final product desorbs immediately from the lattice. If both neighbors are occupied by an atom, the adsorption probability remains to be $p$. However, the reaction probability with one of the neighbor chosen at random is $(1-p)/2$. In this model, reaction rate and desorption rate are infinite. We have used periodical boundary condition in both adsorption and reaction rules. The only relevant parameter of the model is the adsorption probability $p$; the coverage of atoms on the surface is a function of $p$. There

exists a critical value $p_c$, where the system reaches a reactive steady state if $p$ is less than $p_c$; otherwise it reaches a state in which the linear lattice is completely occupied by atoms (poisoned state). The phase diagram of this model is shown in Fig. 48. The transition in this model is second order.

In this model, there are no conservation laws governing the system. Therefore, we expect only one mode to become critical in the transition while the others remain noncritical. This slowest mode is the critical fluctuation in the transition. The transition to absorbing state in the single component RFT requires this fluctuation to vanish below the transition point. This noise mode decays exponentially with time. At the transition point or above, this noise is present at all times; therefore, it prevents the system from being poisoned. This is the picture of the transition for single component RFT, which this system belongs to. It is evident from this picture that essential dynamical behavior near the transition derives from this single mode. Therefore, it is sufficient to learn the dynamical behavior from this relevant single mode. To study this mode, it is necessary to construct the master equation for this model. The major difficult in the construction comes from the large number of states in the system. For a system with n sites, the total number of states is $2^n$. Even for a system with 13 sites, the number of states is enormous. Since we used a periodical boundary condition for this model, the system has translational symmetry. This symmetry of the system was exploited to reduce the number of states.

### 5.5.1 Review of Group Theory

Before we go further, we will briefly review some results from the group theory since it plays an important role in making the problem manageable.

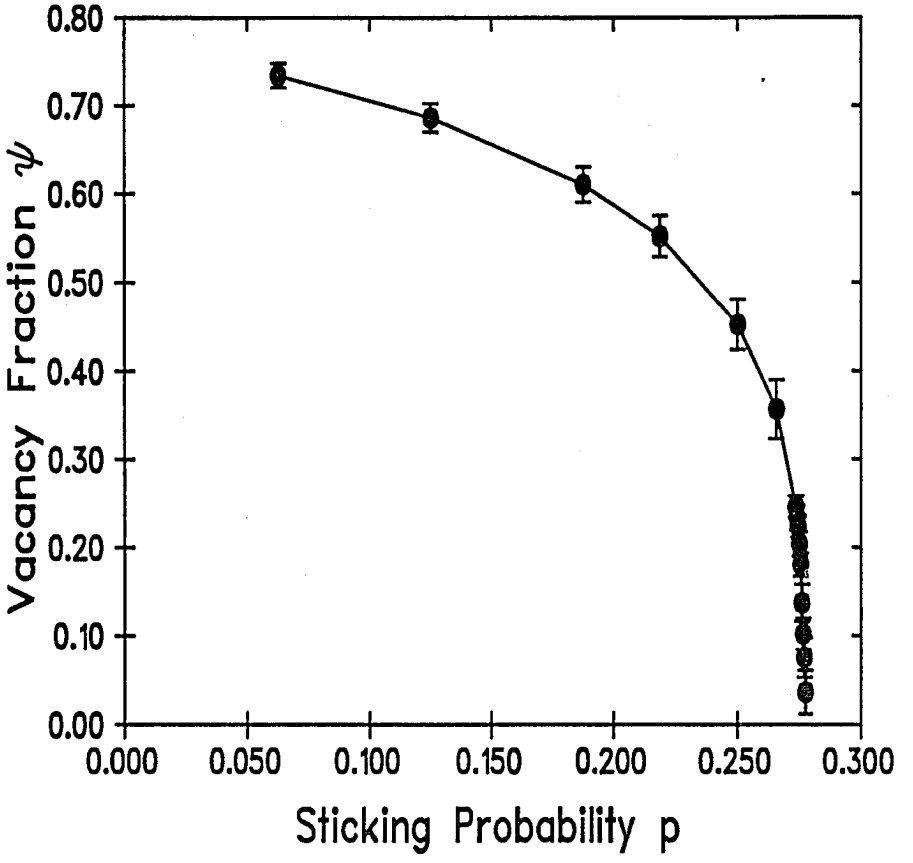


Figure 48: Phase diagram of the Schizo model

A group is a set which is closed with respect to multiplication; in addition, this set must contain a unity and an inverse. The space group, consisting of a rotation and a translation, is the largest group which can be defined for a crystal structure. We will limit this discussion to the one-dimensional translation group, a group within the space group or a subgroup of the space group. If $T(\mathbf{n})$ is an element of the translation group, it acts on some function $\psi(\mathbf{r})$. The net result of the operation is to shift the function in the direction $\mathbf{n}$. This new function $\psi(\mathbf{r}+\mathbf{n})$ looks like the old function, except by a multiplicative phase factor $e^{-2\pi \mathbf{k_i n}}$. We can consider $e^{-2\pi \mathbf{k_i n}}$ as a matrix representation of the translation group $T(\mathbf{n})$. More precisely, a representation of a group is a mapping which maps each elements of the group into a linear transformation. The vector space operated by the group elements is the carrier space. From the group theory we know any representation can be reduced to an irreducible representation. In such a representation, the carrier space is decomposed into the direct sum of various invariant subspaces, each having assigned label. Because of the invariance of the subspace under the action of each group element, the label of each basis function is a conserved quantity. In other words, there is no mixing between functions of different irreducible representation under the action of the group. In the one-dimensional translation group, the wave number $k_i$ is a label for each irreducible representation.

In this model, because the system is translationally invariant, we can decompose the system into various irreducible representation labelled by the wave number $k$. Since kinetic rules for the evolution of the system do not destroy the symmetry of the system, the invariant carrier space of each irreducible representation will remain invariant under the time evolution.

In other words, wave number $k$ will remain to be a good *quantum number* under the action of a time evolution operator, namely the master equation. The matrix elements, which connect basis state of different irreducible representation of the master equation, are zero. Therefore, the master equation is a block diagonal matrix, and each block of the matrix corresponds to an irreducible representation, labelled by the wave vector label $k$. Therefore, we reduce the construction of the full matrix of the master equation to the construction of the master equation of various irreducible representations. The number of states in each irreducible representation is significantly less than the full system. In this one-dimensional model, the field variable, which is the density of the atom on the surface, is not a conserved quantity in time. As we have mentioned previously, we expect the long wave length mode to govern long time behavior of the system. In analogy with the time dependent Landau-Ginzburg model of non-conserved field variables, $k = 0$ mode dominates the critical behavior of the system. Consequently, the study of the essential dynamical behavior reduces to the study of $k = 0$ irreducible representation, and the construction of the master equation is simply the construction of $k = 0$ irreducible representation, a much simpler process that a computer can do.

The basis function for the $k = 0$ irreducible representation is composed of all configurations which are invariance under translation. For example, a system of three sites with only one atom, the basis function is a linear combination of the configurations 100,010,and 001, where 1 represent the atom and 0 is vacancy. From the set of kinetic rules we have described, we can calculate the transition probability among these basis functions, and construct the master equation. The eigenvalues of the transition matrix

represent decay rates of various normal modes. As we have mentioned before, the slowest relaxing state determines the critical behavior of the system, Fig. 49 shows the relaxation rate of the slowest mode and the next mode. As shown in Fig. 49, the second slowest mode relaxes much faster than the slowest mode. In the limit of infinite size, there is only one mode that dominates the dynamic process. Hence, it controls the critical behavior of the system while the rest of the modes act as spectators. In the limit of infinite size system, this mode becomes the true reactive steady state.

### 5.5.2 Finite Size Scaling of Eigenvalues

We calculated the relaxation rates of the slowest relaxing mode for systems size 3 to 14 with various values of $p$. The critical exponent is obtained by finite size scaling.

We define a characteristic time $\tau$ that a vacancy will survive as:

$$\tau = \frac{\sum_t t\ \psi(t)}{\sum_t \psi(t)}\ , \tag{57}$$

where the $\psi(t)$ is the number of vacant sites. We use the following scaling ansatz for $\tau$:

$$\tau = L^z f\left((p - p_c)L^{1/\nu}\right)\ , \tag{58}$$

where $f(x) \propto x^{-z\nu}$ for $x \to \infty$. From the master equation, we can solve directly for the vacancy fraction $\psi(t)$ as a function of time. We write

$$\psi(t) = \sum_i a_i\, e^{-\lambda_i t}\ , \tag{59}$$

where the coefficients $a_i$ are determined by the initial conditions, and $\lambda_i$ is the decay rate of the $i^{th}$ normal mode. We then find from Eq. (57) that $\tau$

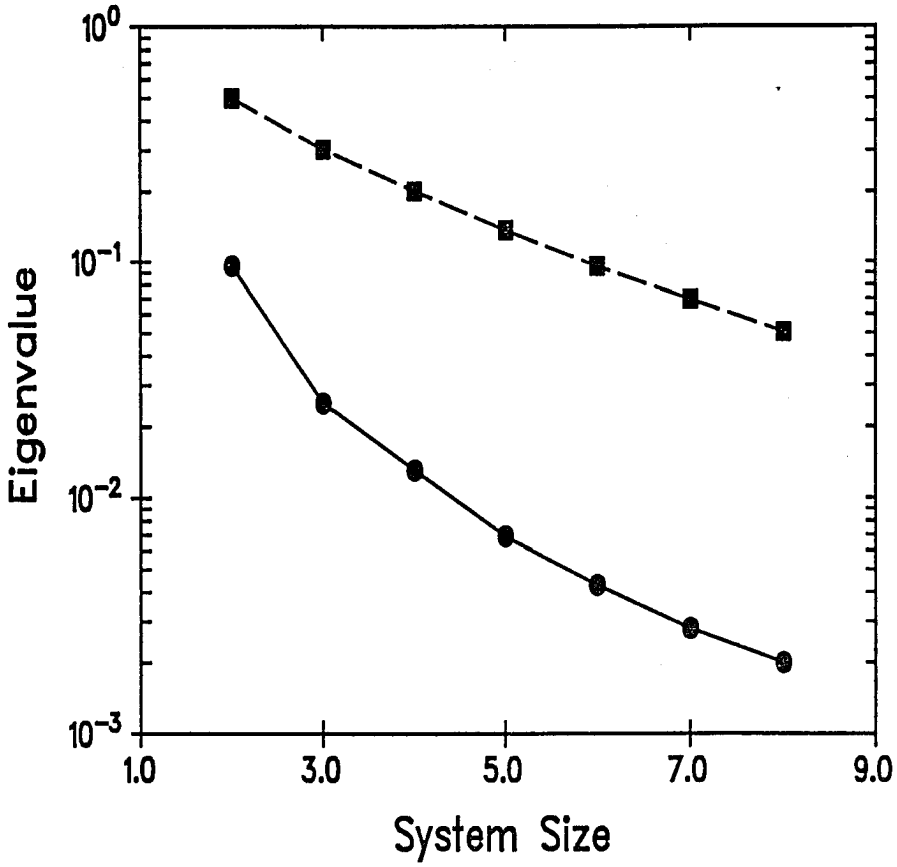


Figure 49: Relaxation of two slowest modes

is given by

$$\tau = \frac{1}{\lambda_1} \frac{1 + \sum_{i>1} \frac{a_i}{a_1} \left(\frac{\lambda_1}{\lambda_i}\right)^2}{1 + \sum_{i>1} \frac{a_i}{a_1} \left(\frac{\lambda_1}{\lambda_i}\right)} . \tag{60}$$

Contributions to $\tau$ from modes other than the slowest mode are evidently included in the summation, but a direct calculation with an initially blank lattice shows the corrections are typically of the order of a few percent for a variety of lattice sizes and thus can be neglected. This is further an evidence that the critical behavior of the system is solely controlled by the lowest normal mode. As the size of the system approaches infinity, the correction to the dynamical exponent vanishes.

The critical point can be determined from $\ln(\tau)$ *vs.* $\ln(L)$ plots for various $p$ values. The value of $p$ which produces a straight line in the plot indicates the critical point $p_c$. This is shown in Fig. 50, and is found to be $0.28 \pm 0.02$. The $p_c$ found by Monte Carlo simulation is 0.277. The slope of the $\ln(\tau)$ *vs.* $\ln(L)$ at the critical point gives the value of dynamical exponent. The dynamical exponent obtained from a least-squares fit is $1.53 \pm 0.12$. This is a further evidence that this model belongs to the RTF and directed percolation universality class. The dynamic exponent for 1+1D given by renormalization calculation is 1.58. By collapse $\ln(\tau L^{-z})$ *vs.* $\ln((p - p_c)L^{1/\mu}$ for a variety of sizes, we found $\mu = 1.05 \pm 0.05$. This is shown in Fig. 51.

## 5.6 Conclusion

In conclusion, we have studied the dynamical phase transition using the master equation. This approach provides a physical picture of the mechanism of dynamical transitions. In this picture, the basic ingredient of

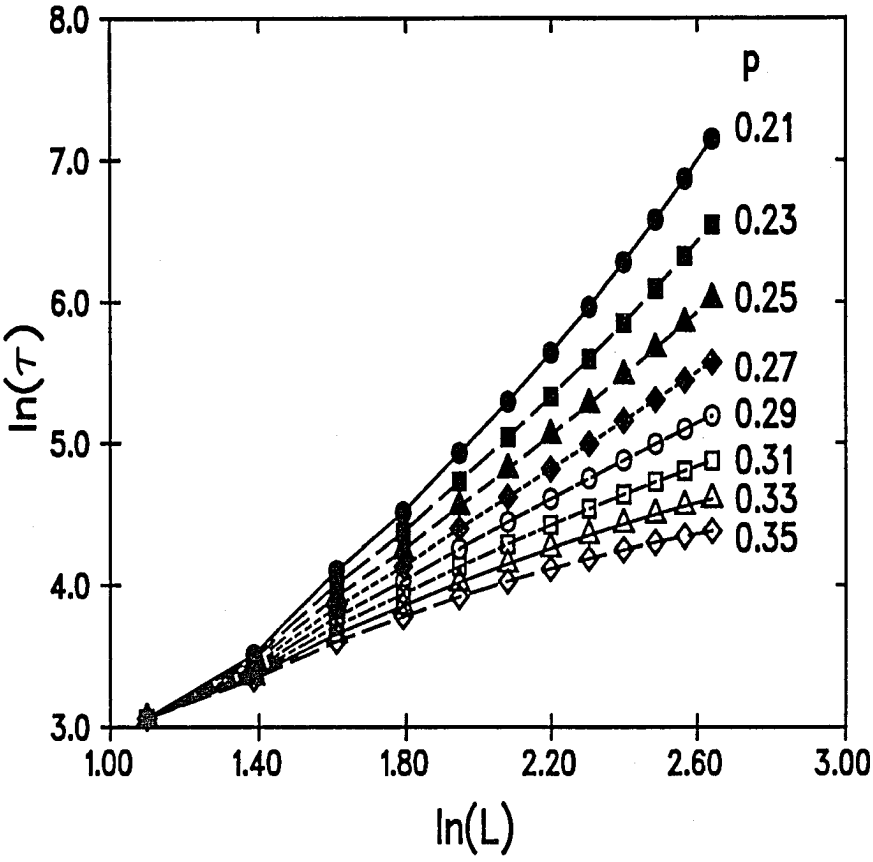


Figure 50: Plots of $\ln(\tau)$ *vs.* $\ln(L)$ for various $p$ values. The value of $p$ which produces a straight line yields the critical point $p_c = 0.27 \pm 0.02$.

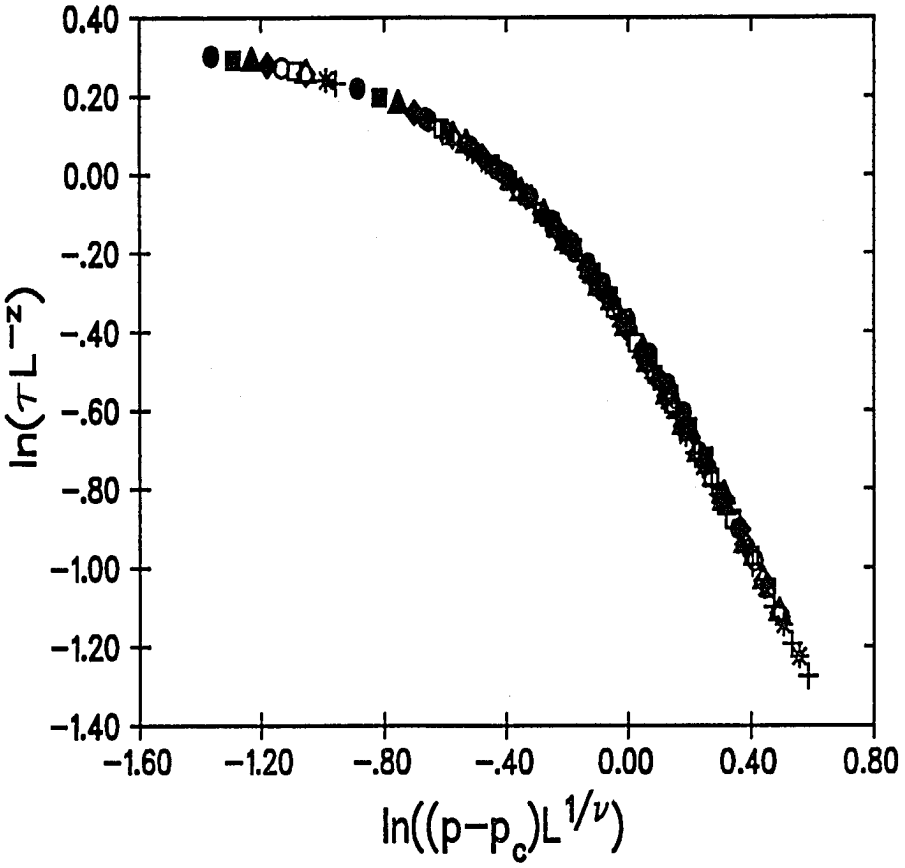


Figure 51: A plot of $\ln(\tau L^{-z})$ *vs.* $\ln\left((p-p_c)L^{1/\nu}\right)$ for various lattice sizes showing the collapse of the data on a single universal curve.

dynamical phase transitions is the appearance of new steady states in the infinite volume limit. In the language of traditional transfer matrix approach, asymptotic degeneracy of the eigenvalues caused by the new steady states contributes to the divergence of the correlation length and the phase transition. Our study of the catalytic model provides numerical support for these views. In this model, we have found an evidence of the generic feature of asymptotic degeneracy in the two largest eigenvalues[72]. Furthermore, We have been able to isolate the relevant mode from the irrelevant modes. These results provided numerical support for the view of the criticality of single mode for the model in the RFT and directed percolation class. This study provided an alternative way of studying dynamical phase transitions. The information of one mode criticality may be utilized in the construction of a longer chain by combining two smaller pieces together in a renormalization approach.

# CHAPTER 6

# CONCLUSIONS

In previous chapters, we have studied kinetic phase transitions and related critical phenomena of a variant ZGB model. In addition, we have provided a generic physical picture of dynamical phase transitions. In our studies we have provided numerical supports for the assertion that this model belongs to the universality class of RFT and directed percolation[48]. Furthermore, the universality is robust in relation to anisotropy and reaction rate.

As our results indicates, critical phenomena of nonequilibrium systems are in many ways reminiscent of critical phenomena of equilibrium systems. The characteristic time scale which measures correlation length in time diverges at a critical point. The dynamical slowing down in the critical region is indicative of this divergence and large fluctuations. Our result also suggests that nonequilibrium critical phenomena are insensitive to the microscopic details. This insensitivity accounts for the universal behavior of critical phenomena in systems of diverse nature. More basically, this universal behavior is related to the topological structure of the parameter space as seen from the perspective of the renormalization group. Although microscopic details play no essential role, other factors such as noise characteristics of the system, dimensionality of the system, and symmetry of the dynamical rules, control the critical behavior.

Our study further indicates that dynamical phase transitions are controlled solely by several slow modes while the fast modes of the system are, in essence, spectators. The dynamical phase transition is in fact a

manifestation of the changes in character of these slow modes. The fundamental mechanism which controls kinetic phase transitions is the degeneracy of steady states. In other words, some slowly decaying modes of a finite volume system metamorphose into steady states in the limit of infinite volume; the appearance of these steady states contributes to the change in dynamic processes and produces phase transitions. In a system which lacks any conservation rules, we expect only one such slow mode to exist and become critical. Consequently, it is the change of characters in this mode which creates dynamical phase transitions. As we have seen in a one-dimensional chemical reaction model, this mode determines the universality class of the system. This is a generic picture of kinetic phase transitions of systems in the universality class of RFT and directed percolation. This mechanism of asymptotic degeneracy in dynamical phase transitions strongly resembles the mechanism of equilibrium transitions.

To recast the physical picture into the language of the transfer matrix[7, 65, 66, 67, 68, 72, 73, 76], asymptotic degeneracy of eigenvalues of the master equation, which is a dynamical counterpart of the static transfer matrix, causes dynamical correlation length to diverge and creates kinetic phase transitions. This asymptotic degeneracy of eigenvalues in a dynamical transition manifests itself in the form of additional steady states. As we have seen, asymptotic degeneracy of eigenvalues of the transfer matrix is the underlying factor of both static and dynamical phase transitions.

Besides phase transitions, a dynamical system also can exhibit more complicated phase structure such as tricritical points. Our studies of the model with finite reactions suggest a tricritical point. The curtailed growth of the susceptibility in conjunction with a lack of reactive steady states

indicated by $\tau$ supports this assertion. Furthermore, a significant deviation of both static and dynamical critical exponents from those of RFT and directed percolation together with the parameters $c_1$ and $c_2$ give further credence to the existence of the tricritical point.

Despite what we have learned about the critical phenomenon of the ZGB model, many aspects of the model are still await to be addressed. Among them is the controversy of the existence of the tricritical point, which warrants further study via analytical means in addition to the existed evidence. One possible way of approaching this problem is to construct an evolution equation for a small system; this equation can then be renormalized. Preliminary effort in this direction has not yet produced any results, however, this lack of results should not be construed as a failure of the approach.

Besides the tricritical problem, other aspects of the oxidation process have not yet been captured by the ZGB model. Noticeably, the question of oscillation and chaos in the catalytic process has not been adequately addressed by the ZGB model. The concentration of CO and O on the surface represents two independent degrees of freedom. It is known that such a system cannot exhibit any chaotic behavior, as a minimum of three degrees of freedom is needed for producing chaos. Therefore, other surface processes may have been neglected by the model that are essential in producing chaos. Because of the theoretical importance of the catalytic oxidation of CO as well as its broad commercial application, further improvement on the model should be made.

Aside from the lack of chaos, the O-poisoned phase of the ZGB model has not been found experimentally. The lack of O-poisoned phase is primarily due to the ability of CO to compactify absorbed O and squeeze out an active

site to absorb and react. The ZGB model has not yet taken into account of this effect. Therefore, further investigation in this direction may be pursued.

Even though the ZGB model produces an O-poisoned phase which is absent in experiments, the fundamental importance of this model should not be overlooked because it has provided an evidence of a universality class in dynamical systems. Moreover, this model demonstrated several generic features of dynamical transitions; these are the important contributions of the ZGB model.

Apart from the ZGB model, the search for a generic approach for the study of dynamical process is still a ongoing process. Despite many similarities between equilibrium and nonequilibrium phase transitions, studies of nonequilibrium phase transitions are more difficult to conduct due to the lack of a generic method to treat them. Even though methods such as the Monte Carlo simulation are available in study these systems, a well developed theory, mirroring the analytical power of the classical mechanics in treating thermodynamic systems, has yet to emerge. Therefore, the search for a comprehensive approach to treat these systems is crucial in providing a fundamental understanding of them as well as in formulating a coherent theory. The approach formulated based on the master equation is a step in this direction. Although this approach is rather generic, the principle disadvantage inherited in it is the difficulty associated with obtaining a solution for a large system. In the limit of an infinite volume system, the master equation is a differential equation in an infinite-dimensional space. It is impractical, if it is not impossible, to obtain a solution of such a mathematical monster, therefore, investigation of other approaches in conjunction with the master equation may be warrant further efforts.

One possible approach in this direction may be the development of a renormalization group method based on the master equation. From our physical picture of kinetic phase transitions, we have established the fact that only the slow modes participate in the transition, and their asymptotic behavior determines the universality class of the system. It is therefore reasonable to expect that starting from a small solvable system, we can coarse-grain irrelevant modes and retain only a small number of slow modes for the construction of a larger system. This process can be repeated in a typical fashion of the renormalization group technique. In view of the conceptual simplicity of the approach, one might expect the implementation of such a procedure will be relatively trivial. However, the successful implementation of this procedure rests largely upon computational resources. The procedure is highly cpu intensive and requires large storage space. Nevertheless, this procedure will provide an alternative to the even more unpalatable possibility of looking for a solution to the master equation of a gigantic system.

In conclusion, we will again emphasis the importance of studying dynamical systems. As we have seen in this study, a substantial amount of efforts have been devoted to the ZGB model, however, away from the details, this model represents a class of dynamical systems, which exhibit common behaviors. The quest for understanding the fundamental processes, which manifest themselves in terms of a universal behavior, motivates this study, and this quest will continue to provide motivation for future studies. It should be noted, however, that the critical phenomenon of nonequilibrium system is only one of many phenomena displayed by the nonequilibrium system. Many fascinating behaviors, such as deterministic chaos, are still beyond our comprehension. The ultimate objective in the study of

dynamical system is to formulate a coherent theory, mirroring the analytic power of statistical mechanics, in treating every dynamical phenomenon. This endeavor is not merely an exercise of intellect, but rather has a more profound impact on our understanding of random processes. The realization of the possibility of creating an order from random processes has far reaching consequences. At the least, this realization has altered the traditional Newtonian association of an order with deterministic forces. Moreover, this realization may eventually provide an answer to the origin of life, which is seemingly derived from random processes. It is this exciting possibility that makes the study of dynamical systems even more important.

## References


[1] J.D. Van Der Waals, *Ph.D. Thesis*, University of Leiden.

[2] P. Weiss, J. Phys. Radium Paris **6**, 667 (1907).

[3] W. Lenz, Z. Phys. B., **21**, 613 (1920).

[4] P. Heller and G.B. Benedek, Phys. Rev. Lett. **8**, 428 (1962).

[5] E.A. Guggenheim, J. Chem. Phys. **13**, 253 (1945).

[6] P.R. Roach, Phys. Rev., **170**, 213 (1968).

[7] L. Onsager, Phys. Rev., **65**, 117 (1944).

[8] L.P. Kadanoff, Physics, **2**, 263 (1966).

[9] K. G. Wilson, Rev. Mod. Phys., **47**, 773 (1975);S.-K. Ma, Rev. Mod. Phys., **45**, 589 (1973)

[10] H.E. Stanley, *Introduction to Phase Transitions and Critical Phenomena*, (Oxford University Press, London, 1971.)

[11] R. Kopelman, S. Parus, and J. Prasad, Phys. Rev. Lett. **56**, 1742 (1986); J. Prasad and R. Kopelman, Phys. Rev. Lett. **59**, 2103 (1987).

[12] G. Nicolis and I. Prigogine, *Self Organization in Nonequilibrium Systems*, (Wiley, New York, 1977).

[13] H. Haken, *Synergetics*, (Springer-Verlag, New York, 1983).

[14] T.M. Liggett, *Interacting Partical Systems*, (Springer-Verlag, New York, 1985.)

[15] F. Schlogl, Z. Phys., **253**, 147 (1972).

[16] T. E. Harris, Ann Probab. **2**, 969 (1974).

[17] W. Kinzel, Ann. Israel Phys. Soc. **5**, 425 (1983); J. L. Cardy and R. L. Sugar, J. Phys. A **13**, L423 (1980); R. C. Brower, M. A. Furman, and M. Moshe, Phys. Lett. B **76**, 213 (1978). The critical exponents in these papers are defined differently from the usual convention. If the

exponents in these papers are denoted with primes, the conversion is $z = z'\nu'/2$.

[18] H. D. I. Abarbanel, J. B. Bronzan, R. L. Sugar, and A. R. White, Phys. Rep. **12C**, 120 (1975).

[19] R. M. Ziff, E. Gulari, and Y. Barshad, Phys. Rev. Lett. **56**, 2553 (1986).

[20] I. Langmuir, Trans. Faraday Soc., **17**, 672 (1922).

[21] C. T. Campbell, G. Ertl, H. Kuipers and J. Segner, J. Chem. Phys. **73**, 5862 (1980).

[22] M. R. Bassett and R. Imbihl, J. Chem. Phys. **93**, 811 (1990).

[23] T. Engel and G. Ertl, J. Chem. Phys. Lett., **54**, 95 (1978).

[24] T. Engel and G. Ertl, J. Chem. Phys. **69**, 1267 (1978).

[25] T. Engel and G. Ertl, Adv. Catal., **28**, 1 (1979).

[26] J.C. Robertson and C.W. Wilmsen, J. Vac. Sci. Tchnol., **9**, 901 (1972).

[27] H. Veillard, Nouv. J. Chim., **2**, 215 (1978).

[28] W. Engler, W. Heiland, and E. Taglauer, Verh. Dtsch. Phys. Ges.[6], **13**, 592, 1978.

[29] J.W. Davenport, Phys. Rev. Lett. **36**, 945 (1976).

[30] C.L. Allyn, T. Gustafsson, and W.E. Plummer, J. Chem. Phys. Lett., **47**, 127 (1977).

[31] R.J. Smith, J. Anderson, and J.G. Lapeyre, Phys. Rev. Lett. **37**, 1081 (1976).

[32] G. Apai, P.S. Wehner R.S. Williams and D.A. Shirley, Phys. Rev. Lett. **37**, 1497 (1976).

[33] J.C. Fuggle, M. Steinkilberg and D. Menzel, J. Chem. Phys. **11**, 307 (1975).

[34] G. Blyholder, J. Chem. Phys. Lett., **68**, 2772 (1964).

[35] G. Doyen and G. Ertl, Surf. Sci. **43**, 197 (1975).

[36] B.H. Chen, D.C. Foyt and J.M. White, Surf. Sci. **67**, 218 (1977).

[37] P.J. Kisliuk, journal J. Phys. Chem. Solids, **3**, 95 (1967).

[38] P.J. Kisliuk, journal J. Phys. Chem. Solids, **5**, 78, (1958).

[39] C. Kohrt and R. Gomer, J. Chem. Phys. **52**, 3283 (1970).

[40] D.A. King and M.G. Wells, Porc. R. Soc. Solids Ser., **A339**, 245 (1974).

[41] P.R. Norton, Surf. Sci. **47**, 98 (1975).

[42] L.J. Taylor, D.E. Ibbotson and W.H. Weinberg, Surf. Sci. **79**, 349 (1979).

[43] M. Ehsasi, M. Matloch, O. Frank, J. H. Block, K. Christmann, F. S. Rys, and W. Hirschwald, J. Chem. Phys. **91**, 4949 (1989).

[44] E. G. Seebauer, A. C. F. Kong, and L. D. Schmidt, J. Chem. Phys. **88**, 6597 (1988).

[45] Luis F. Razon and Roger A. Schmitz, Catal. Rev., **28**(1), 89 (1986).

[46] R. Dickman, Phys. Rev. A **34**, 4624 (1986).

[47] P. Meakin and D. Scalapino, J. Chem. Phys. **96**, 731 (1987).

[48] G. Grinstein, Z.-W. Lai, and D. A. Browne, Phys. Rev. A **40**, 4820 (1989).

[49] H. K. Janssen, Z. Phys. B **42**, 151 (1981); P. Grassberger, Z. Phys. B **47**, 365 (1982).

[50] I. Jensen, H. C. Fogedby, and R. Dickman, Phys. Rev. A **41**, 3411 (1990).

[51] M. Dumont, M. Poriaux, and R. Dagonnier, Surf. Sci. **169**, L307 (1986).

[52] P. Araya, W. Porod, R. Sant, and E. E. Wolf, Surf. Sci. **208**, L80 (1989).

[53] H.-P. Kaukonen and R. M. Nieminen, J. Chem. Phys. **91**, 4380 (1989).

[54] D. Considine, H. Takayasu and S. Redner, J. Phys. A: Math. Gen. **23** L1181, 1990.

[55] H. Jigker abd D. ben-Avraham, J. Phys. A: Math. Gen. **25**, L141, 1992.

[56] R. M. Ziff and B. J. Brosilow 1991 Phys. Rev. Lett. in press.

[57] T. Engel and G. Ertl, *The Chemical Physics of Solid Surfaces and Heterogeneous Catalysis*, Vol. 4, ed. by D. A. King and D. P. Woodruff, (Elsevier, Amsterdam, 1982) p. 92.

[58] P. Flory, J. Am. Chem. Soc. **61**, 1518 (1939).

[59] T. Aukrust, D. A. Browne, and I. Webman, Europhys. Lett. **10**, 249 (1989); Phys. Rev. A **41**, 5301 (1990).

[60] J.W. Evans and .S. Miesch, Phys. Rev. Lett. **66**, 833 (1991).

[61] P. Nightingale, J. Appl. Phys. **53**, 7927, 1982

[62] E. Riedel and F. Wegner, Phys. Rev. Lett. **24**, 730 (1970).

[63] E. Riedel Phys. Rev. Lett. **28**, 675 (1972).

[64] I.D. Lawrie and S. Sarbach, In *Phase Transitions and Critical Phenomena, Vol.* 9,ed. C. Domb and J.L. Lebowitz. New York: Academic Press.

[65] M.E. Fisher, J. Phys. Soc. Japan Suppl. **26**, 87 (1969).

[66] V. Privman and M.E. Fisher, J.Stat. Phys. **33**, 385 (1983).

[67] E. Brezin and J. Zinn-Justin, Nucl. Phys. **B257**[FS14], 867 (1985).

[68] V. Privman and N.M. Svrakic, J.Stat. Phys. **54**, 735 (1989).

[69] W. Kinzel and J.M. Yeomans, J.Phys. **A14**, L163 (1981).

[70] W. Kinzel Ann. Israel Phys. Soc. **5**, 425 (1983).

[71] W. Kinzel, Z.Physik **B58**, 229 (1985).

[72] M. Henkel and V. Privman, Phys. Rev. Lett. **65**, 1777, (1990).

[73] V. Privman and L.S. Schulman, preprint (1991).

[74] Colin J. Thompson, *Mathematical Statistical Mechanics*, (Macmillan, NY, 1972)

[75] W. J. Camp and M. E. Fisher, Phys. Rev. B **6**, 946 (1972)

[76] M. Kac, in . *Brandeis Lectures*, edited by M. Chretien, E.P. Gross and S. Deser (Gordon and Breach, NY, 1968), Vol. 1,p. 241.

[77] S. K. Ma, *Modern Theory of Critical Phenomena* (The Benjamin-Cummings, Reading, MA, 1976.)

[78] W. H. Press, B. P. Flannery, S. A. Teukolsky, and W. T. Vetterling, *Numerical Recipes*, (Cambridge University Press, Cambridge, 1986.)

[79] D. E. Knuth, *The Art of Computer Programming* (Addison-Wesley, Reading, MA. 1971.)

# APPENDIX A

# COMPUTATIONAL CONSIDERATIONS

Monte Carlo simulation is an excellent tool in studying statistical systems. The key of conducting a successful Monte Carlo simulation is to produce a set of results that are free of large statistical fluctuations and free of unwanted correlations. To accomplish these objectives, it is frequently required to average a large number of independent simulations in order to minimize statistical fluctuations. Consequently, the demand on cpu time is significant. It is more so in dealing with systems which undergo a phase transition. The inherit characteristics of critical slow down, together with large fluctuations in a phase transition, often render simulations impossible without judicial design of algorithms to minimize computational time.

In order to achieve higher efficiency, we implemented several time saving techniques, which take advantage of the unique aspect of the problem. The essence of our Monte Carlo procedure is simple: a vacant site on the lattice is selected, and its nearest neighbors are examined to determine if a reaction is possible. Despite the simplicity of the kinetic rules, simulations are time consuming simply because of the intrinsic nature of continuous phase transitions. Much of the time spent in this simulation is in generating random numbers, finding vacant sites, locating nearest neighbors and checking possible reaction partners. Evidently, an efficient and well structured algorithm to accomplish these functions is paramount to the success of the study. The most direct approach toward this direction is to avoid and minimize overhead associated with costly operations. Although there are many things to avoid and minimize in designing an efficient algorithm, a well formulated cookbook approach to produce an efficient algorithm is as yet unavailable. Like everything else in computer science, a well structured and efficient algorithm is largely a function of thoughtfulness and ingenuity

of a programmer. Many times such a design may be closely related to the problem on hand. Therefore, it is not our intention to present here any recipes for efficiency. Rather, we want to record the methods we have been using to achieve efficiency and other computational information pertinent to Monte Carlo simulations.

The most direct approach towards achieving greater efficiency is to avoid costly operations such as subroutine calls, conditional statement.and unnecessary floating point operations. Admittingly, these operations may only play a secondary role in relation to a better structured algorithm. The accumulative effect of repetition of these operations, which is a characteristics of any Monte Carlo simulations, may be significant. In view of this unique aspect of Monte Carlo simulations, efforts in the avoidance of these operations may warrant considerations. In our simulations, the most frequently invoked subroutines is the random number generators. Many invocations are necessary in each Monte Carlo trial. The accumulative overhead in generating random numbers is enormous; to minimize this effect, we generated many random numbers in each invocation and reduced the number of calls to this routine. On a IBM 3090-600E, we were able to achieve a considerable speed up. However, caution must be applied in such a practise. Not all random number generators are created equal and suited for this purpose, in fact, some of the system-supplied random number generators are not suitable in this regard. The reason is that these random number generators do not generate sufficiently random numbers in sequence, and they are only "guarantee that each number is random number individually," but they "don't guarantee that more than one of them is random."[78] These random number generators are usually linear-congruent type with unwanted

correlations. We will discuss them further in appendix B where we will give an overview of how to generate random numbers and how to test a random number generator. Besides this method in reducing the overhead, we have in-line the most frequently used routines as a preventive measure.

In this Monte Carlo simulation, the most frequently executed step is to locate nearest neighbors once a vacant site is chosen. Since this finding nearest neighbors and checking for the boundary conditions require conditional statement; it is desirable to replace this method by some other algorithm, which does not require any conditional statement. This can be achieved by implementing a neighbor-list. For each site on the lattice, we generate a list of the nearest neighbors. If the vacant site is at the boundary, this list will point to its nearest neighbor with the periodic boundary. This list is generated by shifting the index of the lattice. For example, if the 12345 is the index of a five site lattice, 51234 will be the neighbor list which points to the nearest neighbor on the left. The $i^{th}$ element of the neighbor list is the nearest neighbor on the left side of $i^{th}$ site; similarly, we can generate a list for the site on the right. Instead of checking the boundary condition every time a site is selected, no conditional checking is required after implementing the neighbor-list. To find the nearest neighbor is just a matter of indexing now. This greatly reduces the cpu time since indexing is a much faster operation than a conditional operation. The principle of replacing conditional statement with indexing has been employed in other places of the program. We will refrain from further elaboration as the principle is the same.

In addition to these time saving methods, a greater time saving algorithm focuses on the elimination of non-productive operations by taking advantage

of the unique aspect of this model. Since each Monte Carlo trial requires a selection of a vacant site, the method of tracking vacant sites or the lack of it plays an important role. There are two ways to approach this problem. One approach is to randomly chose a site on the lattice and then determine if it is vacant. The disadvantage of this approach is that when the lattice is nearly full, the probability of selecting a vacant site is small; many site selections have to be made before a vacant site will be located. Much of the cpu time are spent on non-productive selection process of picking nonempty sites. Evidently, this method is inefficient in the critical region of the model because vacancies are fewer in this region. Alternatively, one may keep a list of vacant sites. This approach rectified the above problem when the lattice is nearly filled and improves efficiency. Similarly, a list of CO-O pair will improve the efficiency of the reaction cycle. However, there is overhead in maintaining such a list. When the lattice has a substantial number of vacant sites, the overhead of maintaining such a list may exceed the first approach of random selection. The balance is between non-productive site selection in the first approach and the overhead of maintaining the list in the second approach. In our simulation, we implemented both algorithms. In the steady state region and near the first order transition when the lattice has a large number of vacant sites, we used the first approach. Near the second order transition, we used the lists to reduce the computational time. The above mentioned techniques have shorten our simulation time by a factor of 10 or more on an IBM 3090-600E. The reduction in cpu time translated directed into the quality of the simulations by producing more samples thus controlling fluctuations.

As we have seen in the above discussion, a successful Monte Carlo simulation rests on generating a sufficient amount of data to minimize statistical fluctuations as well as minimize unwanted correlations. An essential step to take is to optimize the Monte Carlo simulations in such a way that a large amount of data can be generated within a reasonable time frame. In addition, a prudent selection of a random number generator is of paramount importance in ensuring the quality of data. With these objectivities in mind, the success of simulations is sure to ensue.

# APPENDIX B

# RANDOM NUMBER GENERATIONS

In this appendix we will discuss methods of generating random numbers and methods of testing random numbers. To generate numbers sufficiently random is crucial in producing reliable Monte Carlo results. Different algorithms of generating random numbers are available. We will discuss two of the most commonly used methods: linear congruent method and Fibonacci method.

The widely used method of generating random number in a system-supplied random number generator is the linear congruent method. This method offers a quick way of generating random numbers, according to the following recursion formula:

$$X_{n+1} = (aX_n + c) \; mod \; m \tag{61}$$

The sequence generated by this method is not always random. The random numbers generated by this sequence are sensitive to the choice of $X_0$, a, c, and m. This random number generator generates numbers with a period less than or equal to m. In general it is desirable to generate a sequence of random numbers with a long period. The choice of number c and a is important in determining the period of the sequence. To achieve maximum period m, c has to be relative prime to m, and a-1 is a multiple of a prime divisor of m[79]. The period of the random numbers generated with this choice of a and c is m. The choice of even m is to be avoided. The lower bits of the random number generated by an even modulo are not as random. If the $m = 2^l$, the last l digits have a period of $2^l$ at most. The best choice of m is the largest prime number the system can represent. Even with a judicial choice of parameters, the linear congruent method does not generate a sequence of numbers completely random. It is known that random numbers generators are highly correlated[79]. This correlation of the random

number is intrinsic to the method. The consecutive numbers generated by this algorithm lie on the hyperplane of a hypercube. For our Monte Carlo simulation such planar correlation will give erroneous results due to the bias in site selections. A reliable result requires each cell of the square lattice to be sampled at a uniform rate. The linear congruent type generator does not satisfy this criteria, as we will demonstrate by generating 200 million random numbers. We used $a = 715827550$, $c = 578923381$, and $m = 2147483647$. These parameters are carefully selected to satisfy the criteria we have stated. The random number generated is placed in a suitable bin to produce a histogram as shown in Fig. 52. As demonstrated by the histogram, the random numbers are uniformly distributed over a one-dimensional grid. However, if we use a two-dimensional grid and place these numbers in a corresponding cell, the result is dramatically changed. The number generated tends to aggregate in certain cells indicating correlations as shown in Fig. 53. While there exist ways to correct this, it is out of the scope of our discussion. The point is that linear congruent generators have to be used with care in doing Monte Carlo simulations or any calculations, which require correlation free numbers.

A better way of generating random numbers relatively free of correlation is to use Fibonacci random number generators, and this is what we used in our work. The essence of this generator is to first generate a set of random numbers. Similar to the way of generating Fibonacci sequence, a random number is then generated from this list by adding two numbers of certain distance apart. This generator is relatively free of two-dimensional correlation. We generated 200 million points and placed them in a one- and two-dimensional grid as before; Fig. 54 and Fig. 55 show the distribution of

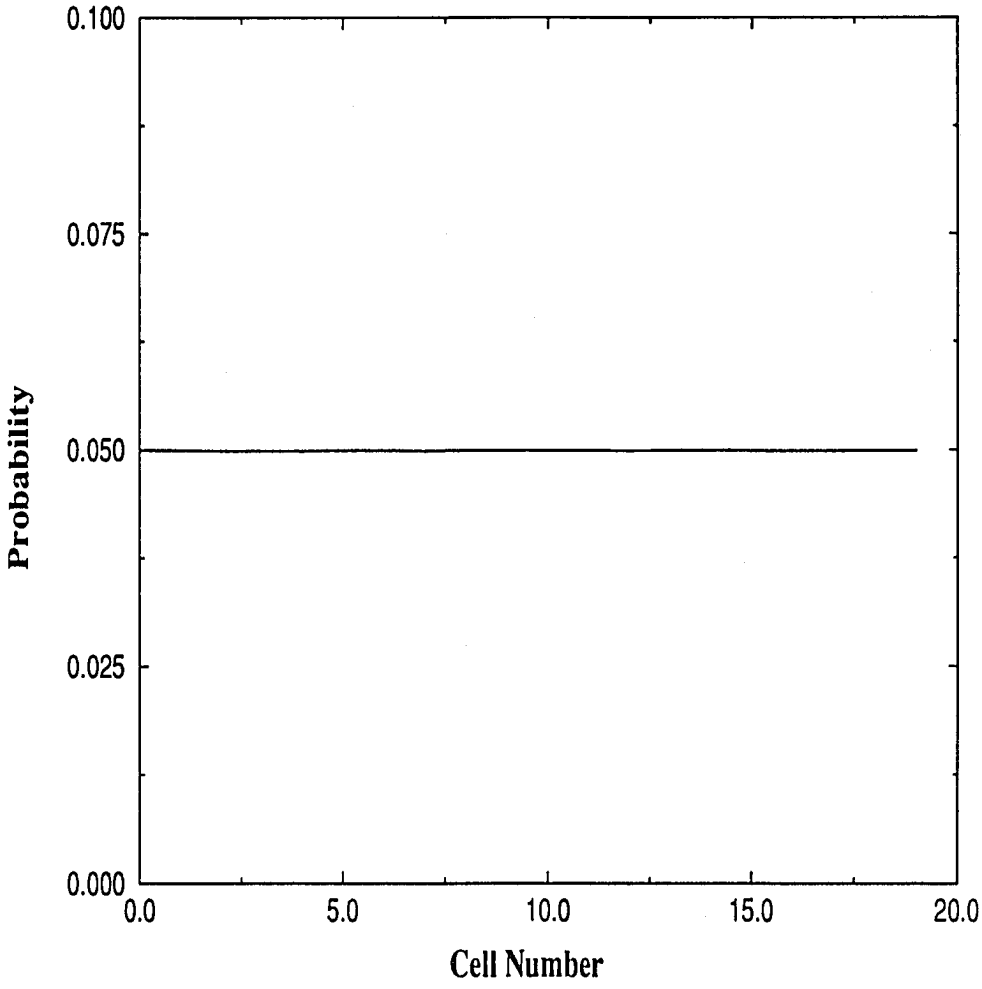


Figure 52: One dimensional distribution of linear congruent random numbers on a linear lattice

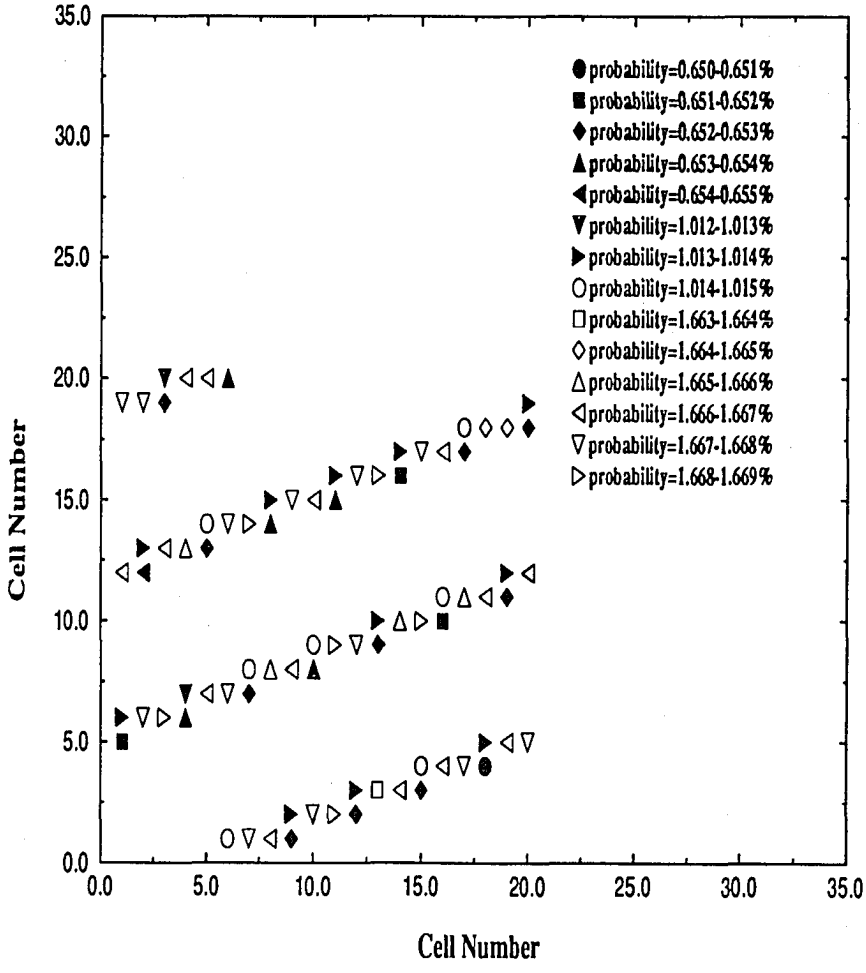


Figure 53: Two dimensional distribution of linear congruent random numbers on a square lattice

these points. It is evident that this generator produces an uniform distribution over one- and two-dimensional grid. In addition to this *parking lot* test, we also performed a pair test and a run test on it. The pair test shows that no pair correlation exist within 92% of the confidence level. The run test indicates that these numbers are random within 89% of the confidence level. For detailed information on testing random number, readers are referred to reference[79].

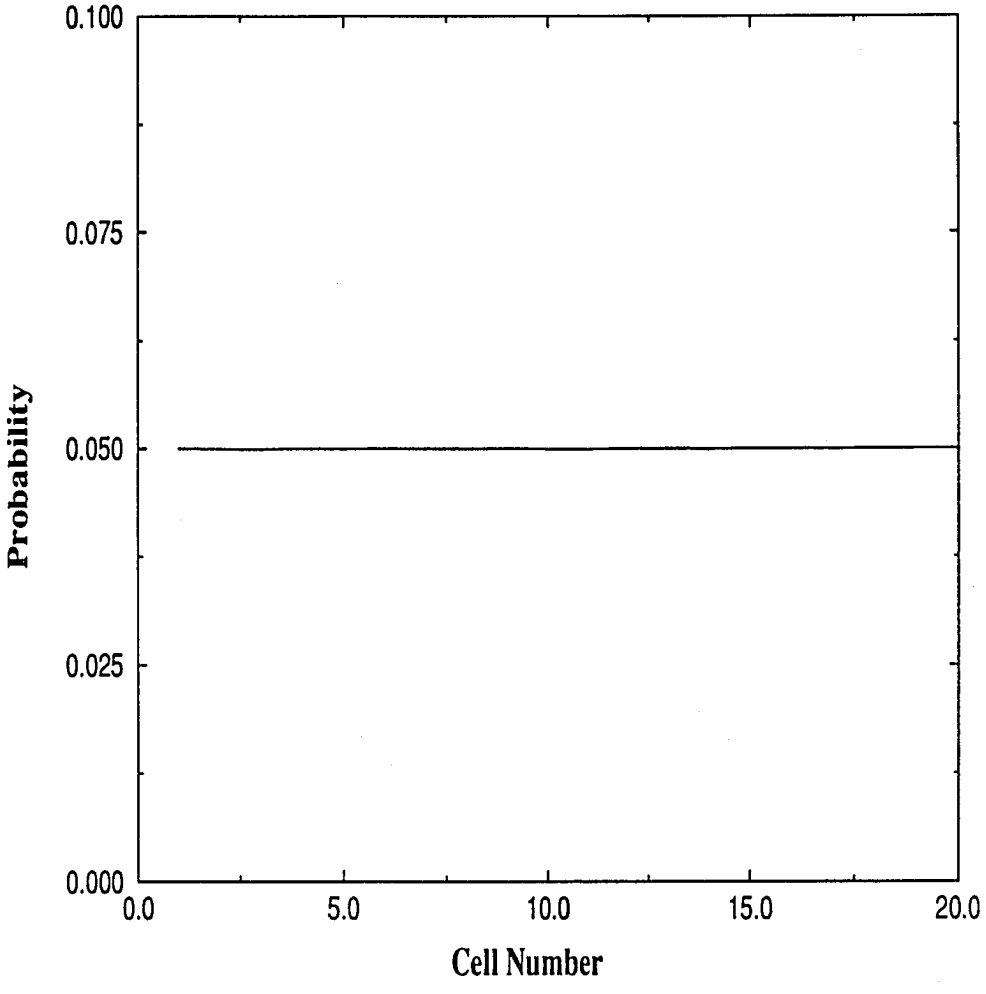


Figure 54: One dimensional distribution of Fibonacci random numbers on a linear lattice

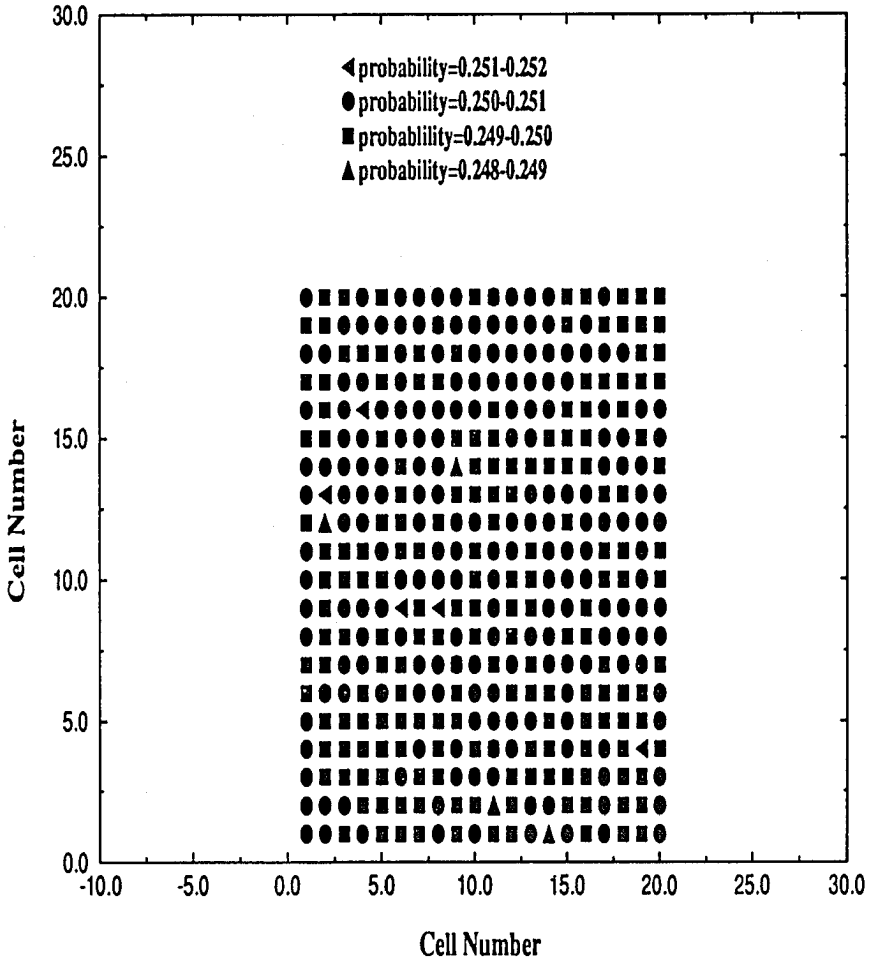


Figure 55: Two dimensional distribution of Fibonacci random numbers on a square lattice

# VITA

The author was born on May 30, 1962 in Shaighai, China. He received B.S. from Louisiana State University in 1985. He continued his graduate study in Louisiana State University in 1986, where he received his master degree in science in 1987. He has worked on the critical phenomena and phase transitions of nonequilibrium systems under the supervision of Prof. Dana Browne.

## DOCTORAL EXAMINATION AND DISSERTATION REPORT

**Candidate:** Bing Yu

**Major Field:** Physics

**Title of Dissertation:** Monte Carlo Studies of the Critical Phenomena in CO Oxidation

**Approved:**

Major Professor and Chairman

Dean of the Graduate School

**EXAMINING COMMITTEE:**

**Date of Examination:**

5 November 1992